MODELLING OF INFRARED RADIATION HEAT TRANSFER FOR YELLOW PEAS IN A PARALLEL TRAY-TYPE GAS-FIRED MICRONIZER

BY

JONG-TAE HONG

A Thesis
Submitted to the Faculty of Graduate Studies
In Partial Fulfillment of the Requirements
for the Degree of

DOCTOR OF PHILOSOPHY

Department of Biosystems Engineering
University of Manitoba
Winnipeg, Manitoba

THE UNIVERSITY OF MANITOBA

FACULTY OF GRADUATE STUDIES

*****

COPYRIGHT PERMISSION

Modelling of Infrared Radiation Heat Transfer for Yellow Peas in a Parallel Tray-Type Gas-Fired Micronizer

BY

JONG-TAE HONG

A Thesis/Practicum submitted to the Faculty of Graduate Studies of The University of Manitoba in partial fulfillment of the requirement of the degree

Of

DOCTOR OF PHILOSOPHY

ABSTRACT

All materials emit energy by virtue of electromagnetic waves due to their body temperatures and this is called radiation. Most energy emitted from a body in the range of wavelengths from 0.7 μm to 100 μm is heat and this is called infrared (IR) radiation. Infrared energy has been used in food processing frequently such as drying, baking or micronizing (cooking partially with high intensity infrared). In spite of many applications of infrared radiation in the food industry, mathematical modelling of infrared processing (micronization) has not been studied thoroughly. To understand the physical phenomena of infrared processing of agricultural products, mathematical models of IR processing using the net-radiation method which is associated with the enclosure theory were developed and validated. The models were developed for a non-moving, fixed-element configuration system and for a moving-element configuration system. The micronization experiments were conducted with yellow peas that were processed in a parallel-tray, gas-fired micronizer. The peas were tempered to 20 - 30% in wet basis moisture content. To validate the mathematical models, several parameters were measured. These included: moisture and temperature gradients, configuration factor from a differential control volume of peas to the emitter surface, mass flowrate, coverage factor, and surface temperatures of emitter and processed peas. The simulation results by the proposed models using the Runge-Kutta 4^{th} order method showed good agreement with the experimental results when the emissivity of peas was assumed to be 0.9 to 0.95. Quantitative results of goodness of fit of the mathematical models are given for all the experiments conducted with the moving and the fixed element configuration. For the comparison by programming algorithm, the

Euler method to solve the model equations was also used, and the simulation results were compared with the results produced by the Runge-Kutta 4^{th} order method. This comparison showed poor fitness to the experimental results when the Euler method was used in the simulation.

ACKNOWLEDGMENTS

First of all, I thank my advisor, Dr. S. Cenkowski, for his invaluable guidance, encouragement, and support during the course of this study. He always made time to advise me for the project whenever I wanted to see him. I learned a lot from him, how to deal with the difficulties in research work. I will never forget all the help and invaluable advice from my co-advisor, Dr. M.G. Scanlon, for this project. He always wished to help me and gave me deep insight on how to define the problems in research and how to access the research problems to solve. I wish to express my sincere gratitude to Dr. W.E. Muir for serving on my thesis committee and providing invaluable advice and feedbacks for me. I thank Dr. S.D. Arntfield in the Department of Food Science for her invaluable advice on the micronization process and for her support to the micronization experiment. Also, I thank Dr. H. Soliman for his advice and discussions on radiation problems which I encountered during my studies. I appreciate all the help from Mr. J. Putnam, D. Bourns, and M. McDonald and their technical assistance.

I acknowledge the financial support from the Natural Sciences and Engineering Research Council of Canada, Centra Gas, Saskatchewan Energy, and InfraReady Products Ltd.

I am grateful to my wife, Kyung-Ae, for her patience and understanding during the long hours of my absence from home, and to my children, Eun-Ah and Jin-Woo, who kept me alive during the periods of troubles. I will never forget all the encouragement, support from and my sisters, Jung-Ok, Jung-Wha, and Sung-Wha. I thank my father-in-law and mother-in-law for their encouragement and support. I thank my father who always wished to see me completing my Ph.D. program successfully.

TABLE OF CONTENTS

LIST OF FIGURES

LIST OF TABLES

TITLE

NOMENCLATURE

Alphabetical

A_i = i-th surface area of the micronizer, m^2

A_S = projected area of the feed on the bottom trough, m^2

C_P = specific heat of the feed, $J/(kg \cdot K)$

F_{d3-j} = configuration factor viewed from the surface, dA_3, to the j-th surface of the micronizer, decimal

H = enthalpy of the feed, J

H = separation distance, m

$\dot{H}$ = rate of enthalpy of the feed, J/s

$\dot{H}_{in}$ = rate of enthalpy of the feed entering the control volume, J/s

$\dot{H}_{out}$ = rate of enthalpy of the feed leaving the control volume, J/s

h_{fg} = heat of vaporization of the moisture, J/kg

ℓ_1, m_1, n_1 = directional cosines in dA_1 with respect to x, y, z-axis, respectively, decimal

L = length of the bottom trough of the micronizer, m

m = mass of the feed in wet basis, kg

$\dot{m}$ = mass flowrate of the feed in wet basis, kg/s

$\dot{m}_{in}$ = mass flowrate of the feed entering the control volume, kg/s

$\dot{m}_{out}$ = mass flowrate of the feed leaving the control volume, kg/s

m_d = mass of the feed in dry basis, kg

$\dot{m}_d$ = mass flowrate of the feed in dry basis, kg/s

m_t = total mass of yellow peas for tempering, kg

M = moisture content of the feed, % wb

M_i = moisture content of raw yellow peas, % wb

M_t = target moisture content of yellow peas, % wb

$\hat{n}_1$ = surface vector of dA_1, (-)

$\hat{n}_2$ = surface vector of A_2, (-)

$\hat{s}_{12}$ = vector pointing from dA_1 to A_2, (-)

$\hat{s}_2$ = vector pointing along the contour A_2, (-)

$dQ_{i,d3}$ = incoming rate of heat on dA_3 surface, W

$q_{i,d3}$ = incoming heat flux on dA_3 surface, W/m^2

$dQ_{o,d3}$ = outgoing rate of heat on dA_3 surface, W

$q_{o,d3}$ = outgoing heat flux on dA_3 surface, W/m^2

t = time, (s)

$t_{R,av}$ = average residence time, (s)

T = temperature of the feed, K

T_j = temperature of j-th surface of the micronizer, K

v_{av} = average travelling velocity of the feed, m/s

W_{add} = amount of water to be added for tempering, kg

w_i, w_j = wieghting factor in Gauss-Quadrature method, (-)

Greek

$\alpha_1, \gamma_1, \delta_1$ = angles between the normal vector of the area dA_1 and the vector $\hat{s}_{12}$ in Figure 3.9.

ε_1 = emissivity of the emitter, decimal

ε_2 = emissivity of open area in enclosure 1, decimal

ε_S = emissivity of the feed, decimal

ε_5 = emissivity of the bottom trough, decimal

Φ = coverage of feed at a given condition, decimal

ρ_S = reflectivity of the feed, decimal

σ = Stefan-Boltzmann constant, $W/(m^2K^4)$

α_S = absorptivity of the feed, decimal

ξ_1 = defined in Eq.(3-22)

ξ_2 = defined in Eq.(3-22)

β = defined in Eq.(3-22)

CHAPTER 1

INTRODUCTION

Thermal processing, which uses heat energy to process materials, of food products is a very common activity to enrich human life by providing better taste for the foods from the raw food materials. Thermal processing in the food industry has been applied in many areas such as drying, cooking, and thermal treatment of food to eliminate microbial counts, such as moulds and yeasts (van Zuilichem et al., 1985; Blenford, 1980). For example, thermal processing in drying reduces the moisture content of the processed materials. By reducing the moisture content of the material the total mass of the material and the water activity can be reduced significantly, therefore the preservation period of the food products being dried can be extended substantially because at low water activity microbes are inactive and simultaneously the cost of storage and transportation can be reduced due to the lower volume or mass (Blenford, 1980). Thermal processing can be classified into three categories: conduction, convection, and radiation. The first two methods have been well established in the theories of heat transfer mechanisms and widely used in industry. On the other hand, thermal processing by radiation is less developed than conduction or convective thermal processing, especially in the food industry due to its complexity (Fasina and Tyler, 2001; Ratti and Mujumdar, 1995). In radiation, the energy is transmitted in the form of electromagnetic waves. Only the range between 0.1 to 1000 μm is called 'thermal radiation' which carries light and heat (Siegel and Howell, 1992). The electromagnetic wave spectrum (Modest, 1993; Siegel and Howell, 1992) is shown in Figure 1.1. Radiative thermal processing has several advantages over conventional heating methods. Radiation transfers energy in the form of electromagnetic waves that can pass through a vacuum, so

a heating medium is not needed to carry thermal energy between the heat source and the product being processed. This feature of direct heating by radiation gives the benefit of environmentally friendly processing of food without generating any waste materials, which occur in conventional cooking such as waste oils in frying and blanch water in blanching. Secondly, heat transfer by radiation between two bodies is proportional to the fourth power of their body temperatures. In high temperature thermal operations, radiation heat transfer dominates the other conventional heating mechanisms and plays the most important role in thermal processing by the combined mode of heat transfer through conduction, convection, and radiation (Siegel and Howell, 1992).

Radiative thermal processing, also known as micronization, is a quick process. The processing time is very short, usually a few minutes (30 s to 5 min) compared to conventional processing methods which have usually 15 to 30 minutes of cooking time (Cenkowski and Sosulski, 1997; Fasina and Tyler, 1997a). Due to the advantages of thermal radiation over conventional heating methods, radiative thermal processing for agricultural products has received considerable attention and was investigated extensively in the 1960s in Russia (Ginzburg, 1969; Hall, 1962). In spite of the advantages of radiative processing, there are some difficulties that prevent using this technology extensively in the food industry. One of these problems is the difficulty of the measurement of radiative properties of agricultural products such as emissivity, absorptivity, and reflectivity, which are essential for the precise design of radiative thermal processing units. Thus, radiative property data for agricultural products are very limited in the literature (Arinze et al., 1987; Ratti and Mujumdar, 1995; Sala, 1986; Singham, 1962). Another difficulty in thermal radiation modelling is that there is no easy way to determine the configuration factor (also known as view factor, angle factor, or shape factor), which represents the energy fraction leaving one surface of an object (i.e., the IR heat emitter) and being intercepted by another object (i.e., the radiated product), for the various geometrical shapes of infrared processing units.

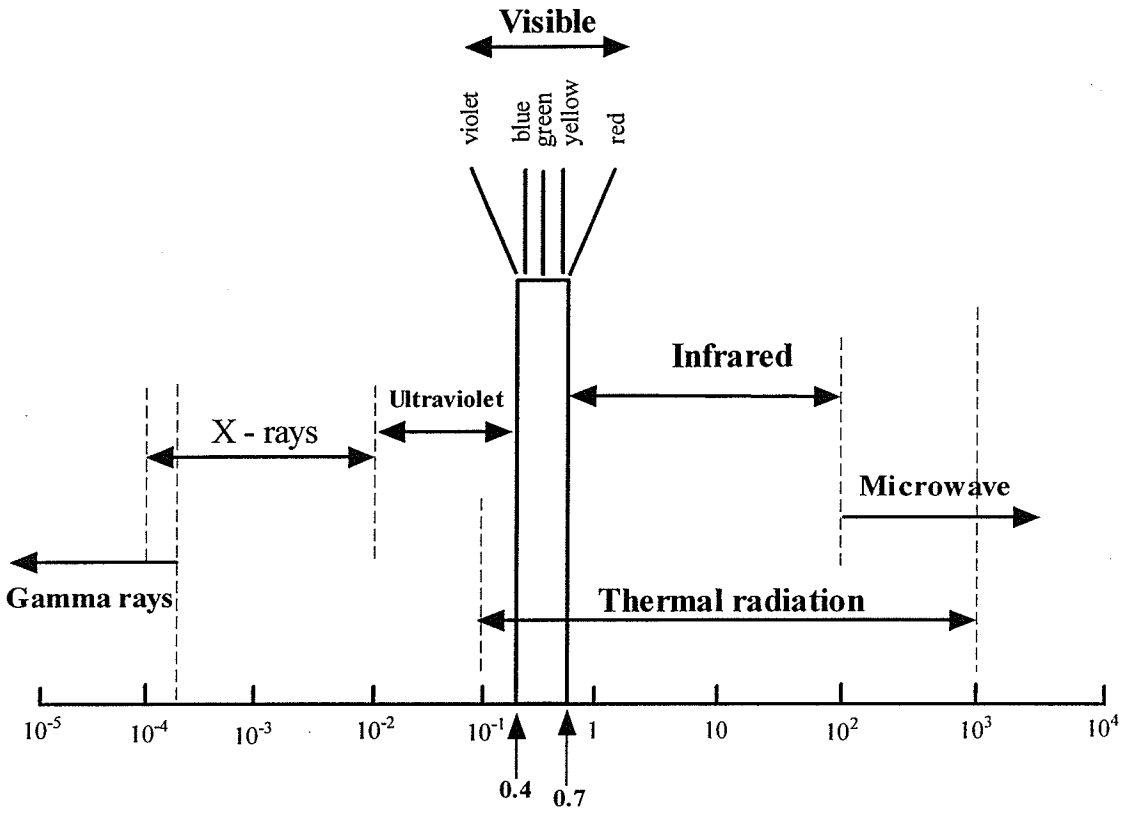

Wavelength, μm

Figure 1.1 Electromagnetic wave spectrum.

For these reasons, most recent investigations on radiation heat transfer have been devoted to finding an easy way to calculate the configuration factor for various geometrical shapes (Chung and Kermani, 1989; Howell, 1982; Hsu, 1967; Sparrow, 1963).

Though the use of infrared energy in the food industry is increasing, only a few studies have been reported on the mathematical modelling of agricultural products subjected to infrared heating (Abe and Tabassum, 1997; Babenko and Shipulina, 1995; Cenkowski et al., 2000; Fasina et al., 1998; Ratti and Mujumdar, 1995). Mathematical modelling is an elegant approach to scaling-up of a process but requires information on radiative properties of the micronized product and the knowledge of thermodynamic interactions between the emitters, the product being processed, and the surroundings. One example would be the determination of the exact values of a configuration factor for various geometries of IR processing units.

A computer model is a helpful device to determine the optimum condition of IR processing for agricultural products, and the control strategies for emitters and the conveying troughs. The computer program must accurately predict temperature and moisture changes in the agricultural products during micronization. The future long term goal is to correlate the processing conditions to textural properties. The specific objectives of this research are to:

1. Develop mathematical models to predict the temperature history and moisture changes of peas processed with high-intensity, infrared radiation (micronization) in two configurations (a moving-element configuration system and a fixed-element configuration system).

2. Develop a mathematical model to calculate the configuration factor for a parallel tray-type, infrared-emitter (micronizer).

3. Evaluate the validity of the proposed models by comparing the experimental results with those obtained through the computer simulation for the two systems (a moving-element configuration system and a fixed-element configuration system).

CHAPTER 2

LITERATURE REVIEW

Infrared (IR) energy has been applied to drying since the early 1940s and the effectiveness of such a process has been investigated for some agricultural products, such as grains, cocoa beans, nut kernels, flour, fruit, and vegetables (Ginzburg, 1969; Hall, 1962). Also, the theories and the applications of IR radiation has been established well over last decades (Fasina et al, 1997b; Modest, 1993; Özisik, 1973; Ratti and Mujumdar, 1995; Siegel and Howell, 1992). In spite of these achievements in IR technology, the use of IR energy in food industry has been limited in the commercial use for several reasons. The reasons are : (a) infrared heating is a surface heating method and the penetrating power of the IR rays on the biological material is not strong enough to penetrate through a deep-bed of processed food. It can penetrate only a few millimeters through the biological materials (Shuman and Staley, 1950), therefore, it is only suitable for processing materials in a thin layer, and (b) scaling-up of the infrared processing unit from laboratory scale to full-plant scale is not easy due to the lack of design data such as emissivity, absorptivity and reflectivity data for the various agricultural products and the lack of mathematical model which describes the processed material under micronizing process (Fasina and Tyler, 2001; Ratti and Mujumdar, 1995). Measurement of radiative properties of agricultural products is rather challenging due to their biological nature. Compared to metals or other non-biological materials, biological materials contain moisture and physicochemical changes take place during thermal processing (Donovan, 1979). Due to the high heat intensity of micronization, the processing time is very short because the radiation energy from the emitter is absorbed instantly at the surface of the product being processed and can last only a couple of minutes (Cenkowski and Sosulski, 1998; van Zuilichem and van der Poel, 1989)

and this feature of short cooking time of micronization compensates for the weak penetrating power for mass production of precooked agricultural products. In this chapter, the effect, the applications, and the mathematical modelling history of IR radiation on agricultural products are surveyed.

2-1 Effects of Infrared on Biological Materials and Its Application

2-1-1 Characteristics of IR on food processing

Electromagnetic waves in the range of wavelength, 0.1 - 1000μm, are associated with heat and light when the beams are incident upon a physical body (Siegel and Howell, 1992). Most thermal radiation is covered by infrared radiation and, traditionally, the infrared spectra are classified into three categories as: near infrared (0.8 - 3.0μm), middle or intermediate infrared (3 - 25μm), and far infrared (25 - 100μm) (Sandu, 1986). When infrared rays impinge on the surface of an agricultural product, some portion of it is reflected at the surface and the rest of it is absorbed into, or transmitted through, the product. The thickness of IR penetration through a biological material is a few millimeters and, usually, most agricultural products can be regarded as opaque materials (Fasina and Tyler, 2001; Fasina et al, 1998; Ratti and Mujumdar, 1995; Shuman and Staley, 1950). Due to its direct heating mechanism of IR transport to processed materials, IR energy is frequently referred to as a 'High Temperature and Short Time (HTST)" process (Blenford, 1980; Nelson, 1962; van Zuilichem and van der Poel, 1989). Infrared was applied to a number of agricultural products to dry flour, malt, fruits, and vegetables, and pasta products (Ginzburg, 1969). But, the depth of penetration by infrared, which depends on the wavelength and the absorbing material, usually is not deep enough, just a few millimeters (usually less than 10 mm). For the processing of bulk materials in multi-layers (or deep-bed) of agricultural products, the products cannot get enough direct heat energy to be cooked from the IR heat source except the first layer of the products which have direct

contact with the IR energy from the IR source. For this reason, infrared energy has been applied widely in industry to dry thin films, such as curing paint and finishes (Nelson, 1962).

Person and Sorenson (1962) demonstrated drying of alfalfa hay of 63% initial moisture content in wet basis using electrical tubular quartz lamps. Their experimental results showed that the higher irradiation intensity and the longer the exposure period enhanced the moisture removal rates. The drying rates for equal intensities depended on the wavelength. Another attempt of applying IR to shelled corn drying was investigated by Headley and Hall (1963) by using a 375 W electrical lamp with a maximum intensity at the wavelength of 1.5μm. They used shelled corn on a stationary and a vibrating tray, which had initial moisture contents of 32% to 35% in dry basis (db), and the moisture content of the shelled corn was reduced to 15% db. They performed IR drying with a single layer; 2.5 cm, 5.0 cm layer of shelled corn. The experimental results showed that the drying time was significantly reduced when the thickness of the shelled corn layer was reduced. Interestingly, for the single layer experiment, the drying time needed to reach 15% moisture content was shorter when a stationary bed of shelled corn was used compared to a vibratory bed.

Recently, many attempts of drying agricultural products with IR have been performed in Japan. By combining convection or conduction with IR radiation, Afzal and Abe (1997, 1998, 1999, 2000) and Abe and Tabassum (1997) investigated the drying rate for rough rice and potatoes using a thin-layer drying model. The combination of IR radiation with convection showed better results in reducing drying time than when only convective drying was used.

2-1-2 IR applications to legume seeds

Originally, the infrared heating technique was applied to animal feed products and cereals to maximize their digestibility (Blenford, 1980). Recently, great attention was paid to food legumes because of the high available starch and proteins after processing with IR (Belitz and Grosch, 1999; Billiaderis, 1992; Cenkowski and Sosulski, 1997; Meyer, 1960). Food legumes are a major part of traditional foods in many countries which include India, Mexico, and many countries in Africa, Central and South America (Deshpande and Damodaran, 1990). They are also a good source of proteins as they contain up to 60% carbohydrates, which are mainly starch components as shown in Table 2.1.1 (Reddy et al., 1989). To broaden the utilization of food legumes, IR processing emerges as a promising technology to shorten the cooking time and to reduce antinutritional factors of legume seeds due to its direct heating feature as an alternative for the conventional thermal processing methods. Cenkowski and Sosulski (1998) reduced the cooking time of split peas by one-third by applying IR heat for 90 s. Major problems for the low utilization of legumes and pulses are the presence of antinutritutional factors, such as trypsin inhibitor, lectins, and tannins, in the legume seeds and also the presence of the microbial growth on the surface of the legumes during the preservation period (van der Poel, 1990). The antinutritional factors damage the gut wall during digestion (lectins), or decrease the digestion of proteins by reducing trypsin activity (trypsin inhibitor), or forms complexes with enzymes or feed proteins and, thus, reduce protein digestibility (tannins) (van der Poel, 1990). To reduce those antinutritional factors, thermal treatment is used as an effective treatment and, among various heating methods, IR heating has shown to be a promising thermal technology due to its 'high temperature short time (HTST)' processing characteristic (Sathe and Salunkhe, 1984; van Zuilichem and van der Poel, 1989; van Zuilichem et al., 1985).

Table 2.1.1 Carbohydrates of food legumes (Reddy et al., 1989).

Legume	Carbohydrates (%)		
	Starch	Amylose	Total
Winged bean seeds	-	-	24.0 - 42.2
Smooth peas	36.9 - 48.6	23.5 - 33.1	56.6
Winkled peas	24.0 - 36.6	62.8 - 65.8	-
Great Northern beans	44.0	10.2 - 30.3	61.2 - 61.5
California small white beans	57.8	29.1 - 32.6	-
Red kidney beans	31.9 - 47.0	17.5 - 37.2	56.3 - 60.5
Navy beans	27.0 - 52.7	22.1 - 36.0	58.4
Pinto beans	51.0 - 56.5	25.8	54.6 - 63.7
Pink beans	42.3	14.9 - 35.3	-
Black-eyed beans	41.2	15.8 - 38.3	-
Black gram	32.2 - 47.9	43.9	56.5 - 63.7
Bengal gram	37.2 - 50.0	31.8 - 45.8	60.1 - 61.2
Mung bean	37.0 - 53.6	13.8 - 35.0	53.3 - 61.2
Red gram	40.4 - 48.2	38.6	57.3 - 58.7
Soybean	0.2 - 0.9	15.0 - 20.0	25.4 - 33.5
Broad bean	41.2 - 52.7	22.0 - 35.0	57.3
Lentil	34.7 - 52.8	20.7 - 45.5	59.7
Cowpea	31.5 - 48.0	-	56.0 - 68.0
Lupine seeds	0.3 - 3.5	-	-

The IR treatment on sorghum was investigated by Shiau and Yang (1982) and they found that micronization improved the starch availability of sorghum and the micronized sorghum at high temperature showed considerable protein solubility.

2-1-3 IR effects on the components of biological materials

For an opaque material, the absorbed IR energy is converted into heat and this increases the body temperature. The increased body temperature of the product by the absorbed IR energy contributes to the change in the physicochemical properties of the products, such as, melting of the starch component when the water content is limited whereas the starch is gelatinized by penetrating of water molecules into the hydrogen bonds of hydroxyl groups in starch when the water content is in excess (Donovan, 1979; Donovan and Mapes, 1980). Most legume starches have a gelatinization temperature from 60 to 90°C when water is in excess as shown in Table 2.1.2 and, unfortunately, the moisture contents of the test materials were not specified in detail (Reddy et al., 1984). Donovan and Mapes (1980) investigated the phase transition of potato starches including acid-treated amylodextrins. When these starches are exposed to heat and to excess water, gelatinization occurs in the temperature range of 65°C to 75°C. Also, Arntfield et al. (1998) showed that water played an important role in reducing cooking time of Laird lentils. They investigated the effects of tempering conditions and moisture contents and found that higher tempering levels (29 - 33%) produced significantly softer micronized lentils than at 25% level. They showed that the moisture content in the seed after micronization had a significant effect on the extent of starch gelatinization whereas the tempering time did not affect starch gelatinization significantly. Fasina et al. (1997a, 1997b) conducted infrared experiments with kidney beans, green peas, black beans, lentils and pinto beans, and measured the physical and mechanical property changes of the micronized products.

Table 2.1.2 Gelatinization temperature of legume starches (Reddy et al, 1984).

Starch source	Gelatinization temperature range (°C)	Reference
Lima beans	70 - 85	Schoch and Maywald, 1968
Lentils	64 - 74	Schoch and Maywald, 1968
	58 - 61	Billiaderis et al., 1981
Yellow peas	63 - 73.5	Schoch and Maywald, 1968
Navy beans	66 - 77	Schoch and Maywald, 1968
	68 - 74	Billiaderis et al., 1981
Garbanzo beans	62.5 - 72	Schoch and Maywald, 1968
	65 - 71	Billiaderis et al., 1981
Mung beans	60 - 78	Schoch and Maywald, 1968
	63 - 69	Billiaderis et al., 1981
Wrinkled peas	69 - 83	Schoch and Maywald, 1968
	> 99	Billiaderis et al., 1981
Black gram	71.5 - 74	Sathe et al., 1982
Black beans	63.8 - 76	Lai and Variano-Marston, 1979
Smooth peas	65 - 69	Billiaderis et al., 1981
Red kidney beans	64 - 68	Billiaderis et al., 1981
Faba beans	61 - 66	Billiaderis et al., 1981
	61 - 69	Lorenz, 1979
Soybeans (Amsoy 71)	73 - 81	Wilson et al., 1978
Peas	54 - 66	Comer and Fry, 1978
Red beans	63 - 70	Lii and Chang, 1981
Adzuki beans	83 - 89	Billiaderis et al., 1981

These researchers concluded that infrared heating caused cracking of the seeds, and the cracking was easily generated at higher moisture contents and at higher surface temperatures (Fasina et al., 1997a). Also, moisture content had more significant effect on seed cracking than did surface temperature because the moisture in the seed built up the vapor pressure and at the end generating pores or bubbles in the product structure (Scanlon et al., 1999). Because of the generated pores the water uptake ability of the seeds precooked by IR was significantly enhanced and the extent of gelatinization of the seeds' starch was also enhanced dramatically (Cenkowski and Sosulski, 1997; Cenkowski and Sosulski, 1998). McCurdy (1992) conducted a series of IR processing experiment on dry peas and canola to investigate the effect of IR heating on the characteristics of dry peas and canola screenings. The micronized peas showed that the protein solubility and bitterness of the raw peas were reduced by infrared heating and also, showed that the infrared heating was effective in partially inactivating myrosinase in canola.

2-1-4 IR effects on microbial populations

Drying is the most common method in food processing to extend the preservation period of food and as a result of drying, the water activity of the food is reduced significantly. Most organisms, which contaminate foods, proliferate at high water activity, mostly at higher water activities than 0.9 (Blenford, 1980). Several investigations which were conducted by researchers (van Zuilichem et al., 1985) in the Netherlands showed that infrared heating of cocoa nibs reduced microbial contamination levels by 95% . The effect of IR heating on the microbial counts of cocoa nibs is shown in Table 2.1.3 (van Zuilichem et al., 1985). They also found that infrared treatment can be used to reduce trypsin inhibitor and other antinutritional factor levels.

Table 2.1.3 Effect of infrared treatment of cocoa nibs on microbial counts (van Zuilichem et al., 1985).

	Before infrared treatment (counts/g)	After infrared treatment (counts/g)
Total count	5×10^6	2×10^5
Enterobacteria	10^4	10
Yeasts	8×10^4	$< 10^2$
Molds	6×10^4	$< 10^2$

2-2 IR Heat Generators

Usually, the generators of infrared radiators can be classified into two categories by their heating source and wavelength of their maximum radiation. According to the wavelength of maximum radiation, the IR radiators or emitters whose surface temperature is in the range of 1773 K (1500 °C) to 2073 K (1800 °C) are called light (short-wave) radiators because the maximum of radiation is less than 1.3μm (visible spectrum is included in this range) (Ginzburg, 1969). Compared to light radiators, the IR generators whose surface temperature is less than 1773 K are called dark (long-wave) radiators which have invisible infrared spectra (Ginzburg, 1969; Fasina and Tyler, 2001). Another classification can be made by the type of heating source used; electrically heated or gas-fired radiators. In electrically heated infrared radiators, the infrared radiation is obtained by passing electrical current through an element of tungsten, and the surface temperature of the electrical radiators can reach higher temperature than gas-fired IR generators. On the other hand, gas-fired IR

generators are generally classified as dark (long-wave) radiators due to their maximum radiation in the invisible infrared range. Gas-fired radiators are made of perforated plates (ceramic or metal) which are heated by gas flames at their surfaces. The characteristics of commercial IR heat sources are represented in Table 2.2.1 for comparison (Strumillo and Kudra, 1986).

Food products are being processed in micronizers and the development of micronizer is now in its third generation (Blenford, 1980; Arntfield et al. 1998; Cenkowski and Sosulski, 1997, 1998; Fasina and Tyler, 2001). The first generation of micronizers were built for the processing of cereals using gas-fired IR heaters and a wedge wire belt conveyor. A wedge wire has triangle shape of the cross-sectional area of the wire (Blenford, 1980). Then, micronizers were modified to use electrically operated IR radiators to be used in areas where electrical energy is less expensive and more easily available than gas (Blenford, 1980). A micronizer of the second generation was developed with a vibratory deck conveyor which replaced the belt conveyor in the first generation and this was found to be effective for cocoa and nuts (Blenford, 1980). The development of the third generation micronizers aims at the efficient processing of powders, which require an extremely different means of conveying and vibrating due to the fine nature of the material and its surface area (Blenford, 1980). The processing time is very short and the powdered material has great heat sensitivity. For these reasons, usually, a stainless steel belt as a conveyor has been used (Blenford, 1980).

Table 2.2.1 Characteristics of commercially used infrared heat sources (Strumillo and Kudra, 1986).

Infrared source		Source temperature		Peak wavelength	Intensitiy
		Usual range (K)	Max (K)	(μm)	(kW/m^2)
Electrically heated radiators					
Non-sheathed radiators	Sylite	1750 - 1800	2200	1.65	Up to 80
	Graphite	2300 - 2800	3500	1.2	Up to 1200
	Metallic-filament tungsten	1900 - 2200	2700	1.2	$(1\text{-}1.4)*10^5$
	Metallic-molybdenum	1600 - 2000	2000	0.9	$(1\text{-}2).*\ 10^5$
Sheathed radiators	Light bulbs	1900 - 2500	2500	1.3	Up to 20
	Quartz lamp	1900 - 2500	2800	1.0	30 - 400
	Plate radiators	700 - 1200	1200	4.0 - 9.0	4 - 14
	Xenon arc lamp	5000 - 10000	10000	0.8 - 1.1	Up to 50
	Tungsten arc lamp	3200 - 4000	7000	0.72	Up to 1400
Gas- heated radiators					
Flame	Direct flame (Bunsen, Teclu, or Mecker burner)	500 - 1600	1800	2.8 - 4.3	20 - 30
	Indirect flame-ceramic element	600 - 800	1500	4.0	50 - 60
	Indirect flame-metallic element	300 - 900	1000	3.6	20 - 30
Flameless	Heated porous plate with internal burning	350 - 850	1200	4.0	40 - 90
	Heated porous plate with external burning	1000 - 1700	2000	1.5 - 2.0	160 - 2400

2-3 Radiative Properties of Biological Materials

When designing an IR food processing unit, one of the most important parts of it is to determine the radiative properties of agricultural products. The averaged radiative properties (hemispherical-total emissivity, absorptivity, and reflectivity) in thermal radiation is essential for the IR processing equipment design for food processing (Ratti and Mujumdar, 1995). The radiative properties of biological materials which are available in the literature are very rare and, even then, the condition of the measurement of the radiative properties of the agricultural products, such as surface conditions and moisture content of a sample are usually not specified in detail (Arinze et al., 1987; Sala, 1986; Singham, 1962).

When applying IR to agricultural products, usually tempering the products is required to prevent overheating of the product surface and to get the best product quality for further processing after micronization (Arntfield et al., 1998; Cenkowski and Sosulski, 1997; Scanlon et al., 1999). Only a limited data of radiative properties for biological materials are available in a limited range of wavelengths due to the difficulty of their radiative property measurement. Massie and Norris (1965) measured spectral reflectance for several grains with the instrument built by them in the range of 0.7 μm to 2.0 μm. The spectral reflectance was 0.2 to 0.6 for wheat of 9, 15, and 25% moisture content and was 0.12 to 0.58 for soybeans of 6 and 24% moisture content. Norris (1958) measured relative light transmittance properties of peaches with the Beckman spectrophotometer and the results was 5% to 100%. Also, Eu (1997) measured the reflectance of wheat in the range of wavelength, 0.35 μm to 1.85 μm. The value of reflectance was 0.12 to 0.57. Typical values of emissivity for agricultural products vary from 0.6 to 0.9 (Arinze et al., 1987; Il'yasov and Krasinikov, 1991). The modelling of IR processing of agricultural products has some problem due to the

difficulty of their radiative property measurement. The device for the radiative properties measurement (hemispherical-total radiative properties) for agricultural products has not been developed well yet (Arinze et al., 1987; Eu, 1997; Norris, 1958).

To best exploit this valuable technology, it is important that we understand the infrared radiation heat transfer mechanism for the IR processing of agricultural products. Also, it is required that an easy and convenient method to measure the radiative properties of agricultural products and this will be quite a challenging task for the research area in IR processing.

2-4 Mathematical Modelling of Infrared Processing

Due to the thermal energy characteristics of infrared radiation, mathematical descriptions of IR processing have been attempted for the last few decades to describe the physical phenomena under IR radiation. Theoretical backgrounds of radiative heat transfer have been developed and well known for several decades since the discovery of the thermal energy of infrared by William Herschel (Siegel and Howell, 1992). Compared to other industries, the applications of radiation theory to food industry has been limited due to several difficulties which can be found in agricultural products. The biological materials experience physicochemical property changes during IR processing (Fasina et al., 1997a; Fasina et al., 1997b). Furthermore, the moisture content of the product affects the radiative properties (Nelson, 1962). Secondly, the limited usage of IR energy on food processing also came from incomplete understanding of the spectral properties of infrared radiation. For example, IR is not strong enough to penetrate the whole thickness of legume seeds (usually less than 10 mm), and this makes IR heater not good for a deep-bed type food processor (Nelson, 1962). The application

of radiation theories to food processing has been devoted mostly to food drying. By drying, one can reduce the mass and the moisture content of agricultural products. Due to this characteristics of IR radiation, IR has been used as a secondary heating option which is combined with convection or conduction heating as a primary drying means to enhance drying efficiency in the paper industry (Blenford, 1980; Fasina and Tyler, 2001). A number of IR mathematical models have been used to study drying thin layer materials such as paper or drying of paint coatings (Ratti and Mujumdar, 1995; Siegel and Howell, 1992). Kuang et al. (1994) developed a mathematical model for paper drying using a gas-fired IR dryer. The model accounted for the mass transfer of water and vapor accompanying conduction, convection and radiation heat transfer. The model was solved with a numerical method of a finite difference method. They showed that IR heat transfer was independent of the mass transfer process and independent of paper sheet temperature. Secondly, they found that an increase of the mass transfer coefficient had a negligible effect on the drying rate.

Parrouffe (1992) proposed a drying model which combined convective and infrared heat transfer for a capillary porous material (such as paper) at the flow conditions in high temperature to simulate paper drying process. He found that there was a link between the evaporation temperature and crust formation on the surface. He also observed that the critical moisture content is independent of the convective drying parameters, sample thickness, overall heat flux, and surface condition. Furthermore, there was an increase of heat transfer coefficient when the surface reached the boiling point of water.

Fernandez and Howell (1996) demonstrated a drying model of infrared radiation for a porous material which simulates paper drying. In this model, they assumed the radiation to be a volumetric phenomena, which represents that absorbed IR energy was expressed in terms of IR energy per unit

volume of the product. Thus, total radiation energy absorbed in the product was obtained by integrating for the whole volume. They analyzed the mass transfer of moisture in the product in three phases, bound water, free water, and water vapor. The volumetric thermal radiation included in the model proved to be an important factor in the drying of paper.

Another interesting mathematical drying model for thick porous materials was suggested by Dostie et al. (1989) by the combination of continuous convective heating with intermittent radiation. They introduced an intermittent function to account for the radiation contribution on the drying experiment and used electrical IR heat intermittently as an external boundary condition and showed significant reduction of drying time, approximately by 50%, when compared to the case of applying convective heating only.

Mathematical modelling of food processed with IR has been attempted for several materials, such as compounds of water and silica or coal and water, which simulate agricultural products. But in some cases, these materials cannot represent well the hygroscopic characteristics of some agricultural products. Hasatani et al. (1988) developed a mathematical model for hybrid drying of granular materials by combining convective heating and IR radiation using an opaque assumption for a batch process. Their drying model included only radiative heating contribution as a boundary condition. But the conditions of radiative heat source and surface temperature of the emitter were not specified. From the energy equation in their model, the convective heat transfer coefficient, h, and overall interchange coefficient (which corresponds to configuration factor or view factor) of thermal radiation, Φ, was obtained by plotting the experimental results to their governing equation of their model. But they used emissivity values of the sample materials instead of overall radiative interchange coefficient which is known as view factor or configuration factor. Also, their usage of

an overall radiative interchange coefficient in the model was not relevant. The overall interchange coefficient between radiative heat source and sample materials could not be the same as the coefficient between the heated air and the sample materials as shown in their model. It seems that they confused the overall radiative interchange coefficient with the emissivity.

A mathematical model of IR drying for a continuous flow along a vibrating bed was developed by Hasatani et al. (1991). The model combined convective and radiative heating which is known as hybrid drying. The equipment used in that experiment is quite similar to the micronizer used in this study which is equipped with a vibrating conveyor to give more exposure to the IR heat to precook the processed products. The fluidization occurred by air through the perforated plates of the vibrated conveyor and the fluidization was effected by the air flow. They assumed that the IR lamps were blackbody, but they did not include the view factor in their radiation model. Furthermore, the evaporation energy term in their governing equation is wrong because they used moisture content of the feed instead of mass flowrate of the feed. They showed the radiation heat was absorbed more effectively on a vibrating bed rather than on a stagnant bed. The drying rate was enhanced with thermal radiation and the calculated results by their model showed satisfactory agreement with the experimental results. But the results are meaningless because their model equation is wrong.

Babenko and Shipulina (1995) proposed a mathematical model for a fluidized bed dryer combined with an electrical IR lamp. They used inclined vibrating bed system under IR radiation for their model by partitioning the bed into several interrelated independent zones. Each zone was a section of a vibrating tray between two injectors of feed additives to the processed product which was heated by infrared radiation. They only included the IR energy which was absorbed in the product volume and they did not analyze the radiative properties of the radiation heat source. The weak point in this

model is that the authors did not include the moisture evaporation energy into the model.

Recently, IR drying investigations of agricultural products were performed actively in Japan. Afzal and Abe (1997, 1998, 1999, and 2000) and Abe and Tabassum (1997) conducted many experiments of IR drying for rough rice, barley, and potato using a thin-layer drying theory for a batch system. They dealt with moisture diffusion by Fick's first law with IR energy as an energy source, but they didn't analyze the energy interactions between the IR source and the processed product. In 1997, Abe and Tabassum (1997) proposed a mathematical model to predict the temperature rise of radiant heated rice in a batch system. They used a small grain container with 3 cm of the bed height and the temperature rise of the rice bed was measured by inserting T-type thermocouple wires. They assumed the surfaces of all the materials which participate in the IR exchange were blackbody and assumed all the materials were opaque. When considering the weak penetrating power of IR to agricultural products, it seems that the experimental setup is lacking reality to simulate biological materials for effective processing of rice. van Zuilichem et al. (1985) suggested a mathematical model to predict the temperature of infrared heated agricultural seeds but they did not include the contribution of moisture evaporation of the seed. Furthermore, the emissivity of the processed product was not included in the model, either. Unfortunately, some parameters, such as the physical meaning of relative temperature in the model is ambiguous and the model was not validated with their experimental results, and the model was lacking in consistency.

Another progress in mathematical modelling of IR processing of agricultural products for a gas-fired micronizer was proposed by Fasina et al. (1998). They investigated heat and mass transfer phenomena using conduction model to predict the temperature profile of an individual grain by including IR energy contribution at the surface of the grain as a boundary condition. There is some

suspicion for the model description because they included configuration factors between the grain and the IR burner and the side plate surfaces of the vibrating conveyor. Their model has only one value, 0.125, of configuration factor between a barley seed on the trough and the emitter. It seems that they included the operating conditions at the exit of the micronizer only and this is physically unrealistic for the entire micronizer length. The configuration factor from a barley kernel to the emitter surface is changing along the micronizer trough and cannot be a constant and has a maximum value aound the middle of the trough. The weak point of the model is that they neglected the energy interactions between the grain and the top side of the vibrating conveyor because there is heat exchange between the seed and the vibrating conveyor when the vibrating conveyor was heated during micronizing processing. Also, one of the boundary conditions of the model at the surface of the processed grain is suspicious because the heat transfer by natural convection at the surface of the grain was calculated by the multiplication of the convective heat transfer coefficient by the temperature difference between the emitter surface and the grain surface. Instead of using the emitter surface temperature, the convective heat transfer must be calculated using the fluid (the mixture of the air and the water vapor which exist between the emitter and the grain) temperature by the definition of convective heat transfer. Also, they measured the grain surface temperature only at the exit of the micronizer and this can be only used as an exit condition or as a boundary condition in their model. The measurement of the grain surface temperature along the vibrating conveyor during micronization for the validation of their model was not explained in their paper.

Also, Cenkowski et al. (2000) proposed a mathematical model of IR processing for a parallel tray-type gas-fired micronizer by using the enclosure theory to predict the temperature history of the pulse crops along the vibratory conveyor for continuous processing. Their sensitivity analysis showed that the configuration factor was the most sensitive to the temperature rise of the processed products.

Also, the model was simulated using the Euler's method and gave rather poor agreement with the experimental results. Hebbar and Rastogi (2001) investigated mass transfer phenomena for cashew kernels during infrared drying by Fick's first law. They estimated the effective diffusion coefficient by adopting a shape factor (sphericity) for the irregular shapes of cashew kernels over a range of temperatures, 100 - 120 °C, and the dependence of the diffusion coefficient was explained by the Arrehnius equation.

Up to now, the mathematical modelling of IR processing for agricultural products is still in the stage of development (Fasina and Tyler, 2001). Some of the proposed models deal with mass diffusion only, and the others include heat transfer phenomena with mass diffusion. For the precise processing of agricultural products, there should be more studies on the heat and mass transfer phenomena by IR radiation such as, the effect of moisture content of the product in mass transfer caused by IR heating (Saravacos and Maroulis, 2001), the effect of surface condition of biological material on IR energy exchange, the effect of operating temperature, the effect of product porosity and product composition on IR energy absorption(Roos, 1995; Schoch and Maywald, 1968; Wray, 1999), and the effect of geometrical configuration of a micronizer (Cenkowski et al., 2000; Fasina and Tyler, 2001; Fasina et al., 1998).

CHAPTER 3

MODELLING

Micronization [high intensity infrared (IR) processing of biological materials, usually legumes] is a complex process because it involves coupled heat and mass transfer. When infrared is applied to agricultural products, the physical phenomena that occur within the products become more complicated to analyze than any other IR processes, such as paper drying or radiative heat dissipation in metallic structures in space, because micronization involves not only coupled mass and heat transfer but also physicochemical changes of the processed products (Ratti and Mujumdar, 1995; Fasina and Tyler, 2001; Blenford, 1980). Typically, micronizers are equipped with vibrating troughs or belt conveyors for conveying product in a continuous fashion. The accurate dynamic behavior of the legumes on a vibratory conveyor is difficult to predict by mathematical equations because of the irregular movement pattern of the materials that can bounce back and forth during IR processing. When the processed material passes under the IR emitters, it experiences complex internal phenomena, such as heat conduction of absorbed radiation energy into the particles, moisture diffusion in those particles, and chemical changes associated with the heat and moisture present (Fasina et al., 1998). In this chapter, the description of the mathematical model and several assumptions for the model derivation are presented, including the heat and mass balance and the configuration factor evaluation for a parallel tray micronizer in continuous processing.

3-1. Description of the Micronization Process

In this study, a lab scale gas-fired infrared heater (micronizer; model MR2, Micronizing Company UK, Ltd.) was installed and used for the experiments. The experimental system is presented in detail in Chapter 4 for a specific configuration. In order to facilitate the understanding of the model proposed in this study, a brief schematic diagram of the experimental setup is depicted in Figure 3.1.

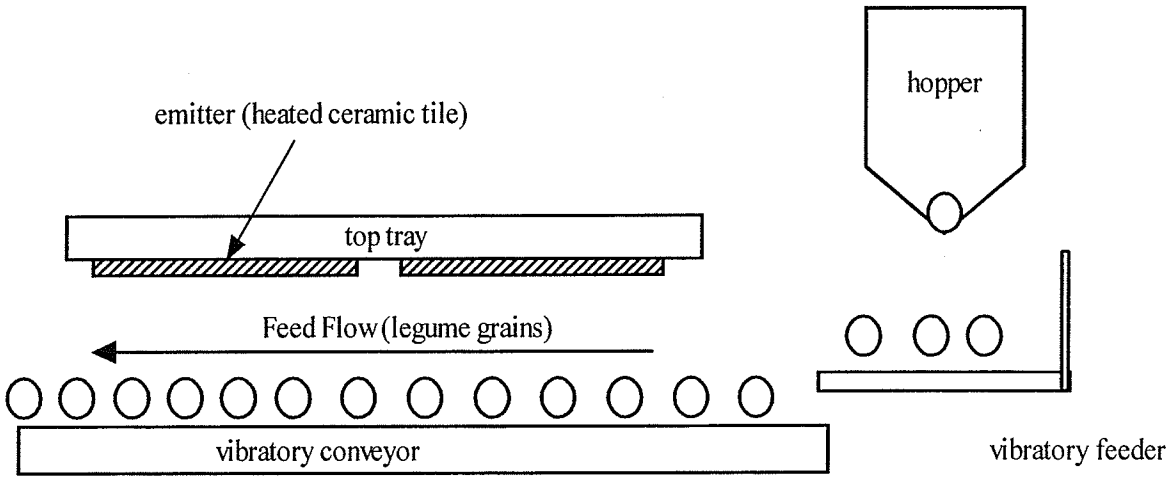

Figure 3.1 Schematic diagram of the the gas-fired infrared heater (micronizer; model MR2, Micronizing Company UK, Ltd.).

The yellow peas are conveyed from the hopper by the vibratory conveyor under the IR emitters which consist of four elements of ceramic tiles in dual line attached to the top tray of the IR heater. As the feed (yellow peas) enters into the heating section, the top surface of the feed is exposed to infrared radiation and is parallel to its emitting surface. Some of the radiation is absorbed by the feed. As the feed travels along the vibratory bottom trough, the temperature of the feed increases and the moisture content decreases due to the radiative heat transfer from the IR emitters. As the feed grains are conveyed by the vibration of the bottom trough (vibratory conveyor), the dynamic behavior of the grains is quite complex to describe in a mathematical expression because the grains bounce back and forth quite irregularly.

3-2 Assumptions for the Model

During infrared processing, a portion of radiation energy coming from the emitters is absorbed by the feed at the surface and another portion of the radiation energy is reflected. The radiation energy absorbed by the feed products is used to increase the temperature of the feed themselves, evaporate moisture, and contribute to physicochemical changes of the feed. These changes include protein denaturation, starch gelatinization in cereals and legumes, enhancement of digestibility, elimination of enzymes such as lipase in oil seeds, and elimination of antinutritional or inhibiting factors such as trypsin and goitrogenic factors (Blenford, 1980; Donovan and Mapes, 1980).

Before the mathematical models of IR processing of biological materials were developed, several assumptions were made:

(1) The processed material is opaque, which means that the radiation energy which penetrates into the body of the material is completely absorbed internally (Siegel and Howell, 1992).

(2) The contribution of the absorbed energy to the physicochemical changes in the feed material is neglected because the amount of energy for the physicochemical changes are small enough to be neglected when it is compared to the latent heat and sensible heat of the

legume feed as can be seen in the literature. The latent heat of water has the value of approximately 2257 kJ/kg where as the enthalpy for starch gelatinization is less than10 kJ/kg (Cenkowski and Sosulski, 1998; Felder and Rousseau, 2000; Sosulski and McCurdy, 1987).

(3) All the surfaces which participate in the radiative heat exchange in IR processing are diffuse-gray. This means that all the radiative properties of the surfaces are independent of the direction and wavelengths of the radiation. This assumption is frequently used in the modelling of IR processing (Fasina and Tyler, 2001).

(4) The surface temperature of the processed product is equal to its internal temperature. This means that the heat transfer in a single particle is fast enough to neglect the temperature gradient in that particle (Ratti and Mujumdar, 1995; Sokhansanj and Bruce, 1987).

(5) The reflected energy at the emitter surface is negligible. The reflected heat energy at the surface of the emitter is small enough to be neglected compared to the radiation energy of the emitter itself (Siegel and Howell, 1992; Modest, 1993).

(6) The "enclosure theory" which are using the 'Net-Radiation Method (NRM)' is applied to the present modelling. The net heat flux from all the surfaces of the enclosure is taken under consideration for the radiative heat exchange among the surfaces. Any surface is considered as completely surrounded by the envelope of a surface of a solid or open areas. This envelope is called an enclosure for the surface (Siegel and Howell, 1992). The enclosure accounts for all directions surrounding the surface.

(7) The temperature of the open areas in the enclosure is considered to be the ambient temperature. This is customarily adopted in the radiation heat exchange in the net-radiation method (Siegel and Howell, 1992; Incropera and DeWitt, 1985).

(8) In this model, only radiative heat transfer mode was included in the model development between the surfaces in the enclosures because no forced convection heat transfer was taking place in the micronizing system used in this experiment (Pabis et al., 1998; Sokhansanj and Bruce, 1987).

3-3 Mathematical Model

To obtain governing equations for the micronization, mass and energy balances will be performed for two kinds of systems: the 'Moving-Element Configuration System (MECS)' and the 'Fixed-Element Configuration System (FECS)'. The 'Moving-Element Configuration System' describes the radiative heat transfer phenomena when the feed is moving with the speed of the bulk materials and thereby the configuration factor of the feed is changing as it moves along the trough. On the other hand, the location of the feed is fixed on the trough which has a constant configuration factor in the 'Fixed-Element Configuration System' where the feed is contained in a stainless steel cage during the bulk material moves along the trough. For the model development for two cases mentioned above, mass and energy balance equations for IR processing of the biological materials under a parallel tray-type infrared heater are formulated and developed with several assumptions which were made in the previous section.

3-3-1 Modelling for a moving-element configuration system

Peas are conveyed in a single layer on a vibrating trough and they pass under IR emitters (Figure 3.2). This figure depicts a schematic diagram of a parallel tray-type micronizer. It is assumed that the movement of the peas on the trough is smooth. As the peas travel along the vibratory conveyor, they experience mass change due to moisture evaporation.

3-3-1-1 Mass balance equation for a moving-element configuration system

A diagram of mass balance for a control volume is shown in Figure 3.3. There are two kinds of methods available to develop a mass balance equation. A mass balance can be written for an elementary volume representing processed peas, which is moving along the feed stream. This approach is called Lagrangian approach or system approach which traces the movement of the control volume. The other approach uses a fixed point in space with the processed feed passing through it and changes that can take place at that point are considered. This approach is called Eulerian approach (Welty et al., 1984). In this chapter, Eulerian method is used. Consider a control volume on the vibratory bottom trough in Figure 3.3. The system has no mass generation or consumption by any chemical reaction and the rate of mass accumulation in the control volume is zero at steady-state. The mass balance can be expressed by the following equation.

$$\begin{pmatrix}\text{rate of mass}\\ \text{into the}\\ \text{control volume}\end{pmatrix} = \begin{pmatrix}\text{rate of mass}\\ \text{out of the}\\ \text{control volume}\end{pmatrix} \tag{3-1}$$

The mass flowrate at the entrance into the control volume is described as:

$$\dot{m}_{in} = \dot{m} \tag{3-2}$$

The mass flowrate leaving the control volume as $\dot{m}_{out}$ in x-direction is:

$$\dot{m}_{out} = \dot{m} + \left(\frac{d\dot{m}}{dx}\right)dx \tag{3-3}$$

Also, the rate of moisture evaporation in the control volume as shown in Figure 3.3 is denoted by $\dot{w}$. By substituting Eq.(3-2), Eq.(3-3), and $\dot{w}$ into Eq.(3-1) one can obtain the following equation:

$$\dot{m}_{in} = \dot{m}_{out} + \dot{w} \tag{3-4}$$

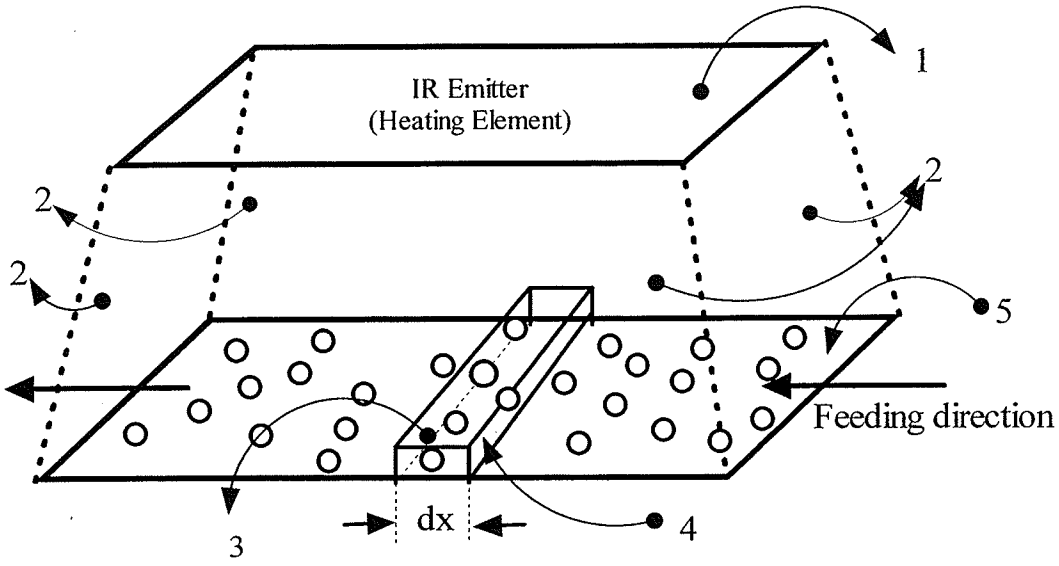

Figure 3.2 Schematic diagram of micronizer planes (enclosure)

1. Heating element inner surface,
2. Side planes (open areas to ambient),
3. Top surface of the control volume,
4. Bottom surface of the control volume,
5. Top surface of the bottom trough

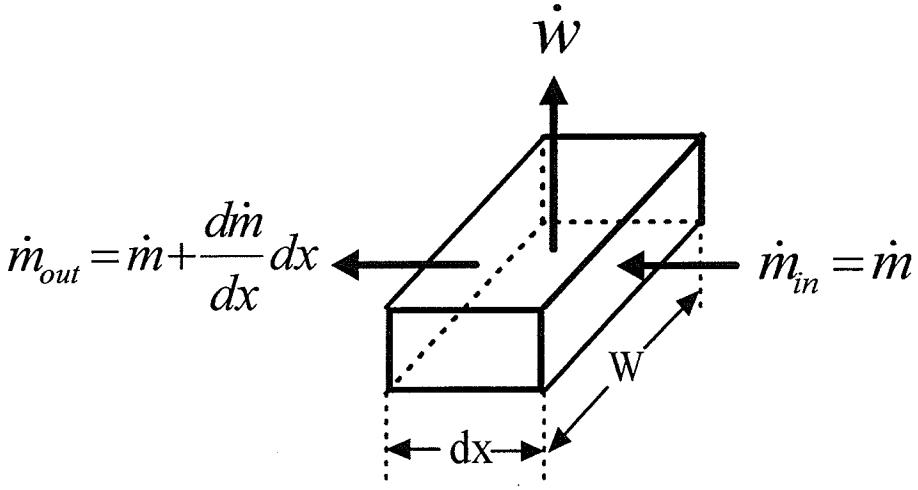

Figure 3.3 Schematic diagram of a control volume for mass balance.

By putting Eq.(3-3) into Eq.(3-4), the mass balance equation was derived as follows:

$$\dot{w} = -\left(\frac{d\dot{m}}{dx}\right) \cdot dx \tag{3-5}$$

3-3-1-2 Energy balance equation for a moving-element configuration system

The radiative heat exchange taking place inside the enclosure is quite complex. The radiation rays leave the surface of the emitter, travel to other surfaces where they are being partially reflected, and then reflected many times within the enclosure with partial absorption at each contact with another surface. Instead of following the radiation pattern, the energy balance can be formulated by using the net-radiation method (Hottel, 1954; Poljak, 1935 cited in Siegel and Howell, 1992). In this method only the net heat flux is considered at the radiated surfaces.

When peas as feed pass through the gas-fired micronizer, the system makes two enclosures. The feed moving along the trough in a single layer separates the micronizer into two enclosures: 'Enclosure 1'and 'Enclosure 2'(Figure 3.4). 'Enclosure 1' consists of the surface of the IR emitter (surface1), open area to the ambient air (surface 2), and the top surface of the feed layer(surface 3) as shown in Figure 3.4. 'Enclosure 2' consists of the bottom surface of the feed layer (surface 4), the open area (surface 6), and the top surface of the bottom trough (surface 5). When the feed passes through the micronizer, the radiation energy from the IR emitter can reach the top surface of the feed layer. A fraction of the radiation energy is absorbed by the feed material and the other fraction is reflected by the surface of the feed back to the emitter and also reflected to the open area of the ambient air of 'Enclosure 1'. As the feed travels through the micronizer, the enthalpy change takes place due to the heat absorption by the feed. This heat exchange can be described using the net-radiation method separately for 'Enclosure 1' and for 'Enclosure 2'. The governing energy equation is derived by taking the energy balance for an elementary control volume in Figure 3.5.

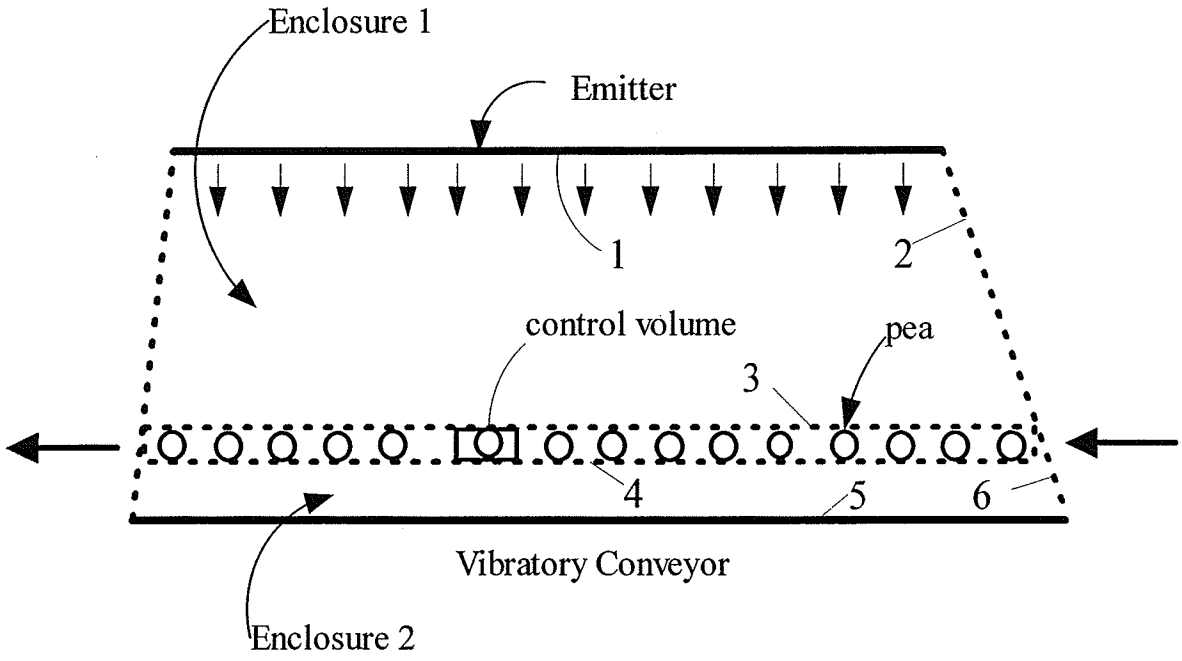

Figure 3.4 Schematic diagram of a gas-fired infrared heater (micronizer)
1, 2, 3 = surface numbers in Enclosure 1,
4, 5, 6 = surface numbers in Enclosure 2.

At steady-state, there is no energy generation, consumption, or accumulation in the control volume. The energy balance equation is expressed as follows:

$$\begin{pmatrix}\text{rate of energy}\\ \text{into the control}\\ \text{volume}\end{pmatrix} = \begin{pmatrix}\text{rate of energy}\\ \text{out of the}\\ \text{control volume}\end{pmatrix} \tag{3-6}$$

All the energy terms for the control volume are classified into two categories, the energy that enters the control volume (feed enthalpy, incoming radiation energy, and net heat radiation from the trough) and energy that leaves the control volume (evaporation, radiosity which represents the emission energy plus the reflected energy at the surface of the control volume, and enthalpy of leaving feed), and are presented in Figure 3.5. The enthalpy of the feed entering the control volume is expressed:

$$\dot{H}_{in} = \dot{H} = \dot{m} \cdot C_p \cdot T \tag{3-7}$$

where,

$\dot{m}$ = mass flowrate of the feed, (kg/s)

C_p= specific heat of the feed, $(\text{J/kg} \cdot \text{K})$

T = temperature of the feed, (K)

$\dot{H}$ = enthalpy of the feed entering the control volume, (J/s)

The radiation energy incident upon the top surface of the control volume (surface 3) is expressed as:

$$dQ_{i,d3} = q_{i,d3} \cdot dA_S \tag{3-8}$$

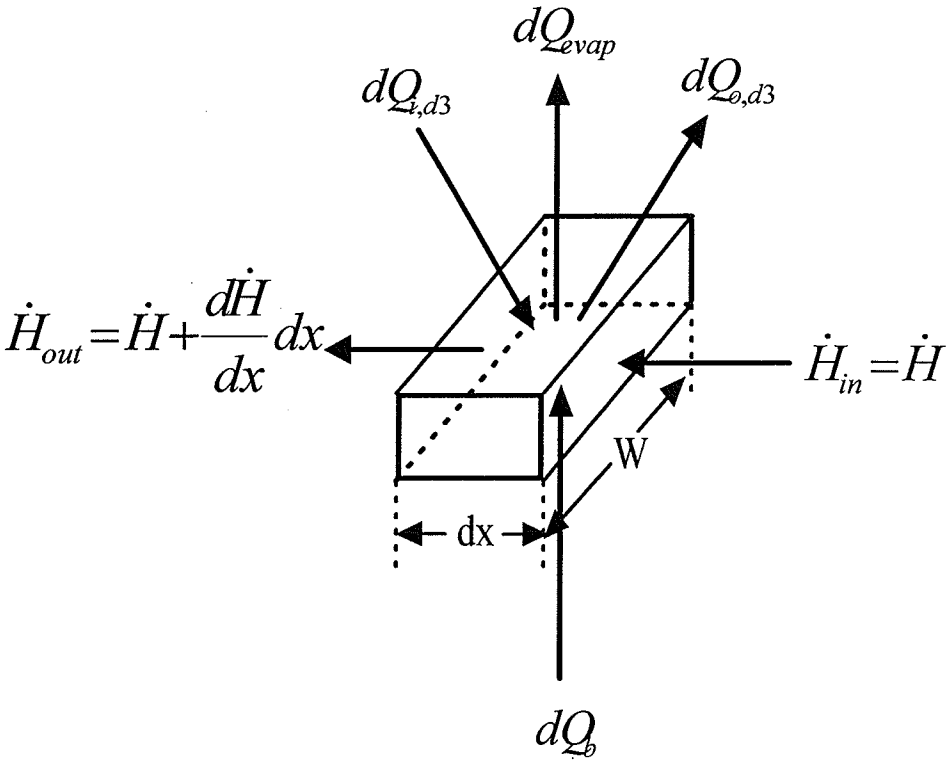

Figure 3.5 Schematic diagram of energy balance for a control volume (moving-element configuration system).

where $q_{i,d3} \cdot dA_S$ =

incoming radiative heat flux on the top surface of the control volume (J/s· m^2) **x** area occupied by the feed material in the control volume (m^2).

The elementary control volume consists of the feed and the spaces between the feed particles. The top surface area of the control volume (dA_3) is greater than the projected area of the feed (dA_S) when the feed moves along the trough in a single layer. Therefore, a ratio of these two areas is introduced and named coverage, Φ:

$$\Phi = \frac{dA_S}{dA_3} = \frac{A_S}{A_3} = \text{constant} \tag{3-9}$$

where A_S is the projected area of the feed layer only and A_3 is the surface area which includes the feed surface plus the spaces between the feed particles.

Incoming heat flux ($q_{i,d3}$) is a summation of the outgoing heat flux from other surfaces in Enclosure 1 and is described as follows:

$$q_{i,d3} \cdot dA_S = \sum_{j=1}^{N} \left(q_{o,j} \cdot A_j \cdot dF_{j-dS} \right) \tag{3-10}$$

where N is the number of surfaces in Enclosure 1, the subscript 'S' denotes the feed sample, and dF_{j-dS} is the configuration factor from the j-th surface to the top surface of the feed occupying the control volume. A_j is the area of j-th surface in the enclosure. By virtue of the configuration factor reciprocity, the following relationship is valid (Siegel and Howell, 1992):

$$A_j \cdot dF_{j-dS} = dA_S \cdot F_{dS-j} \tag{3-11}$$

where F_{dS-j} is the configuration factor from the surface dA_S to the j-th surface (A_j), and the configuration factor for the j-th surface in Enclosure 1 has the following relationship:

$$F_{dS-j} \approx F_{d3-j} \tag{3-12}$$

Therefore, by incorporating the last four relationships into Equation (3-8), we obtain:

$$\begin{aligned} q_{i,d3} \cdot dA_S &= q_{i,d3} \cdot \Phi \cdot dA_3 \\ &= \sum_{j=1}^{N} \left(F_{d3-j} \cdot q_{o,j} \right) \Phi \cdot dA_3 \end{aligned} \tag{3-13}$$

After the rearrangement of the last equation , the incoming radiation heat flux onto the elemental surface is expressed as:

$$q_{i,d3} = \sum_{j=1}^{N} \left(F_{d3-j} \cdot q_{o,j} \right) \tag{3-14}$$

When the radiation energy from the surfaces of the two enclosures is absorbed by the feed, the moisture of the feed evaporates into the air and this causes a decrease of the mass flowrate of the feed. The rate of the heat needed for the evaporation of the moisture from the control volume is expressed by:

$$dQ_{evap} = h_{fg} \cdot \dot{w} = h_{fg} \cdot \left(-\frac{d\dot{m}}{dx} \right) dx \tag{3-15}$$

where, h_{fg} = heat of evaporation of moisture, (J/kg).

As the feed absorbs the radiation energy from the surfaces of both enclosures, its temperature increases so that it also emits radiation energy corresponding to the surface temperature of the feed. This outgoing radiation energy from the feed surface of the control volume is written as:

$$dQ_{o,d3} = q_{o,d3} \cdot \Phi \cdot dA_3 \tag{3-16}$$

The outgoing radiation heat flux (radiosity), $q_{o,d3}$, is expressed as a summation of the heat emitted by the processed feed and the heat reflected as a portion of the heat flux that reaches the surface of the feed layer (incoming radiation). Eq.(3-16) therefore can be written as:

$$q_{o,d3} \cdot \Phi \cdot dA_3 = \left(\varepsilon_S \cdot \sigma \cdot T^4 + \rho_S \cdot q_{i,d3}\right)\Phi \cdot dA_3 \tag{3-17}$$

For diffuse-gray opaque materials:

$$\alpha_S = \varepsilon_S \quad \text{and} \quad \alpha_S + \rho_S = 1 \tag{3-18}$$

where, α_S, ε_S, and ρ_S represent absorptivity, emissivity, and reflectivity of the feed, respectively. After incorporating Eq.(3-18) into Eq.(3-17), Eq.(3-16) reduces to the following form:

$$dQ_{o,d3} = \left[\varepsilon_S \sigma T^4 + \left(1 - \varepsilon_S\right) q_{i,d3}\right]\Phi \cdot dA_3 \tag{3-19}$$

At the exit from the control volume, the rate of change of the enthalpy of the feed is described as follows:

$$\dot{H}_{out} = \dot{H} + \left(\frac{d\dot{H}}{dx}\right) dx \tag{3-20}$$

In Enclosure 2, there is a radiation heat exchange between the bottom surface of the control volume (surface 4) and the surface of the vibratory conveyor (surface 5, Figure 3.4). The open area of the ambient air (surface 6) in Enclosure 2 is small enough because the ratio of the width of the trough over the open area in Enclosure 2 was less than 0.08. So, the radiation exchange by the open area was neglected in the model development (Figure 3.4). The bottom surface of the feed layer (surface 4) emits the radiation energy onto the surface of the trough (surface 5) and the same surface 5 emits back the energy to the bottom surface of the feed layer (surface 4). The net heat flux is obtained by

adding the two heat fluxes which leave each surface (surface 4 and surface 5) in Enclosure 2. The net heat flux from the bottom trough is expressed as:

$$dQ_b = q_b \cdot \Phi \cdot dA_3 = \left\{ \frac{\xi_2 \left[\Phi \left(1 - \varepsilon_S \right) - 1 \right] - \varepsilon_5 \xi_1}{1 - \Phi \left(1 - \varepsilon_5 \right)\left(1 - \varepsilon_S \right)} \right\} \Phi \cdot dA_3 \tag{3-21}$$

where,

$$\begin{aligned} \xi_1 &= \Phi \cdot \varepsilon_S \cdot \sigma \cdot T^4 + \beta, \\ \xi_2 &= -\varepsilon_5 \cdot \sigma \cdot T_5^4, \\ \beta &= (1 - \Phi) q_{i,d3} = (1 - \Phi) \left[F_{d3-1} \cdot \varepsilon_1 \cdot \sigma \cdot T_1^4 + \left(1 - F_{d3-1} \right) \varepsilon_2 \cdot \sigma \cdot T_2^4 \right] \end{aligned} \tag{3-22}$$

The derivation of Eq.(3-21) is presented in detail in Appendix I. When the items presented above are incorporated into Eq. (3-6), then

$$\dot{H}_{in} + dQ_{i,d3} + dQ_b = \dot{H}_{out} + dQ_{o,d3} + dQ_{evap} \tag{3-23}$$

By replacing the symbols in Eq.(3-23) with developed relationships we obtain:

$$\dot{H} + \Phi \cdot dA_3 \cdot q_{i,d3} + q_b \cdot \Phi \cdot dA_3 = \left[\dot{H} + \frac{d\dot{H}}{dx} dx \right] + q_{o,d3} \cdot \Phi \cdot dA_3 + h_{fg} \left(- \frac{d\dot{m}}{dx} \right) dx \tag{3-24}$$

Also, dA_3 can be expressed as follows:

$$dA_3 = W \cdot dx \tag{3-25}$$

where, W is the width of the bottom trough (m).

By inserting Equation (3-25) into Equation (3-24) and dividing both sides of the equation by 'dx' we

obtain:

$$\Phi \cdot W \cdot q_{i,d3} + q_b \cdot \Phi \cdot W = \frac{d\dot{H}}{dx} + q_{o,d3} \cdot \Phi \cdot W + h_{fg}\left(-\frac{d\dot{m}}{dx}\right) \tag{3-26}$$

The mass flowrate, $\dot{m}$, in wet basis is expressed as a function of the mass flowrate of dry mass and its moisture content in wet basis [%]:

$$\dot{m} = \dot{m}_d\left(\frac{100}{100 - M}\right) \tag{3-27}$$

where,

$\dot{m}_d$=dry mass flowrate, $\left(\text{kg solid/s}\right)$

M = moisture content in wet basis, $\left(\text{kg } H_2O/\text{kg feed}\right)$

The total mass flowrate and enthalpy of the feed are functions of moisture content and temperature. From equation (3-27), $d\dot{m}/dx$, and $d\dot{H}/dx$ are expressed as functions of the moisture content and temperature as follows:

$$\frac{d\dot{m}}{dx} = \frac{d}{dx}\left[\dot{m}_d\left(\frac{100}{100 - M}\right)\right] = \frac{100\dot{m}_d}{(100 - M)^2}\left(\frac{dM}{dT}\right)\left(\frac{dT}{dx}\right) \tag{3-28}$$

$$\frac{d\dot{H}}{dx} = \frac{100\dot{m}_d}{(100 - M)}\left(\frac{dT}{dx}\right)\left[\left(\frac{C_P}{100 - M} + \frac{dC_P}{dM}\right)\frac{dM}{dT} \cdot T + C_P\right] \tag{3-29}$$

By introducing the developed relationships [Eq.(3-28) and Eq.(3-29)] back into Equation (3-26), we obtain:

$$\frac{dT}{dx} = \frac{\Phi \cdot W \cdot \varepsilon_S \left[\frac{q_b}{\varepsilon_S} + F_{d3-1} \cdot \varepsilon_1 \cdot \sigma \cdot T_1^4 + \left(1 - F_{d3-1}\right)\varepsilon_2 \cdot \sigma \cdot T_2^4 - \sigma \cdot T^4 \right]}{\left(\frac{100 \cdot \dot{m}_d}{100 - M}\right)\left[\left(\frac{C_P}{100 - M} + \frac{dC_P}{dM}\right)\frac{dM}{dT}T + C_P - \frac{h_{fg}}{100 - M}\left(\frac{dM}{dT}\right)\right]} \tag{3-30}$$

where, q_b is derived from Eq.(3-21) as :

$$q_b = \frac{\xi_2\left[\left(1 - \varepsilon_S\right)\Phi - 1\right] - \varepsilon_5\xi_1}{1 - \Phi\left(1 - \varepsilon_S\right)\left(1 - \varepsilon_5\right)} \tag{3-31}$$

The derivation of Eq.(3-31) was shown in Appendix I in detail. Also the derivation of Eq.(3-28) and (3-29) were shown in Appendix II. The term dC_P/dM becomes zero if the specific heat of the feed is assumed constant throughout processing. The parameters ξ_1, ξ_2, and β are described by Eq.(3-22).

Eq.(3-30) has a form of the first order non-linear differential equation. To solve this equation, numerical solution is required.

3-3-2 Modelling for a fixed-element configuration system

When a certain amount of feed is placed at a fixed position under the emitters, the energy flux that reaches the surface of the feed is constant during micronization with a constant configuration factor. Except for the location of the feed, other operating conditions in the fixed-element configuration system are the same as the conditions of the moving-element configuration system. Figure 3.6 and 3.7 depict schematic diagrams of a control volume for mass and energy balance for the feed material positioned at a fixed location on the trough and the formulation is presented through Eq.(3-32) to Eq.(3-40) by the Lagrangian approach.

3-3-2-1 Mass balance equation for a fixed-element configuration system

In the Lagrangian approach, the concept of mass balance for the control volume located at a fixed position is shown in Figure 3.6. The material in the control volume experiences unsteady-state conditions. The difference between the Eulerian method and the Lagrangian method is that the mass contained in the control volume stays within the control volume in the Lagrangian method (the control volume is the mass itself) while in the Eulerian approach the mass in the control volume is moving with time through the boundary of the control volume. As the processing time passes, the moisture in the feed is evaporated into the air ($\dot{w}$) and this makes the change of the mass in the control volume (dm/dt). Thus, the mass balance equation is formulated as:

$$\begin{pmatrix}\text{rate of mass}\\ \text{into the}\\ \text{control volume}\end{pmatrix} - \begin{pmatrix}\text{rate of mass}\\ \text{out of the}\\ \text{control volume}\end{pmatrix} = \begin{pmatrix}\text{rate of mass}\\ \text{accumulation in the}\\ \text{control volume}\end{pmatrix} \qquad (3\text{-}32)$$

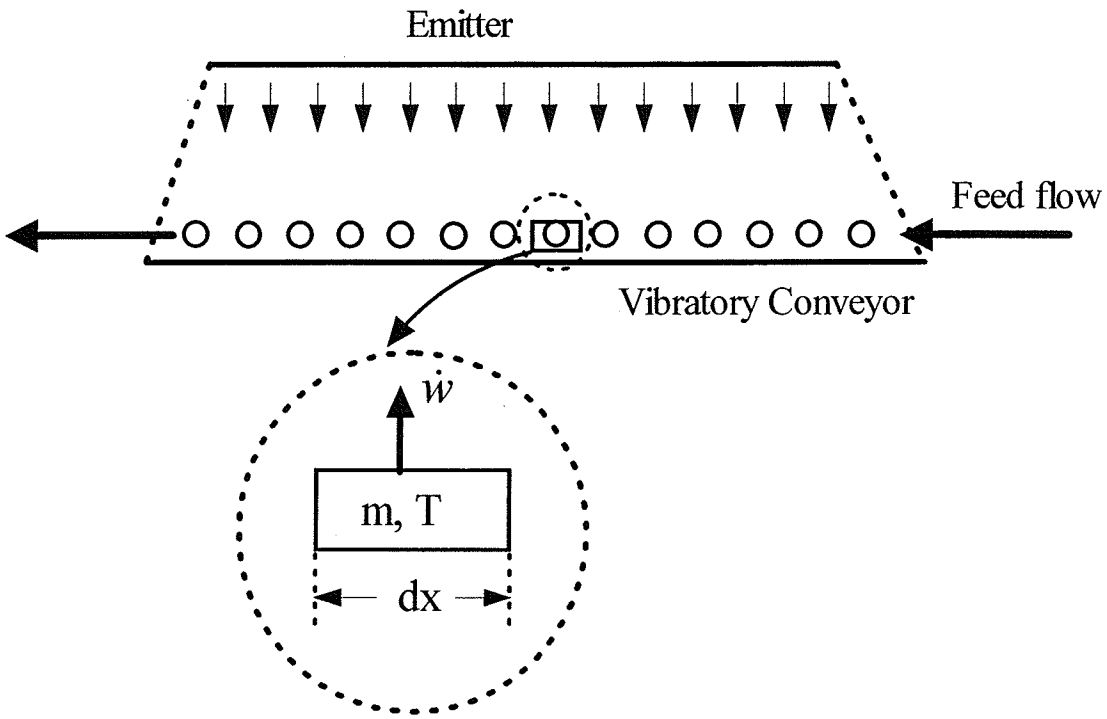

Figure 3.6 Control volume for mass balance in a fixed-element configuration model.

In Eq.(3-32), the rate of mass into the volume is equal to zero and by introducing the rate of moisture evaporation ($\dot{w}$) and rate of mass accumulation (dm/dt) into Eq.(3-32) , we obtain:

$$-\dot{w} = \frac{dm}{dt} \tag{3-33}$$

By rearranging Eq.(3-33), we obtain:

$$\dot{w} = -\frac{dm}{dt} \tag{3-34}$$

where, t = processing time (s).

The rate of moisture evaporation is equal to the rate of mass change in the control volume with respect to time.

3-3-2-2 Energy balance equation for a fixed-element configuration system

Similarly to the derivation of the heat transfer equation in the moving-element configuration model as presented in section 3-3-1-2, we can write the energy balance for a control volume (Figure 3.7). The only difference in the energy balance between the moving-element configuration system and the fixed-element configuration system is that the enthalpy in the fixed-element configuration system is changing with time (unsteady-state). The energy balance equation for a fixed-element control volume is formulated as:

$$\begin{pmatrix}\text{rate of energy}\\ \text{into the}\\ \text{control volume}\end{pmatrix} - \begin{pmatrix}\text{rate of energy}\\ \text{out of the}\\ \text{control volume}\end{pmatrix} = \begin{pmatrix}\text{rate of energy}\\ \text{accumulation in}\\ \text{the control volume}\end{pmatrix} \tag{3-35}$$

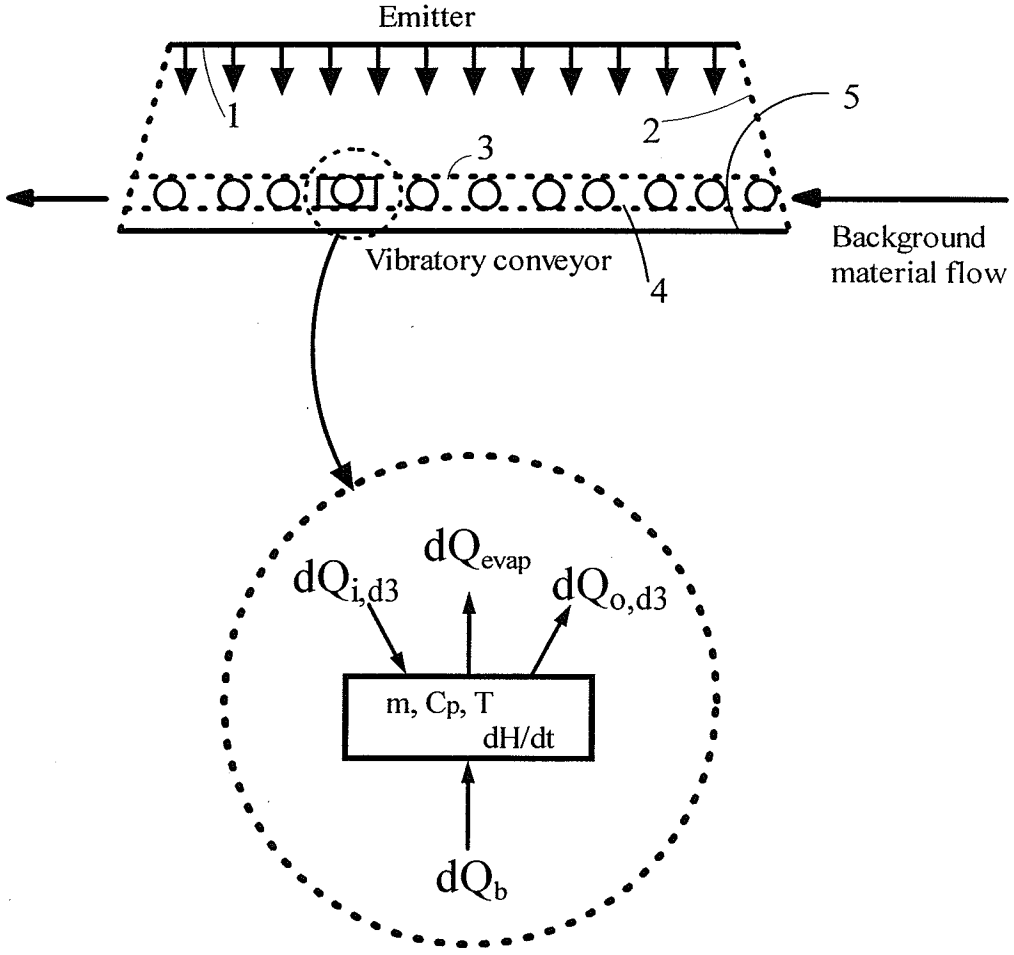

Figure 3.7 Schematic diagram of energy balance on a control volume (fixed-element configuration model).

The enthalpy change of the fixed control volume is expressed as follows:

$$\frac{d}{dt}(H) = \frac{d}{dt}\left(m \cdot C_P \cdot T\right) \tag{3-36}$$

The other energy terms are the same as the terms in the moving element configuration system derived in section 3-3-2, except for the differential element term (dx) which is replaced with the differential time (dt). Therefore, Eq.(3-8), Eq.(3-15), Eq.(3-19), Eq.(3-21), and Eq.(3-36) can be incorporated into the energy balance equation [Eq.(3-35)] which has the same form as Eq.(3-6).

Referring to Figure 3.7, the energy balance gives the following equation.

$$\left[dQ_{i,d3} + dQ_b\right] - \left[dQ_{evap} + dQ_{o,d3}\right] = \frac{dH}{dt} \tag{3-37}$$

By rearranging and incorporating Eq.(3-8), Eq.(3-15), Eq.(3-19), Eq.(3-21) and Eq.(3-36) into Eq.(3-37), we get:

$$\begin{aligned} &\left(\frac{100 \cdot m_d}{100 - M}\right)\left(\frac{dT}{dt}\right)\left[\left(\frac{C_P}{100 - M} + \frac{dC_P}{dM}\right)\frac{dM}{dT}T + C_P - \left(\frac{h_{fg}}{100 - M}\right)\frac{dM}{dT}\right] \\ &= \Phi \cdot W \cdot \varepsilon_S \cdot dx\left[F_{d3-1}\varepsilon_1\sigma T_1^4 + \left(1 - F_{d3-1}\right)\varepsilon_2\sigma T_2^4 - \sigma T^4 + \frac{q_b}{\varepsilon_S}\right] \end{aligned} \tag{3-38}$$

By rearranging Eq.(3-38), we obtain the final equation for the fixed element configuration model as follows:

$$\left(\frac{dT}{dt}\right) = \frac{\Phi \cdot W \cdot \varepsilon_S \cdot dx\left[F_{d3-1}\varepsilon_1\sigma T_1^4 + \left(1-F_{d3-1}\right)\varepsilon_2\sigma T_2^4 - \sigma T^4 + \frac{q_b}{\varepsilon_S}\right]}{\left(\frac{100\cdot m_d}{100-M}\right)\left[\left(\frac{C_P}{100-M}+\frac{dC_P}{dM}\right)\frac{dM}{dT}T + C_P - \left(\frac{h_{fg}}{100-M}\right)\frac{dM}{dT}\right]} \tag{3-39}$$

where,

$$\begin{aligned} q_b &= \frac{\xi_2\left[\left(1-\varepsilon_S\right)\Phi - 1\right] - \varepsilon_5\cdot\xi_1}{1-\Phi\left(1-\varepsilon_S\right)\left(1-\varepsilon_5\right)}, \\ \xi_1 &= \Phi\cdot\varepsilon_S\cdot\sigma\cdot T^4 + \beta, \\ \xi_2 &= -\varepsilon_5\cdot\sigma\cdot T_5^4, \\ \beta &= \left(1-\Phi\right)\left[F_{d3-1}\cdot\varepsilon_1\cdot\sigma\cdot T_1^4 + \left(1-F_{d3-1}\right)\varepsilon_2\cdot\sigma\cdot T_2^4\right] \end{aligned} \tag{3-40}$$

For the increment dx≈Δx, Eq.(3-39) can be rewritten as:

$$\left(\frac{dT}{dt}\right) = \frac{\Phi \cdot W \cdot \varepsilon_S \cdot \Delta x\left[F_{d3-1}\varepsilon_1\sigma T_1^4 + \left(1-F_{d3-1}\right)\varepsilon_2\sigma T_2^4 - \sigma T^4 + \frac{q_b}{\varepsilon_S}\right]}{\left(\frac{100\cdot m_d}{100-M}\right)\left[\left(\frac{C_P}{100-M}+\frac{dC_P}{dM}\right)\frac{dM}{dT}T + C_P - \left(\frac{h_{fg}}{100-M}\right)\frac{dM}{dT}\right]} \tag{3-40a}$$

3-3-3 Special cases : governing equations for constant specific heat

3-3-3-1 Moving-element configuration system

Some simplifications were introduced to the developed mathematical model, constant value of specific heat was assumed for proposed the model [Eq.(3-26)]. The governing equation for a general case (Eq. 3-26) is expressed as follows:

$$\Phi \cdot W \cdot q_{i,d3} + q_b \cdot \Phi \cdot W = \frac{d\dot{H}}{dx} + q_{o,d3} \cdot \Phi \cdot W + h_{fg}\left(-\frac{d\dot{m}}{dx}\right) \tag{3-26}$$

If the specific heat stays constant it will affect the $d\dot{H}/dx$ term. The enthalpy change for the constant specific heat can be expressed as follows:

$$\begin{aligned} \frac{d\dot{H}}{dx} &= \frac{d}{dx}\left(\dot{m} \cdot C_P \cdot T\right) = C_P \frac{d}{dx}\left(\dot{m} \cdot T\right) \\ &= \dot{m} \cdot C_P \frac{dT}{dx} + C_P \cdot T \frac{d\dot{m}}{dx} \end{aligned} \tag{3-26a}$$

From Eq.(3-27) and (3-28), the mass flowrate of the feed and derivative of mass flowrate are:

$$\dot{m} = \dot{m}_d\left(\frac{100}{100 - M}\right) \tag{3-27}$$

$$\frac{d\dot{m}}{dx} = \frac{d}{dx}\left[\dot{m}_d\left(\frac{100}{100 - M}\right)\right] = \frac{100\dot{m}_d}{(100 - M)^2}\left(\frac{dM}{dT}\right)\left(\frac{dT}{dx}\right) \tag{3-28}$$

By putting Eq.(3-27) and (3-28) into Eq.(3-26a), Eq.(3-26a) reduces to:

$$\frac{d\dot{H}}{dx} = \left(\frac{100}{100 - M}\right)\dot{m}_d \cdot C_P \cdot \frac{dT}{dx}\left[1 + \left(\frac{T}{100 - M}\right)\frac{dM}{dT}\right] \tag{3-26b}$$

Now, incorporating Eq.(3-26b) into Eq.(3-26) gives the governing equation which assumes a constant specific heat as follows:

$$\frac{dT}{dx} = \frac{\Phi W \varepsilon_S\left[F_{d3-1} \cdot \varepsilon_1 \cdot \sigma \cdot T_1^4 + (1 - F_{d3-1})\varepsilon_2 \cdot \sigma \cdot T_2^4 - \sigma \cdot T^4 + \frac{q_b}{\varepsilon_S}\right]}{\left(\frac{100\dot{m}_d}{100 - M}\right)\left[C_P + \left(\frac{C_P T - h_{fg}}{100 - M}\right)\frac{dM}{dT}\right]} \tag{3-26c}$$

3-3-3-2 Fixed-element configuration system:

Similarly to the simplified case presented in section 3-3-3-1, in the fixed-element configuration system the assumption of constant specific heat affects the enthalpy term in Eq.(3-37). This equation is introduced into this section one more time for convenience:

$$\left[dQ_{i,d3} + dQ_b\right] - \left[dQ_{evap} + dQ_{o,d3}\right] = \frac{dH}{dt} \tag{3-37}$$

The enthalpy change [Eq.(A2-10), see Appendix II] is expressed as:

$$\frac{dH}{dt} = \left(\frac{100\dot{m}_d}{100 - M}\right)\frac{dT}{dt}\left[C_P + \left(\frac{C_P \cdot T}{100 - M}\right)\frac{dM}{dT}\right] \qquad \text{(A2-10)}$$

By incorporating Eq.(A2-10) and the developed relationships in section 3-3-2-2 into Eq.(3-37), we get the final equation for the constant specific heat of the feed as:

$$\frac{dT}{dt} = \frac{\Phi \cdot W \cdot dx \cdot \varepsilon_S\left[F_{d3-1} \cdot \varepsilon_1 \sigma T_1^4 + \left(1 - F_{d3-1}\right)\varepsilon_2 \cdot \sigma \cdot T_2^4 - \sigma \cdot T^4 + \frac{q_b}{\varepsilon_S}\right]}{\left(\frac{100 \cdot m_d}{100 - M}\right)\left[C_P + \left(\frac{C_P T - h_{fg}}{100 - M}\right)\frac{dM}{dT}\right]} \qquad \text{(3-27c)}$$

3-4 Configuration Factor

In radiation heat transfer, there is a very unique parameter which appears only in radiation heat exchange. This parameter is called a configuration factor which is also known as a view factor, a shape factor, or an angle factor. Configuration factor represents the fraction of radiation energy that arrives at a surface being in direct view with the surface that radiates this energy. In this section, the derivation of a configuration factor for a differential strip viewing a finite area of an IR source that is parallel to the differential strip is presented.

3-4-1 Derivation of the configuration factor

In this work, all the surfaces (material and enclosures) are assumed diffuse-gray, which means that the radiative properties of the surfaces do not depend on the direction and wavelength of infrared rays. There are several mathematical techniques available for determination of the configuration factor such as Hottel's Crossed-String method, Contour Integration method, and the Unit-Sphere method (Modest, 1993). Hottel's Crossed-String method is very useful in determining the

configuration factor when it is related to a 2-dimensional geometry. The Unit-Sphere method was introduced by Wilhelm Nusselt and this method uses a hemisphere of a unit radius to determine the configuration factor. The Contour Integration method gives a very convenient tool for determination of the configuration factor by Stokes' theorem which is used to transform multiple integrations over a surface area to a single curve integration around the boundary of the area. This method is more general than the others. It is applicable to various shapes of geometry and was used in this work to derive the configuration factor for parallel tray-type infrared heaters.

According to Stokes' theorem, the configuration factor from a differential element to a finite area ($F_{d1\text{-}2}$) is expressed in a vector form (Modest, 1993; Özisik, 1973) as follows:

$$F_{d1-2} = \frac{1}{2\pi}\oint_{C_2} \frac{\left(\hat{s}_{12} \times \hat{n}_1\right)\cdot d\hat{s}_2}{S^2} \tag{3-41}$$

where, $\hat{S}_{12}$ is the vector pointing from the elemental surface of dA_1 to a point on the contour of A_2 which is described by vector $\hat{S}_2$ and $d\hat{S}_2$ is a vector pointing along the contour A_2 (Figure 3.8). In the Cartesian coordinate system, the vector form of the configuration factor in Eq.(3-41) is expressed as follows (Siegel and Howell, 1992) and the configuration for the Cartesian coordinate system is shown in Figure 3.9:

$$\begin{aligned} F_{d1\text{-}2} = {} & \frac{\ell_1}{2\pi}\oint_{C_2} \frac{(z_2-z_1)dy_2-(y_2-y_1)dz_2}{S^2} \\ & + \frac{m_1}{2\pi}\oint_{C_2} \frac{(x_2-x_1)dz_2-(z_2-z_1)dx_2}{S^2} \\ & + \frac{n_1}{2\pi}\oint_{C_2} \frac{(y_2-y_1)dx_2-(x_2-x_1)dy_2}{S^2} \end{aligned} \tag{3-42}$$

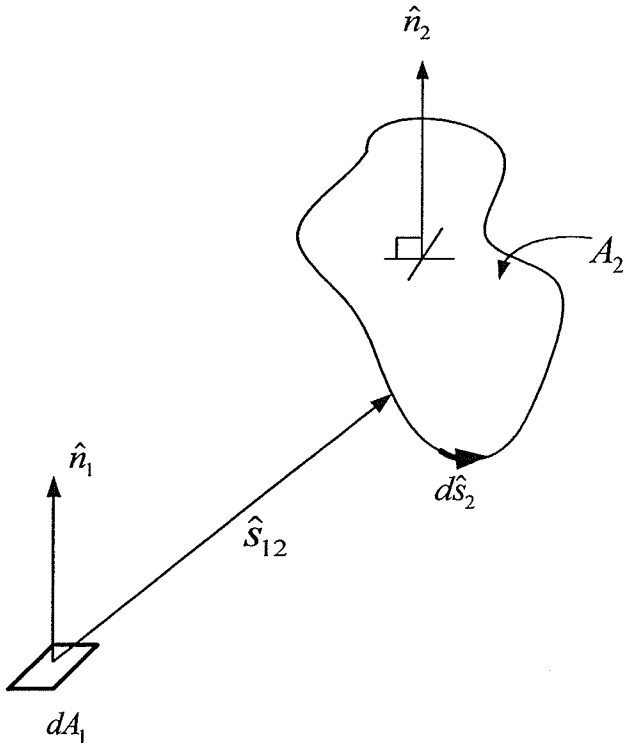

Figure 3.8 Diagram of configuration factor from a differential element to a finite area by Stokes' theorem.

where,

ℓ_1, m_1, n_1
= directional cosines of vector $\hat{n}_1$ with respect to x, y, z- axis in dA_1.

x_1, y_1, z_1 = position coordinates of area dA_1.

x_2, y_2, z_2 = position coordinates of area A_2.

C_2 = boundary of area A_2.

$S^2 = \|\hat{s}_{12}\|^2 = (x_2 - x_1)^2 + (y_2 - y_1)^2 + (z_2 - z_1)^2$

If α_1, γ_1, δ_1 are the angles between the axes (x, y, z) of coordinates and the normal vector of differential element of dA_1, the directional cosines are defined by the angle between the normal vector of dA_1 and the coordinate system. x-axis is the width of the trough, y-axis representing the length of the trough, and z-axis is parallel to the normal axis was shown in Figures 3.9 and 3.10:

$$\ell_1 = \cos \alpha_1,\ m_1 = \cos \gamma_1,\ \text{and}\ \ n_1 = \cos \delta_1 \tag{3-43}$$

For surface areas which are parallel to each other, the directional cosines of the element dA_1 have the following values (Figure 3.10):

$$\begin{aligned} \ell_1 &= \cos \alpha_1 = 0 \ \text{ for } \alpha_1 = 90^\circ \\ m_1 &= \cos \gamma_1 = 0 \text{ for } \gamma_1 = 90^\circ \\ n_1 &= \cos \delta_1 = 1 \ \text{ for } \delta_1 = 0^\circ \end{aligned} \tag{3-44}$$

By substituting the above results for Eq.(3-42), the configuration factor for two parallel trays between the differential element dA_1 and the finite area A_2 (Figure 3.10) can be reduced as follows:

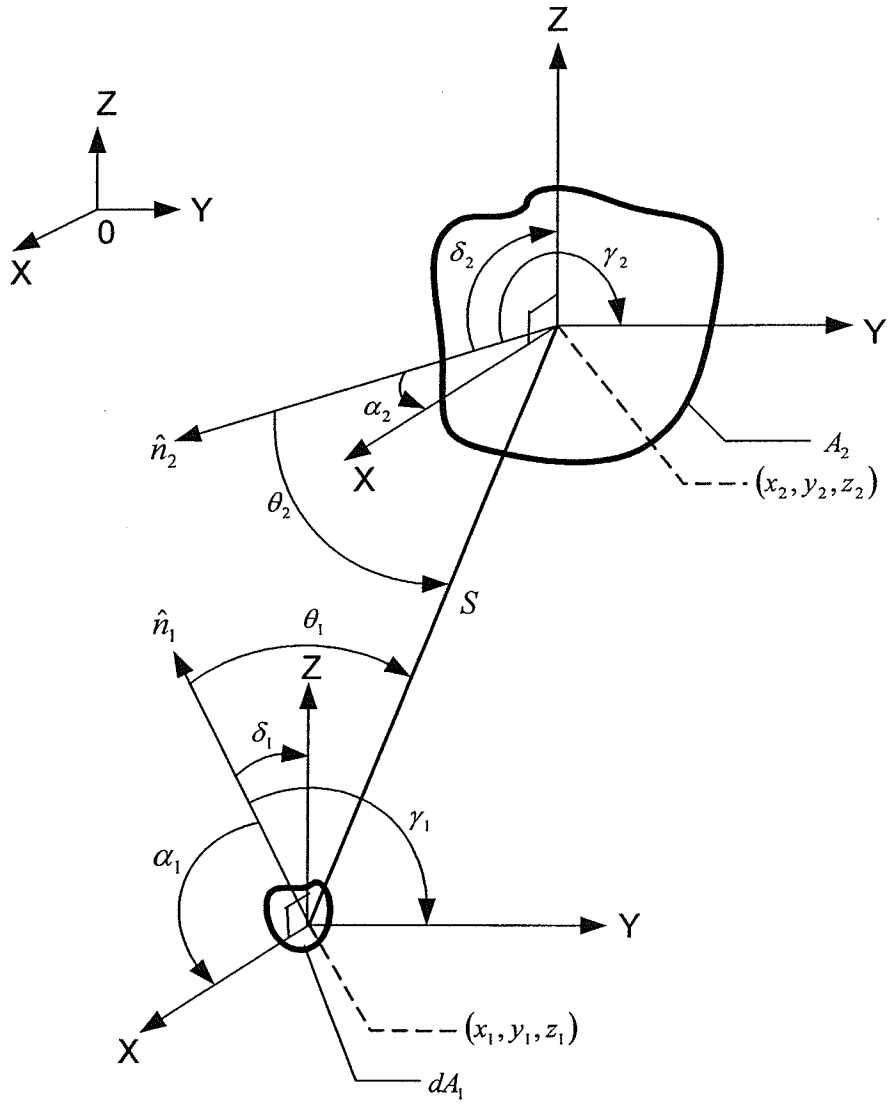

Figure 3.9 Geometry of contour integration for the configuration factor between a differential element and a finite area.

$$F_{d1\text{-}2} = \frac{1}{2\pi}\oint_{C_2}\frac{(y_2\text{-}y_1)\,dx_2 - (x_2\text{-}x_1)\,dy_2}{S^2}$$

$$= \frac{1}{2\pi}\oint_{(I,II,III,IV)}\frac{(y_2\text{-}y_1)\,dx_2 - (x_2\text{-}x_1)\,dy_2}{(x_2\text{-}x_1)^2+(y_2\text{-}y_1)^2+(z_2\text{-}z_1)^2} \qquad (3\text{-}45)$$

$$= \frac{1}{2\pi}\oint_{(I,II,III,IV)}\frac{(y_2\text{-}y_1)\,dx_2 - (x_2\text{-}x_1)\,dy_2}{(x_2\text{-}x_1)^2+(y_2\text{-}y_1)^2+H^2}$$

where,

$z_2\text{-}z_1=H$,

I, II, III, IV = boundary sections of A_2 (Figure 3.10).

When considering the model, the control volume was selected by a differential strip. Therefore, the configuration factor [Eq.(3-46)] should be chosen from a differential strip of control volume to a finite area of the emitter and it is obtained by integrating Eq.(3-45) for the entire width of the bottom trough and dividing by the width of the trough. The configuration factor from strip 1 to A_2 ($F_{dstrip1\text{-}2}$; Figure 3.10) can be expressed as follows:

$$F_{dstrip1\text{-}2} = \frac{1}{(b_1\text{-}a_1)}\int_{a_1}^{b_1} F_{d1\text{-}2}\;dx_1, \qquad (3\text{-}46)$$

where, $(b_1\text{-}a_1) = W =$ width of the trough.

The configuration factor $F_{dstrip1\text{-}2}$ is equivalent to the configuration factor $F_{d3\text{-}1}$ which is used in the governing equation of the model [Eq.(3-30) and Eq.(3-39) in Chapter 3]. The boundary of the emitter surface (area A_2) consists of boundary I, II, III, and IV shown in Figure 3.10 and the configuration factor $F_{d1\text{-}2}$ can be obtained by the summation of each boundary section of A_2 of rectangular shape. For the emitter of a rectangular shape, the boundary can be separated into four sections shown in Figure 3.10 and each boundary section can be integrated with some intervals of

variables as follows. The symbols a_i, b_i, c_i, and d_i in the equations of boundary conditions denote lower and upper limits for the line integrations and have the physical meaning of the dimension of the emitter. The subscript 1 and 2 denotes the variables in the trough A_1 and in the emitter A_2, respectively (Figure 3.10):

(i) Boundary I:

boundary conditions:

$$y_2=d_2,\ dy_2=0$$
$$a_2 \le x_2 \le b_2,\ dx_2 \neq 0$$

$$F_{d1\text{-}2}^{I} = \frac{1}{2\pi}\int_{a_2}^{b_2} \frac{(y_2\text{-}y_1)dx_2\text{-}(x_2\text{-}x_1)dy_2}{(x_2\text{-}x_1)^2+(y_2\text{-}y_1)^2+H^2} = \frac{1}{2\pi}\int_{a_2}^{b_2} \frac{(d_2\text{-}y_1)dx_2}{(x_2\text{-}x_1)^2+(d_2\text{-}y_1)^2+H^2} \tag{3-47}$$

(ii) Boundary II:

boundary conditions:

$$x_2=b_2,\ dx_2=0$$
$$c_2 \le y_2 \le d_2,\ \ dy_2 \neq 0$$

$$F_{d1\text{-}2}^{II} = \frac{1}{2\pi}\int_{d_2}^{c_2} \frac{(y_2\text{-}y_1)dx_2\text{-}(x_2\text{-}x_1)dy_2}{(x_2\text{-}x_1)^2+(y_2\text{-}y_1)^2+H^2} = \frac{1}{2\pi}\int_{d_2}^{c_2} \frac{-(x_2\text{-}x_1)dy_2}{(x_2\text{-}x_1)^2+(y_2\text{-}y_1)^2+H^2}$$
$$= \frac{1}{2\pi}\int_{c_2}^{d_2} \frac{(b_2\text{-}x_1)dy_2}{(b_2\text{-}x_1)^2+(y_2\text{-}y_1)^2+H^2} \tag{3-48}$$

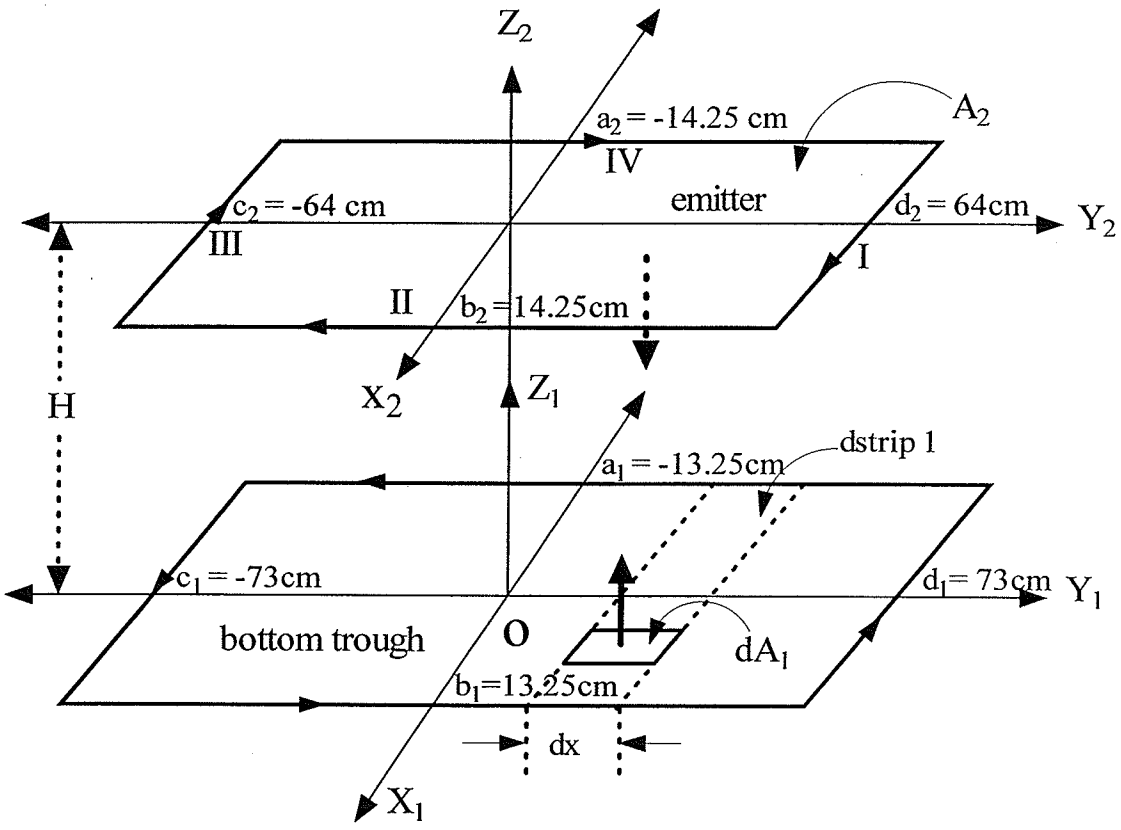

Figure 3.10 Schematic diagram of configuration factor between two parallel trays.

(iii) Boundary III:

boundary conditions:

$$y_2=c_2,\ dy_2=0$$
$$a_2 \le x_2 \le b_2,\quad dx_2 \ne 0$$

$$F_{d1\text{-}2}^{III}=\frac{1}{2\pi}\int_{b_2}^{a_2}\frac{(y_2-y_1)dx_2-(x_2-x_1)dy_2}{(x_2-x_1)^2+(y_2-y_1)^2+H^2}=\frac{1}{2\pi}\int_{a_2}^{b_2}\frac{-(c_2-y_1)dx_2}{(x_2-x_1)^2+(c_2-y_1)^2+H^2} \tag{3-49}$$

(iv) Boundary IV:

boundary conditions:

$$x_2=a_2,\quad dx_2=0$$
$$c_2 \le y_2 \le d_2,\ dy_2 \ne 0$$

$$F_{d1\text{-}2}^{IV}=\frac{1}{2\pi}\int_{c_2}^{d_2}\frac{(y_2-y_1)dx_2-(x_2-x_1)dy_2}{(x_2-x_1)^2+(y_2-y_1)^2+H^2}=\frac{1}{2\pi}\int_{c_2}^{d_2}\frac{-(x_2-x_1)dy_2}{(x_2-x_1)^2+(y_2-y_1)^2+H^2}$$
$$=\frac{1}{2\pi}\int_{c_2}^{d_2}\frac{-(a_2-x_1)dy_2}{(a_2-x_1)^2+(y_2-y_1)^2+H^2} \tag{3-50}$$

where,

$F_{d1\text{-}2}^{I}$, $F_{d1\text{-}2}^{II}$, $F_{d1\text{-}2}^{III}$, and $F_{d1\text{-}2}^{IV}$

= configuration factor for each boundary section from dA_1 to A_2.

The summation of the above integrations from Eq.(3-47) to (3-50) represents the configuration factor from area dA_1 to A_2 in Figure 3.10 and is shown in Eq.(3-51):

$$\begin{aligned} F_{d1\text{-}2} &= F^{I}_{d1\text{-}2} + F^{II}_{d1\text{-}2} + F^{III}_{d1\text{-}2} + F^{IV}_{d1\text{-}2} \\ &= \frac{1}{2\pi}\int_{a_2}^{b_2}\frac{(d_2-y_1)dx_2}{(x_2-x_1)^2+(d_2-y_1)^2+H^2} + \frac{1}{2\pi}\int_{c_2}^{d_2}\frac{(b_2-x_1)dy_2}{(b_2-x_1)^2+(y_2-y_1)^2+H^2} \\ &+ \frac{1}{2\pi}\int_{a_2}^{b_2}\frac{-(c_2-y_1)dx_2}{(x_2-x_1)^2+(c_2-y_1)^2+H^2} + \frac{1}{2\pi}\int_{c_2}^{d_2}\frac{-(a_2-x_1)dy_2}{(a_2-x_1)^2+(y_2-y_1)^2+H^2} \end{aligned} \tag{3-51}$$

By integrating Equation (3-51) over the entire width of the trough and averaging the result, the desired configuration factor $F_{dstrip1\text{-}2}$ is expressed as Eq.(3-52).

$$\begin{aligned} F_{dstrip1\text{-}2} &= \frac{1}{(b_1-a_1)}\int_{a_1}^{b_1} F_{d1\text{-}2}\ dx_1 = \frac{1}{(b_1-a_1)}\int_{a_1}^{b_1}\left(F^{I}_{d1\text{-}2}+F^{II}_{d1\text{-}2}+F^{III}_{d1\text{-}2}+F^{IV}_{d1\text{-}2}\right)\ dx_1 \\ &= \frac{1}{2\pi(b_1-a_1)}\int_{a_1}^{b_1}\int_{a_2}^{b_2}\frac{(d_2-y_1)\cdot dx_2dx_1}{(x_2-x_1)^2+(d_2-y_1)^2+H^2} + \frac{1}{2\pi(b_1-a_1)}\int_{a_1}^{b_1}\int_{c_2}^{d_2}\frac{(b_2-x_1)\cdot dy_2dx_1}{(b_2-x_1)^2+(y_2-y_1)^2+H^2} \\ &+ \frac{1}{2\pi(b_1-a_1)}\int_{a_1}^{b_1}\int_{a_2}^{b_2}\frac{-(c_2-y_1)\cdot dx_2dx_1}{(x_2-x_1)^2+(c_2-y_1)^2+H^2} + \frac{1}{2\pi(b_1-a_1)}\int_{a_1}^{b_1}\int_{c_2}^{d_2}\frac{-(a_2-x_1)\cdot dy_2dx_1}{(a_2-x_1)^2+(y_2-y_1)^2+H^2} \end{aligned} \tag{3-52}$$

The final expression of the configuration factor is expressed as Eq.(3-52) and it consists of four terms of double integrations. It is difficult to obtain an analytical solution for this integration. To solve this integration numerically, Gauss-Quadrature numerical method was used and is presented in the following section.

3-4-2 Numerical formulation of the configuration factor

Eq. (3-52) is difficult to solve analytically, therefore this double integration will be solved by a numerical method. For simplicity and accuracy of the four double integrals, the number of sampling

points were extended from 5 points to 20 points of Gauss-Quadrature (Chapra and Canale, 1989; Stroud and Secrest, 1966). Double integration of a function f(x,y) can be approximated between the lower limit of "-1" and the upper limit of "+1" as follows:

$$\int_{-1}^{1}\int_{-1}^{1} f(x,y)\,dxdy = \sum_{i=1}^{N}\sum_{j=1}^{N} w_i \cdot w_j \cdot f(x_i,y_j) \tag{3-53}$$

where,

w_i, w_j = weighting factors (or weights),

N = number of sampling points,

x_i, y_j = sampling points.

To use Gauss-Quadrature method, the upper and lower limit of the integration should have +1 and -1. For this reason, the derived configuration factor integration should be transformed to a proper form to get the upper and lower limit value of +1 and -1. The procedure is shown below. In boundary I as shown in Figure (3-10) (the first component on the right hand side of Eq.(3-52)), the configuration factor can be expressed as follows:

$$\begin{aligned} F^{I}_{dstrip1\text{-}2} &= \frac{1}{2\pi(b_1 - a_1)}\int_{a_1}^{b_1}\int_{a_2}^{b_2}\frac{(d_2 - y_1)dx_2dx_1}{(x_2 - x_1) + (d_2 - y_1) + H^2} \\ &= \frac{1}{2\pi(b_1 - a_1)}\int_{-1}^{1}\int_{-1}^{1} f_1(X_1,X_2,y_1)dX_2dX_1 \end{aligned} \tag{3-54}$$

The upper and lower limits of integration of the original integral can be converted to the upper limit of +1 and the lower limit of -1 by using the following linear transformation:

$$x_1=g_1(X_1)=\frac{1}{2}\left[(b_1+a_1)+(b_1-a_1)X_1\right],\ b_1\geq a_1$$
$$x_2=g_2(X_2)=\frac{1}{2}\left[(b_2+a_2)+(b_2-a_2)X_2\right],\ b_2\geq a_2 \tag{3-55}$$

and

$$\begin{aligned} &x_1=a_1\ at\ X_1=-1,\ \text{and}\ x_1=b_1\ at\ X_1=1,\\ &dx_1=\frac{1}{2}(b_1-a_1)dX_1\ ,\\ &x_2=a_2\ at\ X_2=-1,\ \text{and}\ x_2=b_2\ at\ X_2=1,\\ &dx_2=\frac{1}{2}(b_2-a_2)dX_2 \end{aligned} \tag{3-56}$$

By using the linear transformation shown above, the configuration factor can be converted to the form of Gauss-Quadrature integration as follows:

$$\begin{aligned} F^{I}_{dstrip1\text{-}2}&=\frac{1}{2\pi(b_1-a_1)}\int_{a_1}^{b_1}\int_{a_2}^{b_2}\frac{(d_2-y_1)\,dx_2dx_1}{(x_2-x_1)^2+(d_2-y_1)^2+H^2}\\ &=\frac{1}{2\pi(b_1-a_1)}\int_{-1}^{1}\int_{-1}^{1}f_1(X_1,X_2,y_1)\,dX_2dX_1\\ &=\frac{1}{2\pi(b_1-a_1)}\sum_{i=1}^{N}\sum_{j=1}^{N}w_i\cdot w_j\cdot f_1(X_{1i},X_{2j},y_1) \end{aligned} \tag{3-57}$$

where,

$$f_1(X_1,X_2,y_1)=\frac{(b_1-a_1)(b_2-a_2)(d_2-y_1)}{4\left[(x_2-x_1)^2+(d_2-y_1)^2+H^2\right]},$$

$$x_1=g_1(X_1)=\frac{1}{2}\left[(b_1+a_1)+(b_1-a_1)X_1\right],$$

$$x_2=g_2(X_2)=\frac{1}{2}\left[(b_2+a_2)+(b_2-a_2)X_2\right],$$

X_{1i}, X_{2j} = sampling points for X_1 and X_2, respectively,

w_i, w_j = weighting factors.

By the same manipulation, the other configuration factors for the Boundary II (the right hand side of Eq.(3-52)) are:

$$\begin{aligned} F^{II}_{dstrip1-2} &= \frac{1}{2\pi(b_1-a_1)}\int_{-1}^{1}\int_{-1}^{1} f_2(X_1,Y_2,y_1)\,dY_2\,dX_1 \\ &= \frac{1}{2\pi(b_1-a_1)}\sum_{i=1}^{N}\sum_{j=1}^{N} w_i\cdot w_j\cdot f_2(X_{1i},Y_{2j},y_1) \end{aligned} \tag{3-58}$$

where,

$$f_2(X_1,Y_2,y_1)=\frac{(d_2-c_2)(b_1-a_1)(b_2-x_1)}{4\left[(b_2-x_1)^2+(y_2-y_1)^2+H^2\right]},$$

$$y_2=g_3(Y_2)=\frac{1}{2}\left[(d_2+c_2)+(d_2-c_2)Y_2\right],$$

$x_1=g_1(X_1)$,

X_{1i}, Y_{2j} = sampling points for X_1 and Y_2, respectively.

The same as the above solution is applicable for boundary III from the strip 1 to A_2:

$$F^{III}_{dstrip1-2} = \frac{1}{2\pi(b_1 - a_1)} \int_{-1}^{1}\int_{-1}^{1} f_3(X_1, X_2, y_1)\,dX_2\,dX_1$$
$$= \frac{1}{2\pi(b_1 - a_1)} \sum_{i=1}^{N}\sum_{j=1}^{N} w_i \cdot w_j \cdot f_3(X_{1i}, X_{2j}, y_1) \qquad (3\text{-}59)$$

where,

$$f_3(X_1, X_2, y_1) = -\frac{(c_2 - y_1)(b_2 - a_2)(b_1 - a_1)}{4\left[(x_2 - x_1)^2 + (c_2 - y_1)^2 + H^2\right]} \quad ,$$

$x_1 = g_1(X_1)$ and $x_2 = g_2(X_2)$.

For boundary IV,

$$F^{IV}_{dstrip1-2} = \frac{1}{2\pi(b_1 - a_1)} \int_{-1}^{1}\int_{-1}^{1} f_4(X_1, Y_2, y_1)\,dY_2\,dX_1 \quad ,$$
$$= \frac{1}{2\pi(b_1 - a_1)} \sum_{i=1}^{N}\sum_{j=1}^{N} w_i \cdot w_j \cdot f_4(X_{1i}, Y_{2j}, y_1) \qquad (3\text{-}60)$$

where,

$$f_4(X_1, Y_2, y_1) = \frac{-(d_2 - c_2)(b_1 - a_1)(a_2 - x_1)}{4\left[(a_2 - x_1)^2 + (y_2 - y_1)^2 + H^2\right]} \quad ,$$

$y_2 = g_3(Y_2)$

X_{1i}, Y_{2j} = sampling points.

3-5 Summary of the Chapter

In this chapter, a comprehensive description of the derivation of the mathematical models for IR processing of granular material (yellow peas in this study) using a parallel tray-type micronizer has been presented. The models were developed using the concept of net-radiation with the assumptions of the material having diffuse-gray surfaces. These models are general and can be used for any granular products whose physical properties have been defined. A coverage factor (Φ) was introduced to account for the change in the IR heat intensity due to the movement of the feed material. The mathematical models are in the form of a first order non-linear differential equation.

CHAPTER 4

EQUIPMENT AND EXPERIMENTAL METHODS

To investigate the change in temperature and moisture content of yellow peas under infrared processing, a laboratory scale infrared heating system (IR heater or micronizer), manufactured by Micronizing Company Ltd. UK, was used. This chapter describes the configuration of the lab-scale micronizer system as well as the function and characteristics of its major parts, followed by a description of experimental methods, materials and instruments for data acquisition used in this study.

4-1 Laboratory Scale Infrared Heating (Micronization) System

4-1-1 Configuration of the micronizer

The infrared heating system (micronizer) used in this research is shown in Figure 4.1a and 4.1b. The gas-fired micronizer uses natural gas and has a minumum heat energy of 31.6 kJ and 100 kJ in the maximum nominal power. This unit consists of three principal elements: (1) four gas-fired infrared heaters and air-gas mixing system with a combustion air fan: (2) a feeding system with a hopper which consists of a vibrating feeder and a vibrating conveyor: (3) a control panel for the slope adjustment of the vibratory conveyor and the vibratory feeder frequency. This gas-fired micronizer (model MR2, Micronizing Company Ltd., UK) consists of two parallel trays, top and bottom.

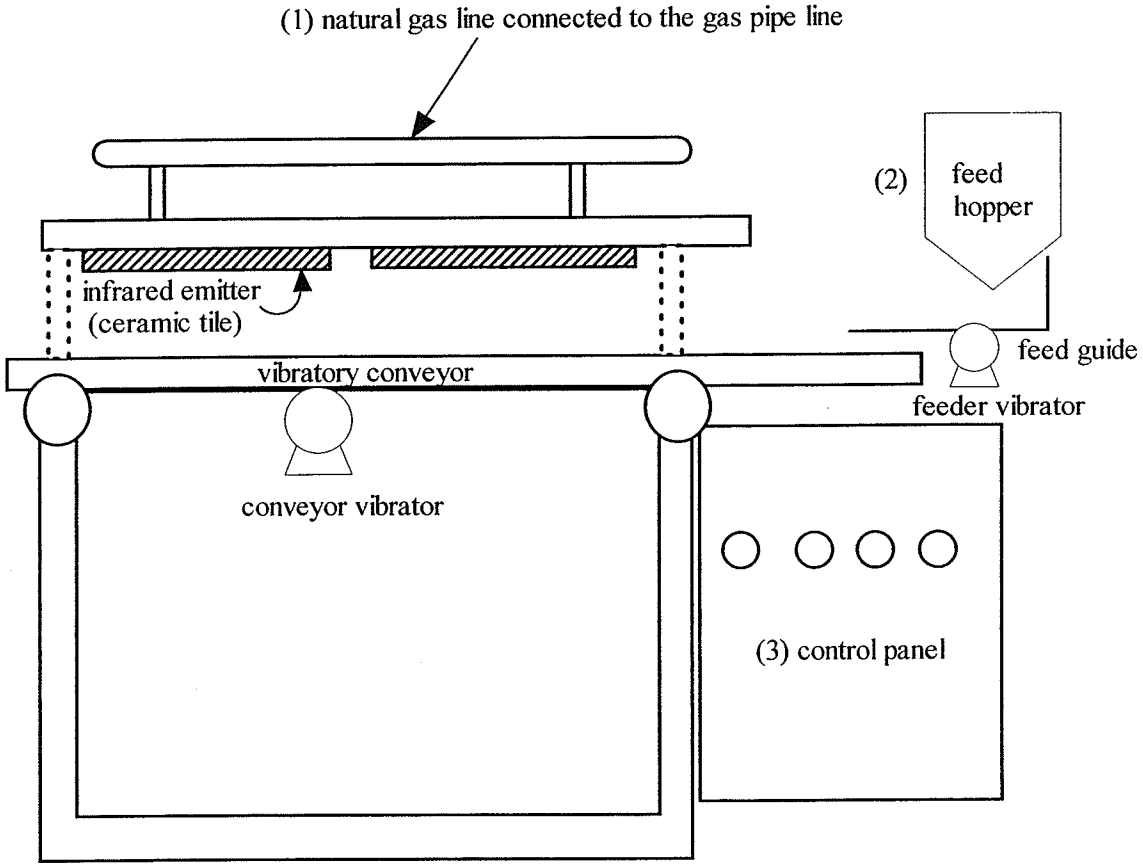

Figure 4.1a Schematic diagram of a lab scale gas-fired infrared heater (micronizer; model MR2, Micronizing Company Ltd., UK).

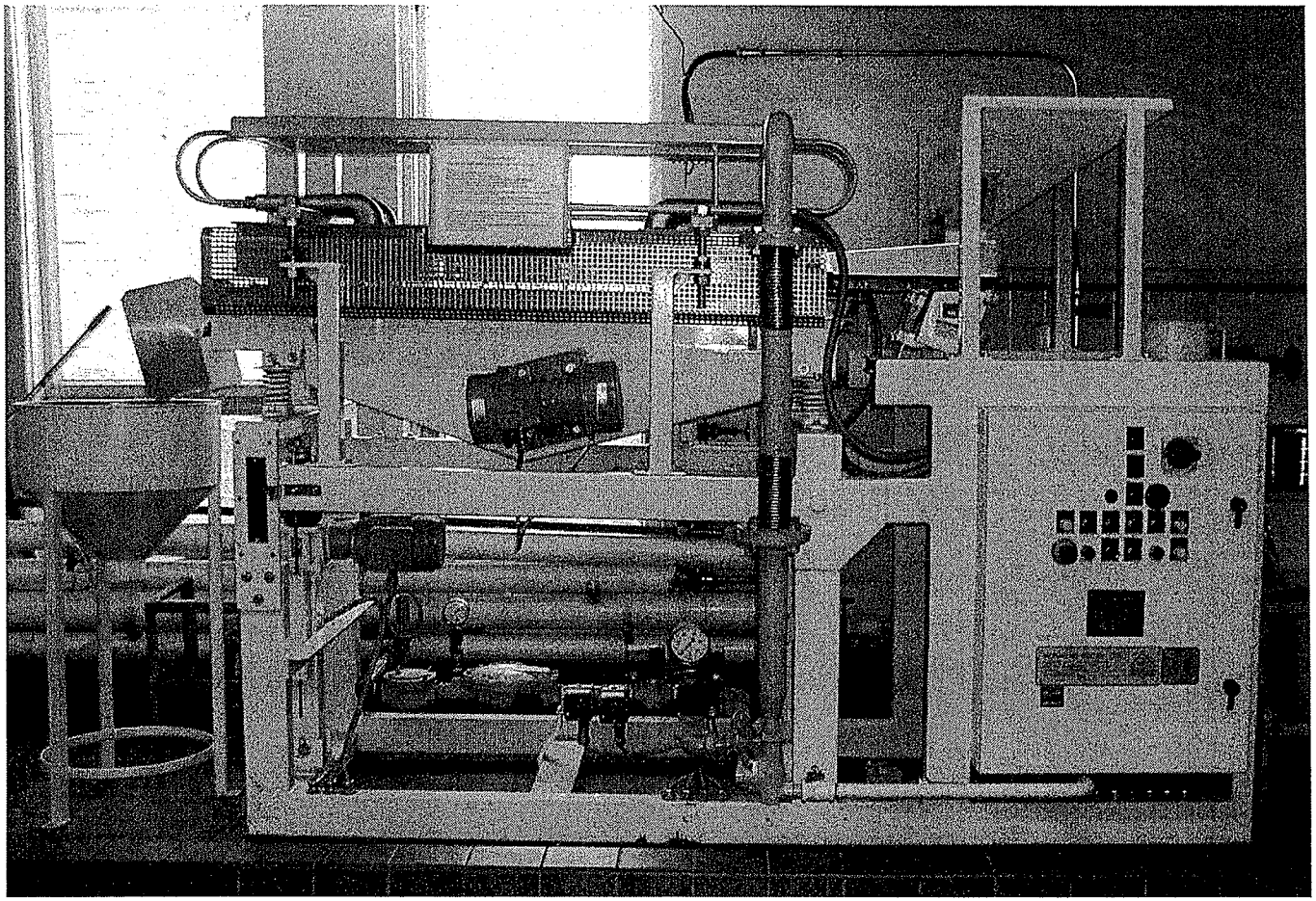

Figure 4.1b Lab-scale gas-fired infrared heater (micronizer; model MR2, Micronizing Company Ltd., UK).

4-1-2 Description of the data acquisition system

For data recording, a 'Multiscan1200' (Omega Engineering Inc., P.O. Box 2669, Stamford, CT 06906, USA) data acquisition system was used to record the temperatures of the enclosure surfaces which were described in Chapter 3. The enclosure surfaces include the surface of the infrared emitter, the bottom trough, ambient air surface which encloses the side of the micronizer and the surface of feed material. The data were acquired every 2 s and the surface temperatures were acquired through K-type thermocouple wires (model; HH-K-type 24, Omega Engineering Inc.) to the computer system. The IR processing system in this experiment generates high temperatures. For this reason, K-type thermocouples were selected for the experiments. A brief overview of the system showing thermocouple locations is given in Figure 4.2.

4-1-3 Operating Conditions

The operating conditions of the micronizer can be adjustable with the switches in the control panel of the micronizer. To control the mass flowrate of the feed (yellow peas), the slope of the trough was set to zero position of the scale and the vibratory feeder was set to 60 of the scale. For the natural gas flow rate control, the valve of the natural gas was set to 9. To get constant infrared heat intensity from the emitter to the feed product, the separation distance of infrared emitters to the feed was fixed to 12 cm and this distance affects the IR intensity at the surface of the feed from the emitter.

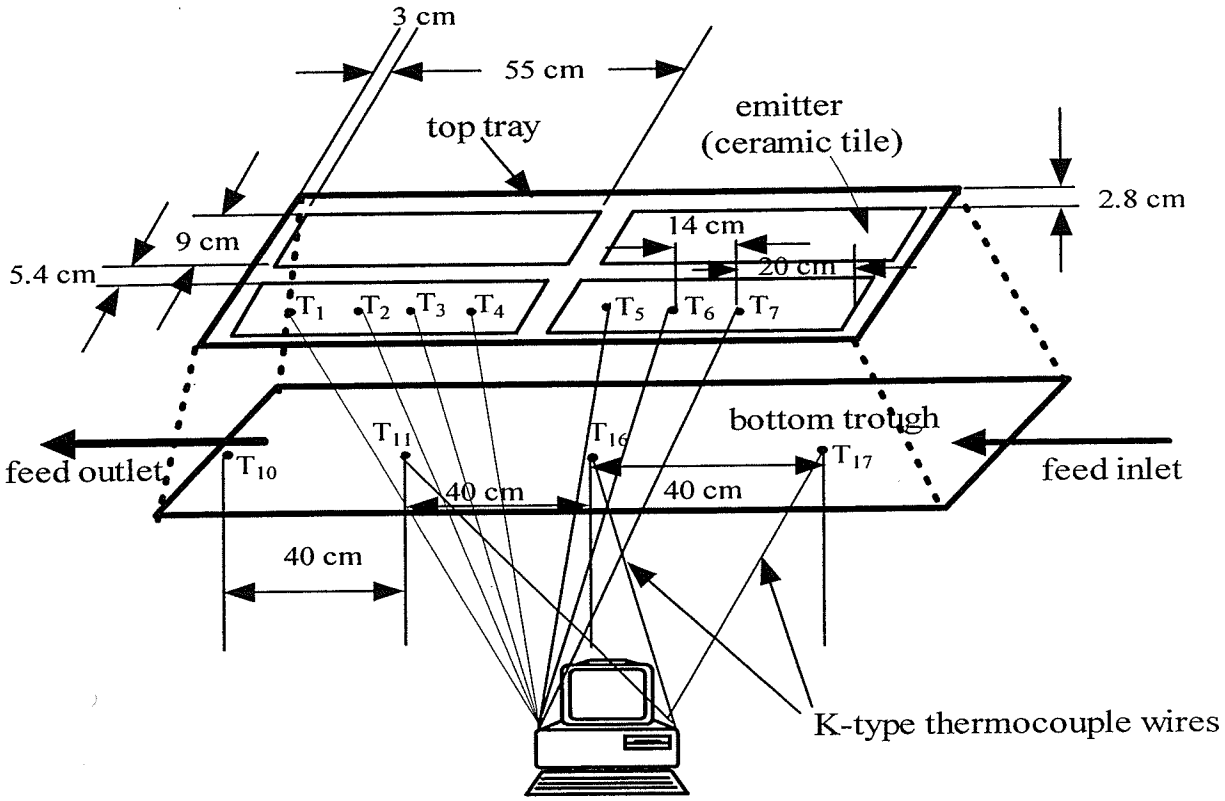

Figure 4.2 Schematic diagram of thermocouple points connected to the data acquisition system.

4-2 Experimental Methods

4-2-1 Sample preparation

In this study, whole yellow peas were used as a test product. The peas were purchased from 'Roy Legumex of Landmark Ltd. (Manitoba)'. The moisture content of the raw peas was required to prepare enough amount of bulk pea samples of desired moisture content for the continuous IR processing. The moisture content of raw yellow peas was in the range of 10 - 13%. The moisture content was determined by the AACC two-stage standard method (AACC, 1995). After obtaining the moisture content of the raw yellow peas, the raw bulk peas of 15 to 25 kg were tempered with distilled water to get a desired initial moisture content of 20 to 30% for the experiments. For the tempering, 15 to 25 kg of raw yellow peas were placed in a rotating mixer [model Big Cat (type B), Redlion, Canada] and the appropriate amount of distilled water was added to the mixer. The opening of the mixer was covered with a plastic bag and sealed tightly with elastic strings to prevent moisture escaping into the air. Then the mixer was kept rotating for 10 to 16 h to get uniform equilibration of moisture in all samples used in each experiment. The amount of water to be added to the raw yellow peas was calculated by Eq.(4-1) (Arntfield et al., 1998) which was derived from a mass balance of water and the peas.

$$W_{add} = \frac{m_t\left(M_t\text{-}M_i\right)}{\left(100\text{-}M_t\right)} \tag{4-1}$$

where,

m_t = total mass of raw yellow peas, (kg)

M_i = moisture content of raw yellow peas, (% wb)

M_t = target moisture content of yellow peas, (% wb)

W_{add} = amount of water to be added, (kg)

4-2-2 Micronization processing and sample collection

Two types of experiments were performed in this study: i) a fixed-element configuration (FEC) and ii) a moving-element configuration (MEC). In the fixed-element configuration, the test samples were contained in a small cage made of steel, which had an open top so that the peas could be irradiated by the emitter. In the FEC the cage was placed on the vibratory conveyor at a distance of 40 cm from the end of the trough. This location has a configuration factor of 0.67. The yellow peas were processed in 30, 60, 90, 120, 150, and 180 s, respectively. The processed peas of each run were collected in individual plastic containers sealed with a plastic lid and cooled down to room temperature. After that, the moisture content of the processed peas was determined by a standard two-stage air-oven drying method (AACC, 1995). During FEC processing, tempered peas were flowing on the vibratory conveyor as background materials to simulate real processing conditions. In the moving-element configuration, an aluminum trough (insert) which had the same dimensions (same width, same length and depth) as the vibratory conveyor was devised and was used for sampling . The 1 mm thick aluminum insert was attached to the vibratory conveyor with C-clamps. The aluminum insert was pulled out of the micronizer at the end of each MEC processing, and the samples at marked positions on the insert were collected into the plastic containers that were sealed with plastic lids. The moisture content was determined in the same way as in the FEC experiments.

4-2-3 Temperature measurement

To validate the mathematical models, temperatures of the feed samples, emitters, and reflecting enclosure surfaces (Figure 3.4 in Chapter 3) which participate in the heat exchange through radiative heat transfer with the feed samples must be measured. The equation to predict the temperature history of the processed peas along the trough requires information on the surface temperature of the

IR emitter (Figure 3.4 in Chapter 3). This enclosure consists of the emitter (heated ceramic tiles), the bottom trough (vibratory conveyor), the enclosed open area between the emitter and the trough, and the surface of the layer of moving peas (Figure 3.4). The end tips of the thermocouple wires to measure the temperature were attached onto the surfaces of each tray (the emitter and the bottom trough) and inserted into some of the peas. The peas with inserted thermocouples were attached to a movable wooden support and placed at the inlet position on the bottom trough (Figure 4.3). Then the wooden support with peas was pulled by rewinding rod operated by a motor which was connected to an adjustable power supply (Model 1711, BK precision, Placentia, CA). The speed of the motor was set at an average speed of bulk peas. During IR processing, the temperature of each enclosure surface was also recorded by the data acquisition system. Each experiment was performed after 30 min of a warm-up period of the micronizer to reach stable temperatures of micronizer surfaces (the emitter and the bottom trough).

4-2-4 Determination of the moisture gradient

During infrared processing, the moisture content of the peas decreases and the temperature of the materials increases as the peas pass along the bottom trough. Due to this reason, the moisture change of peas per temperature change (dM/dT) has a negative value. The moisture-temperature gradient (dM/dT) can be evaluated in two steps as follows:

As a first step, the changes of moisture content and temperature change of the material with processing time, dM/dt and dT/dt are evaluated. After that, the moisture content change with time is divided by the temperature change with time as follows.

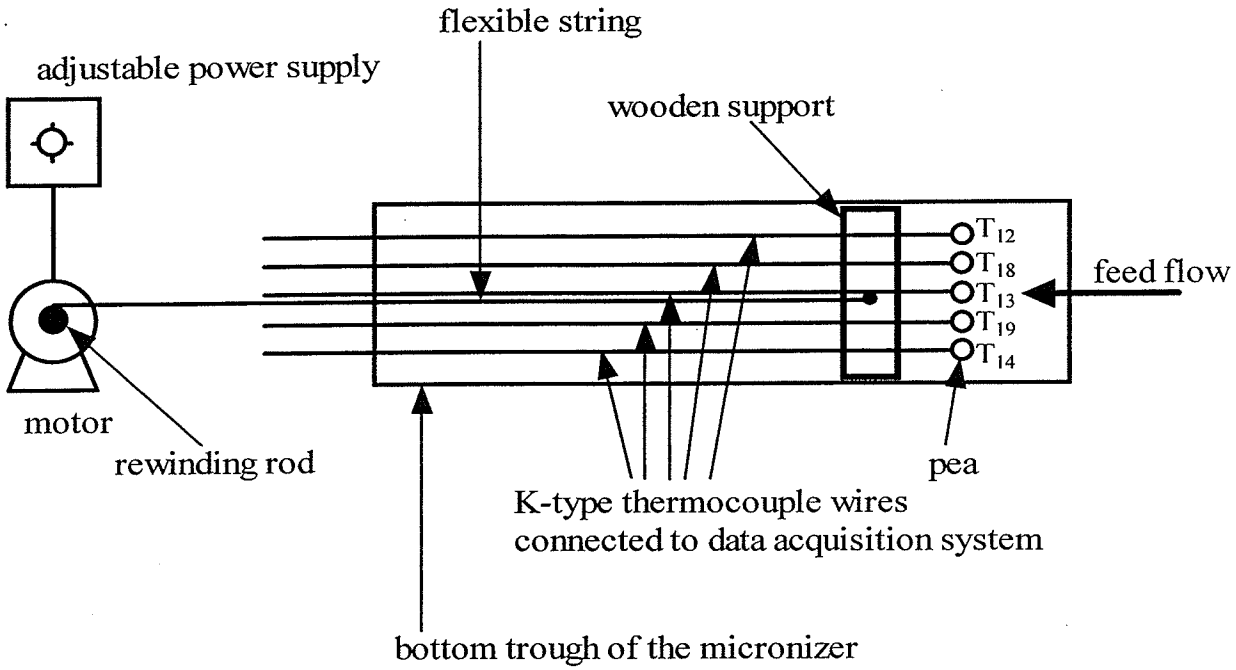

Figure 4.3 The wooden support for the temperature measurement of peas for the moving-element configuration system.

$$\frac{dM}{dT} = \left(\frac{dM}{dt}\right) \Big/ \left(\frac{dT}{dt}\right) \qquad (4\text{-}2)$$

where,

M = moisture content of peas, (% wb)

T = temperature of peas, (K)

t = IR processing time, (s)

This moisture gradient, dM/dT, from the experimental data can be expressed as a function of time for the fixed-element configuration model or as a function of distance along the bottom trough for the moving-element configuration model for a continuous process.

4-2-5 Determination of coverage

To deal with the particle type bulk material as a continuum, a coverage factor, Φ, was intorduced and it is defined by the ratio of the projected area of the peas on the bottom trough over the area of the bottom trough during micronization. This parameter was introduced with the assumption that the trough is covered with a single layer of processed peas as a continuum. As frequently seen in the paper industry, the wetted sheet paper in IR drying is considered as a continuum, therefore it's easy to develop a mathematical model of IR drying (Kuang et al, 1994). On the contrary, biological materials such as peas or grains in food processing by micronization are single-layered discrete elements and it is easier to be considered as a continuum. The coverage is expressed by the following equation as shown in Chapter 3.

$$\Phi = \frac{A_S}{A_5} = \frac{dA_S}{dA_5} = \text{constant} \tag{4-3}$$

where,

A_S= projected area of the pea which covered the bottom trough, (m^2)

A_5= area of the bottom trough of the micronizer, (m^2)

After running the experiment with the aluminum trough, the micronizer was stopped and the tray was pulled out of the micronizer. The peas on the aluminum trough were gathered into a densely packed single-layer and the area covered by the material was measured.

4-2-6 Measurement of mass flowrate

During IR processing, the test material undergoes a change in mass due to moisture evaporation from the materials into the air. This is caused by radiative heat from the IR source to the feed and this heat makes the moisture of the peas evaporate. Although the mass of the peas changes during IR processing, the mass flowrate of the solid content of the peas is assumed constant during the steady-state IR processing if evaporation of other components of the material can be neglected. If the moisture content in wet basis and mass flowrate in wet basis at any location on the vibrating conveyor is known, the dry mass flowrate is calculated by the following relationship:

$$\dot{m}_d = \dot{m}\left(\frac{100 - M}{100}\right) \tag{4-4}$$

where,

M = moisture content of the peas in wet basis, (% wb)

$\dot{m}_d$= mass flowrate of the peas in dry basis, $\left(\text{kg solid/s}\right)$

$\dot{m}$ = mass flowrate of the peas in wet basis, $\left(\text{kg/s}\right)$

In Eq.(4-4), the mass flowrate in wet basis can be determined at any position on the vibratory conveyor by sampling the processed peas in that location. In this study, the mass flowrate in wet basis was measured at the exit of the micronizer trough for the convenience of sampling for 1 or 2 min interval.

4-2-7 Measurement of residence time

The dynamic behaviour of the feed material on the bottom trough is quite irregular, bouncing forwards and backwards along the trough. This is the characteristic of spherical shape of biological materials on a vibratory conveyor. The residence time of the peas which travel along the bottom trough was measured by using black painted peas and a stopwatch. The painted peas were dropped at the inlet location of the trough and the travelling time of the painted peas to pass the bottom trough were measured. The total length of the trough was 146 cm. The residence time was calculated by dividing the total length of the trough by the travelling time of the marked peas which was measured and was averaged. The averaged residence time was used to evaluate average velocity for the peas under a given operating condition.

$$v_{av} = \frac{L}{t_{R,av}} \tag{4-5}$$

where,

v_{av} = average travelling velocity of peas, $(\mathrm{m/s})$

L = length of the vibratory conveyor, (m)

$t_{R,av}$ = average residence time, (s)

The average travelling velocity of the pea was used as a conversion factor to convert processing time to the location of the peas at a given time for the proposed model.

CHAPTER 5

EXPERIMENTAL RESULTS

To validate the proposed mathematical models in Chapter 3, a series of experiments using a lab-scale micronizer was performed to provide the information for practical applications. The results are described in this chapter and include the temperature of the emitter surface, moisture content changes and temperature history of the test materials during micronization, coverage of the material, and residence time of the material during IR processing.

5-1 Emitting Surface Temperature

In IR processing of biological materials, the surface temperature of the emitter is one of the most important variables to understand the physical phenomena of radiative heat transfer in gas-fired IR units (Ratti and Mujumdar, 1995). In this study, a series of experiments were conducted to measure the surface temperatures of the emitters in the gas micronizer. Nine experiments were conducted. The temperature of the emitter surface was measured at seven locations and the results were averaged. After the micronizer is fired-up, the surface temperature of the emitters becomes stable and reaches a constant level after approximately 20 min of a warm-up period. Figure 5.1.1 shows the temperature history at various locations on the emitter surface after approximately 20 min of warm-up period. The average temperature at measured locations (T_1 to T_7) falls in the range between 660 °C and 760 °C. The vertical bars indicate the standard deviations for the nine runs and shows that there is good reproducibility.

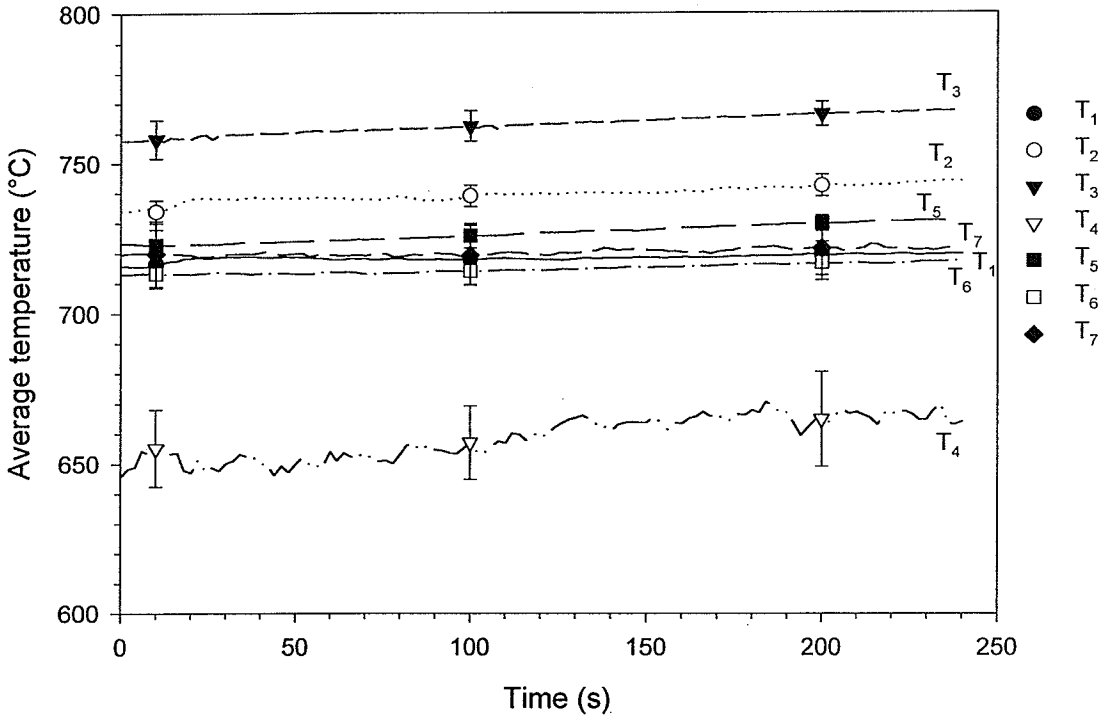

Figure 5.1.1 Average temperature of emitting surfaces after a 20-minute warm-up period. Each temperature line represents the average of nine experiments.

Except for thermocouple T_4, the temperatures of the emitter were within the range of 720°C to 760°C with ± 18.2 °C (standard deviation). The possible reasons for the T_4 point being lower could be that this thermocouple did not have a good contact with the ceramic emitter, or the thermocouple junction was oxidized. The overall average temperature of the emitter without T_4 was 730 ± 18.2 °C. The thermocouples were calibrated with the room temperature. And the temperatures of the thermocouple wires were higher or lower than the room temperature when the thermocouple wire was exposed to an ambient air, and in that case, the wire was replaced with new one.

5-2 Moisture Loss During Micronization

During IR processing of the peas, the feed material loses moisture due to high heat intensity at the surface of the peas from the emitter. Moisture was measured in two different setups: a) when the feed sample was exposed to the IR heat intensity at a fixed location on the trough (constant configuration factor) which is also named 'a fixed-element configuration model', and b) when the micronization experiment was performed and samples were collected from several selected locations along the vibrating trough (moving-element configuration model). Figures 5.2.1 to 5.2.3 show the moisture content of peas when micronized at the fixed location (40 cm from the exit of the trough) where the calculated configuration factor was 0.67.

The target tempered moisture in experiments shown in Figure 5.2.4 was approximately 20 % but due to the tempering process in measuring the weight of water and the mass of yellow peas using scales, the initial moisture in runs MMC1 to MMC3 went down by 1 to 2 %. Figures 5.2.4 to 5.2.6 show the moisture along the vibrating trough positioned horizontally (the angle of the slope = 0°).

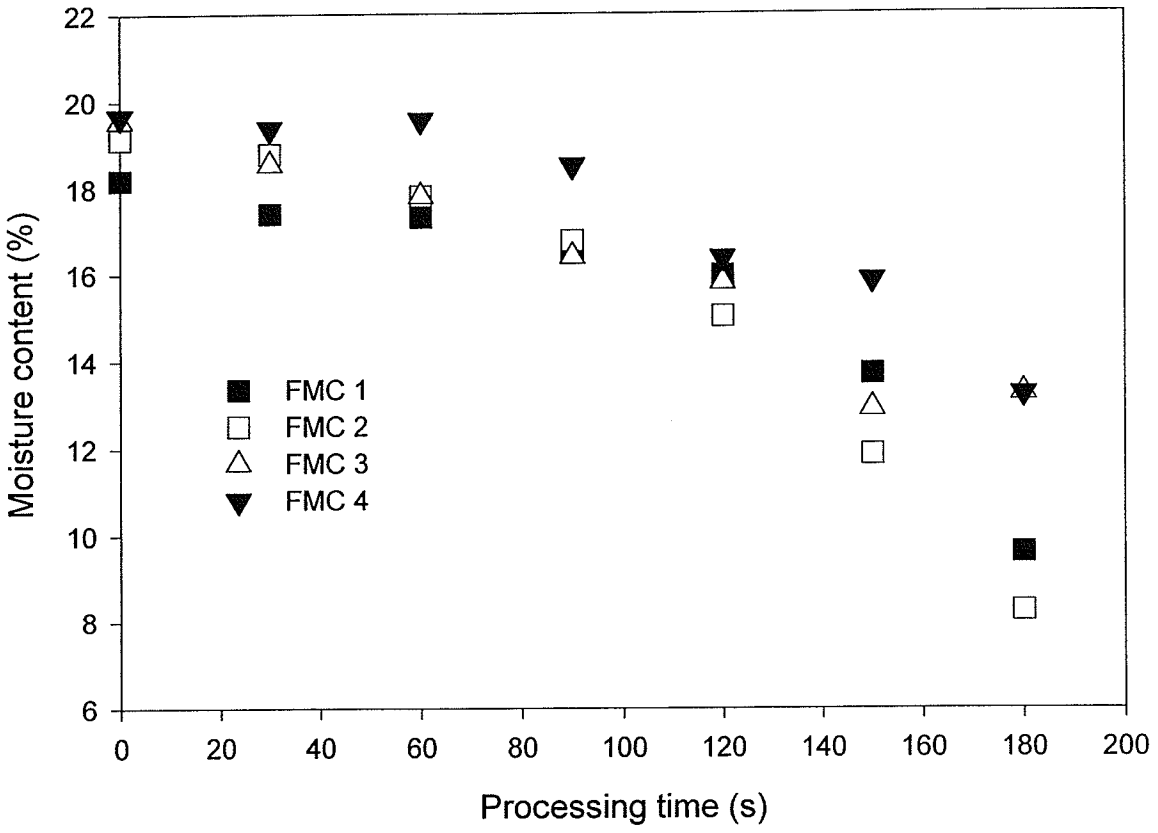

Figure 5.2.1 Moisture content of peas initially at 20% micronized at constant heat intensity (fixed-element configuration) where the configuration factor is 0.67. The data show four tests (FMC1 to FMC4).

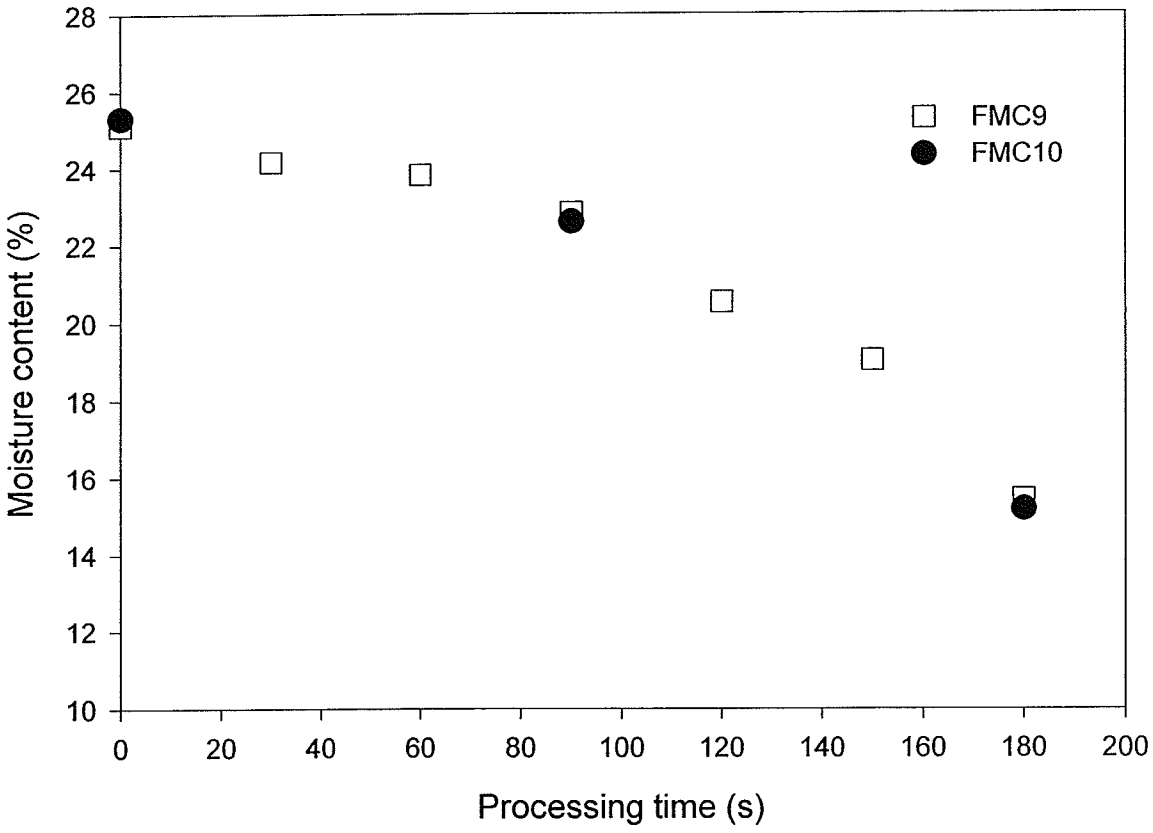

Figure 5.2.2 Moisture content of peas initially at 25% micronized at constant heat intensity (fixed-element configuration) where the configuration factor is 0.67. The data show two tests (FMC9 and FMC10).

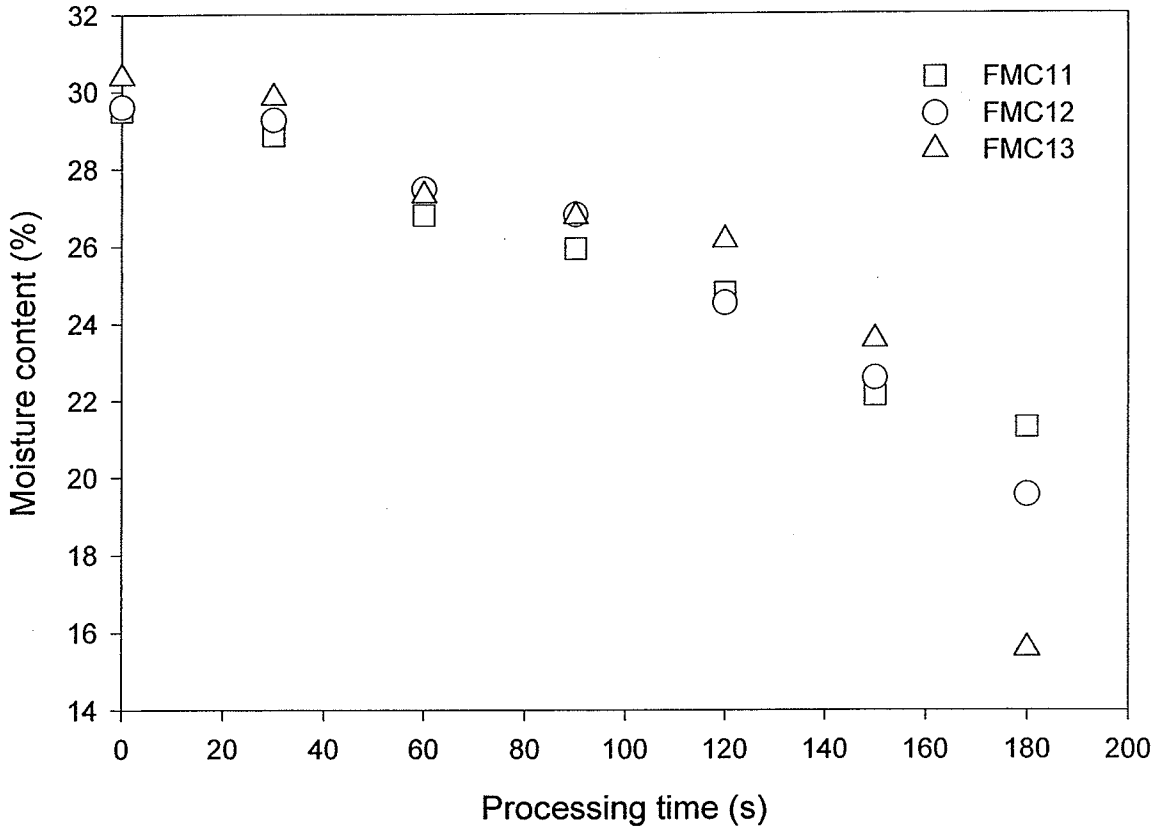

Figure 5.2.3 Moisture content of peas initially at 30% micronized at constant heat intensity (fixed-element configuration) where the configuration factor is 0.67. The data show three tests (FMC11 and FMC13).

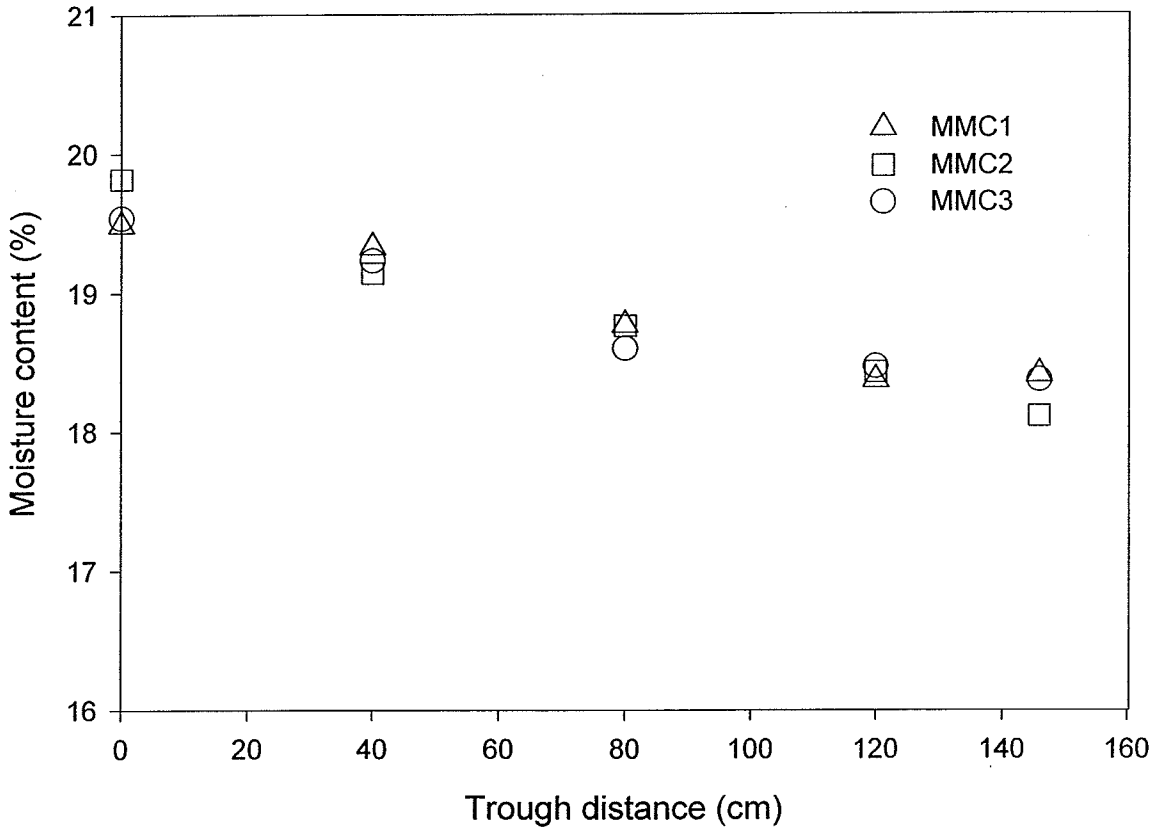

Figure 5.2.4 Moisture content of peas initially at 20% along the trough during micronization of peas on the vibratory conveyor for three runs for the moving-element configuration (MMC1 to MMC3). The slope of the trough was 0 degrees.

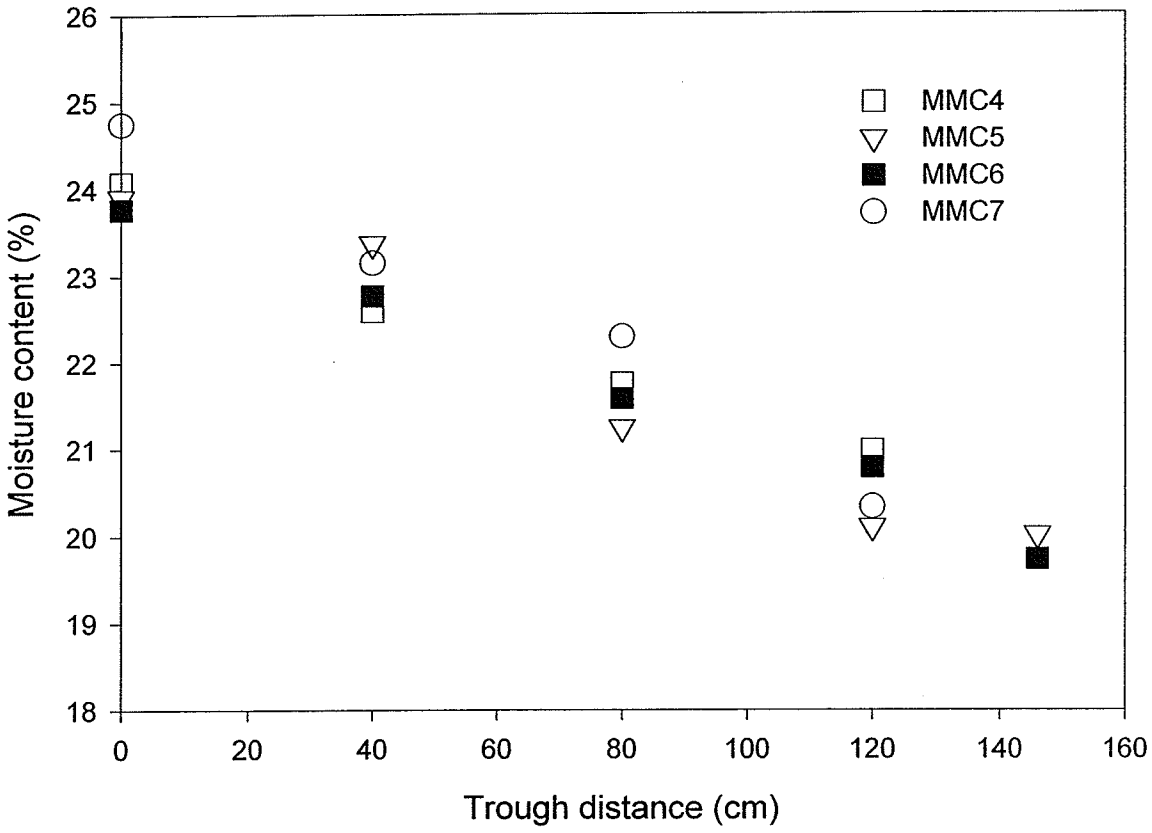

Figure 5.2.5 Moisture content of peas initially at 25% along the trough during micronization of peas on the vibratory conveyor for four runs for the moving-element configuration (MMC4 to MMC7). The slope of the trough was 0 degrees.

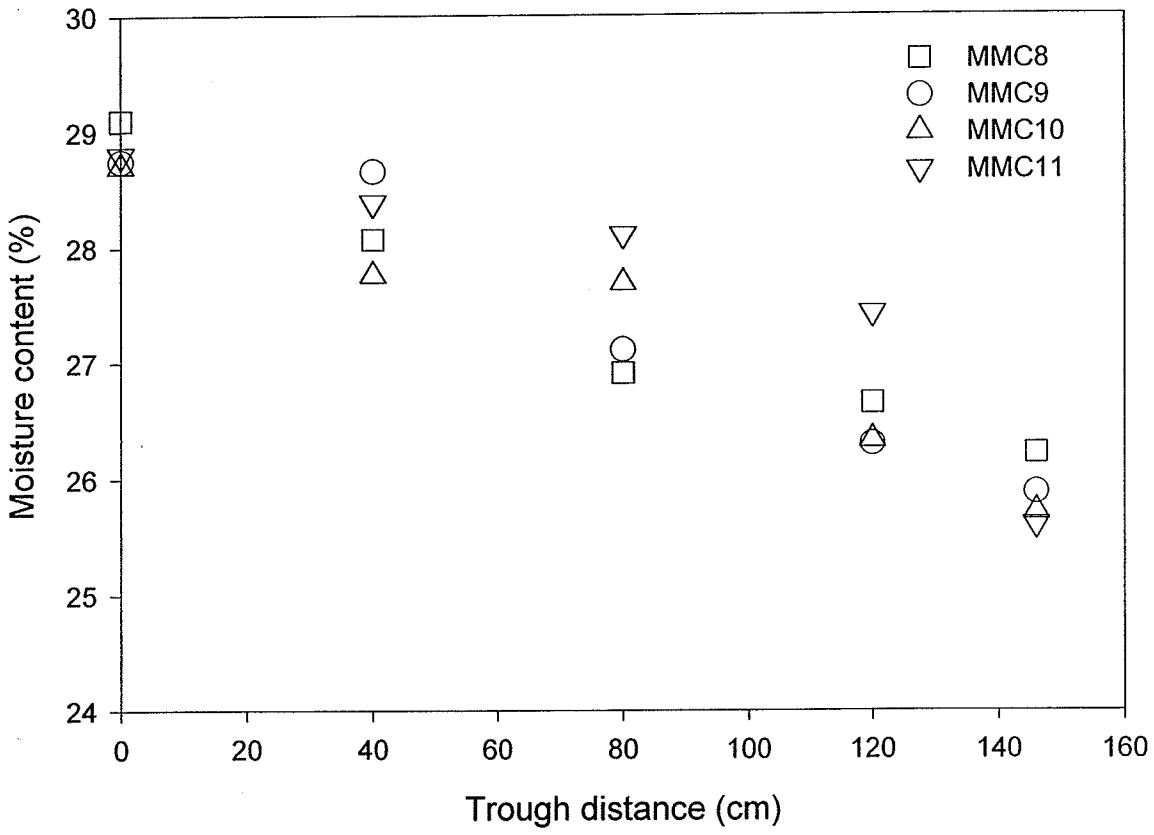

Figure 5.2.6 Moisture content of peas initially at 30% along the trough during micronization of peas on the vibratory conveyor for four runs for the moving-element configuration (MMC8 to MMC11). The slope of the trough was 0 degrees.

For the moisture at the fixed position shown in Figure 5.2.1 to 5.2.3, the moisture loss in 3 min of processing time was 10 to 14 % on a wet basis. On the other hand, the moisture loss for the moving samples for the slope zero was within the range of 2 to 5 % but the residence time was only approximately 1 min. There were some difference between the target moisture contents and attained moisture content in tempering process. The values were shown in Table 5.2.1.

Table 5.2.1 Comparison the target moisture contents and attained moisture contents in tempering process.

Target MC[a]	Attained MC for MECS[b]	Attained MC for FECS[c]
20% wb	19.6 ± 0.2% wb	19.1 ± 0.7% wb
25% wb	24.1 ± 0.4% wb	25.2 ± 0.1% wb
30% wb	28.8 ± 0.2% wb	29.8 ± 0.5% wb

[a] MC= moisture content,
[b] MECS = moving-element configuration system,
[c] FECS = fixed-element configuration system.

5-3 Temperature Measurement

Temperatures in peas tempered to 20, 25, 30% moisture, and exposed to micronization at a fixed position (constant heat intensity at a configuration factor of 0.67) are shown in Figures 5.3.1 to 5.3.3. The symbols 'F', 'M', and 'R' used in labels denotes fixed-element configuration system, moving-element configuration system, and the run number, respectively. The 'Ch' represents the number of the thermocouple channel connected to the peas. The average temperature attained for the sample tempered to 20, 25, and 30% MC was approximately 146°C, 120°C, and 117°C, respectively. As expected, the temperature increased as the initial moisture content of the sample decreased. Figures 5.3.1 to 5.3.3 indicate temperature rises during micronization and the maximum temperature rise was higher when its moisture content decreased. Figures 5.3.4 to 5.3.6 show the temperature changes of peas for peas moving along the trough at a separation distance of 12 cm from the infrared source. The slope of the trough was maintained at zero degree angle. The residence time in the experiments shown in Figure 5.3.4 and 5.3.5 were 42.5 and 59.9 s, respectively, and in the third experiment (Figure 5.3.6) in which peas were at the 30% initial moisture content, the average residence time increased to 98 s. During micronization process, some of the peas which were inserted by K-type thermocouple wires were placed at the inlet location of the trough. For the second or the third consecutive experiment for the moving-element configuration system, the pea samples with the thermocouples were heated due to the heated surfaces of the micronizer.

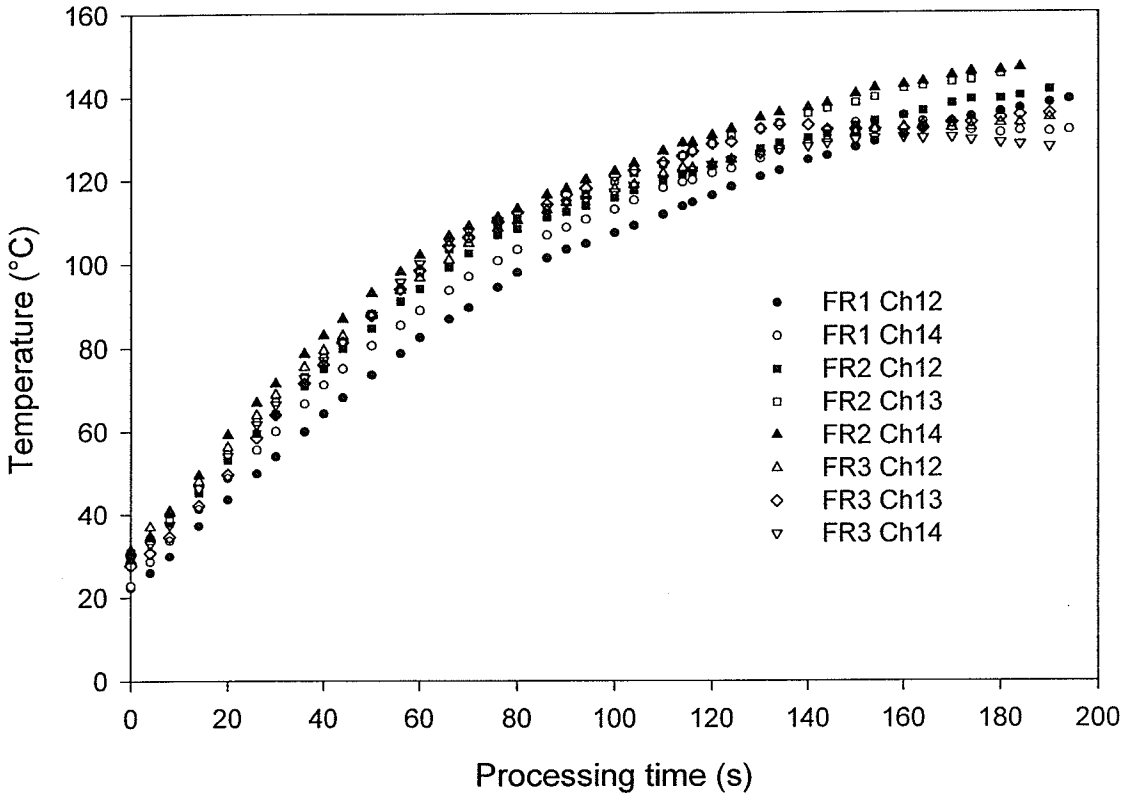

Figure 5.3.1 Temperatures of peas during micronization at a fixed-element configuration and tempered to 20% initial moisture content. Sample was positioned at 40cm from the end of the bottom trough where the configuration factor was 0.67. Data show three runs (FR1 to FR3) for pea temperatures measured by thermocouples on channel 12 to 14(Ch12 to Ch14).

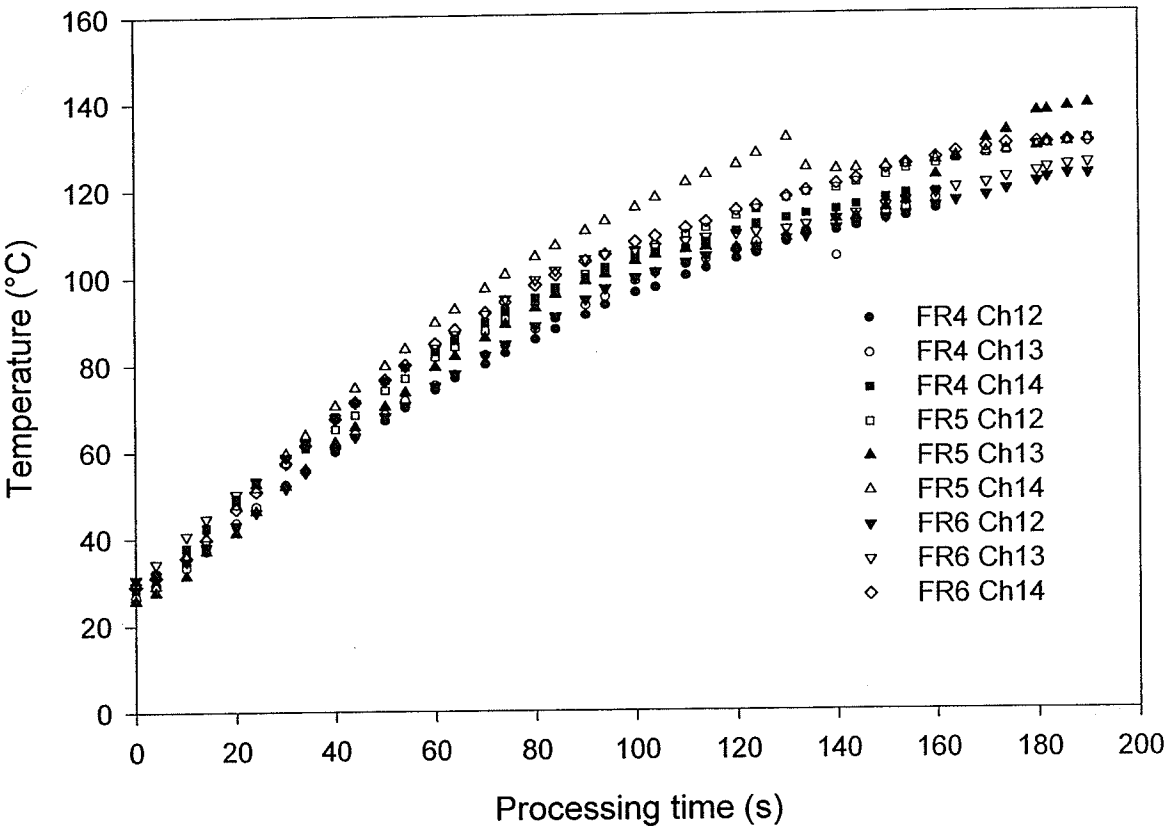

Figure 5.3.2 Temperatures of peas during micronization at a fixed-element configuration) and tempered to 25% initial moisture content. Sample was positioned at 40cm from the end of the bottom trough where the configuration factor was 0.67. Data show three runs (FR4 to FR6) for pea temperatures measured by thermocouples on channel 12 to 14 (Ch12 to Ch14).

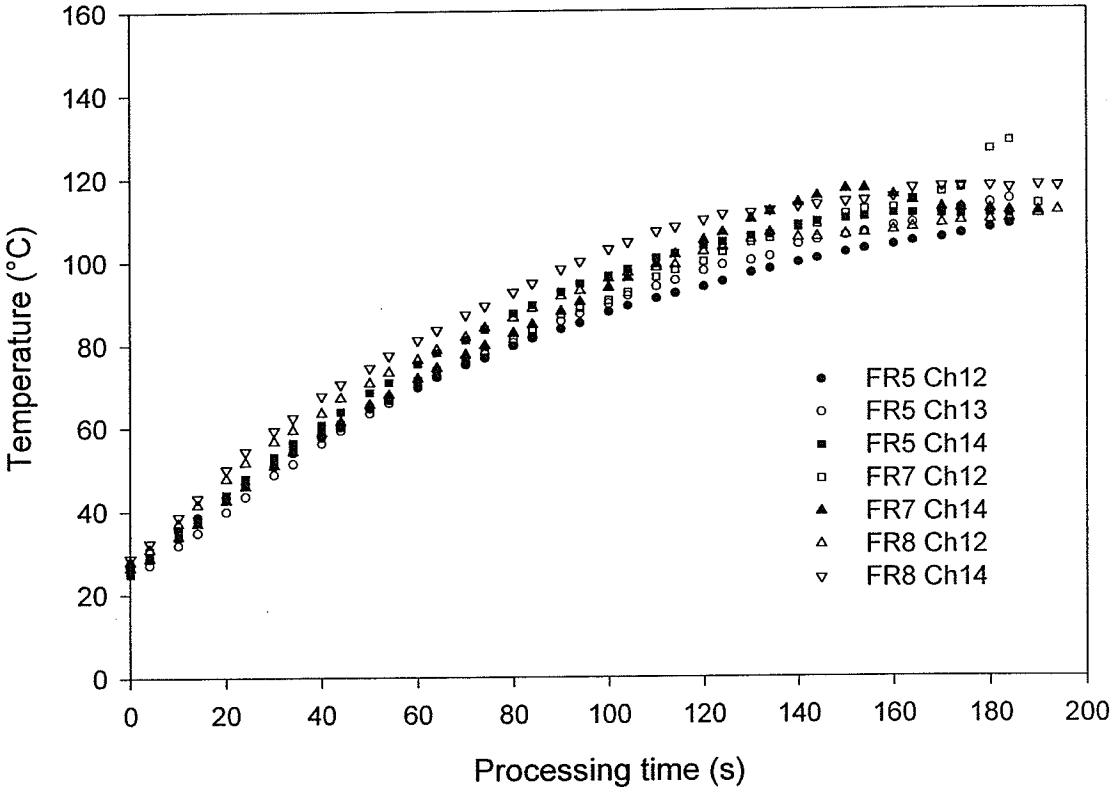

Figure 5.3.3 Temperature of peas during micronization at a fixed-element configuration) and tempered to 30% initial moisture content. Sample was positioned at 40cm from the end of the bottom trough where the configuration factor was 0.67. Data show three runs (FR5 to FR8) for pea temperatures measured by thermocouples on channel 12 to 14 (Ch12 to Ch14).

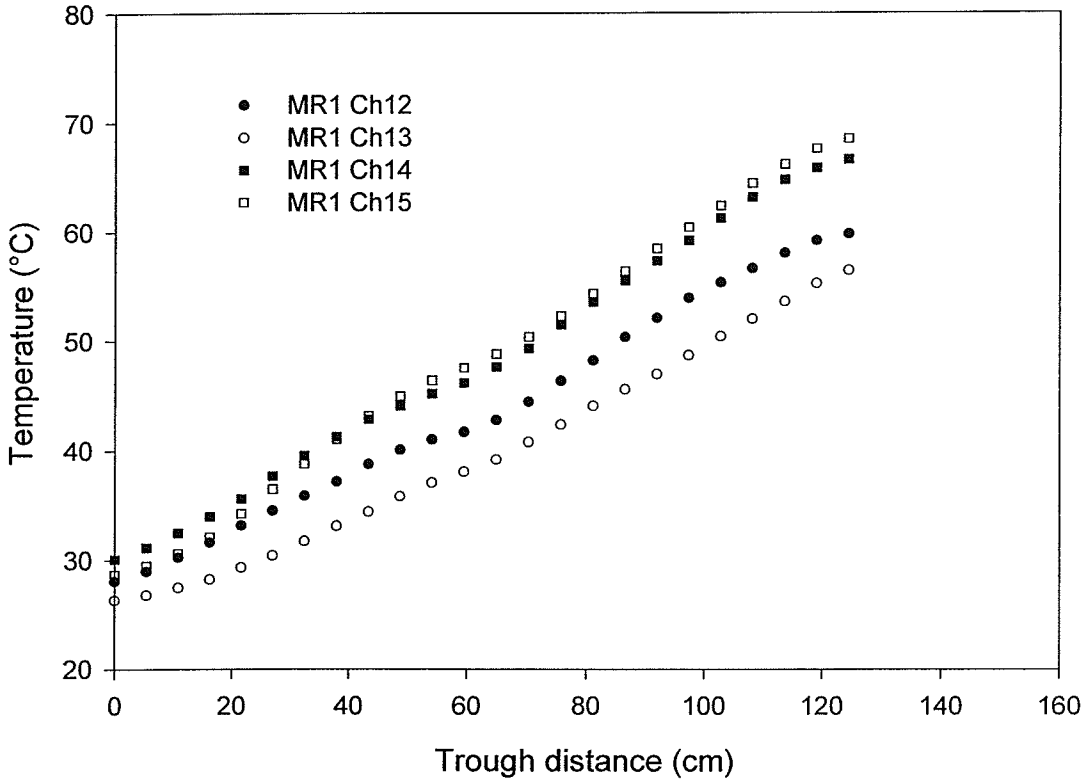

Figure 5.3.4 Temperatures of peas during micronization for a moving-element configuration and tempered to 20% initial moisture content. Data show one run (MR1) for pea temperatures measured by thermocouples on channel 12 to 15 (Ch12 to Ch15).

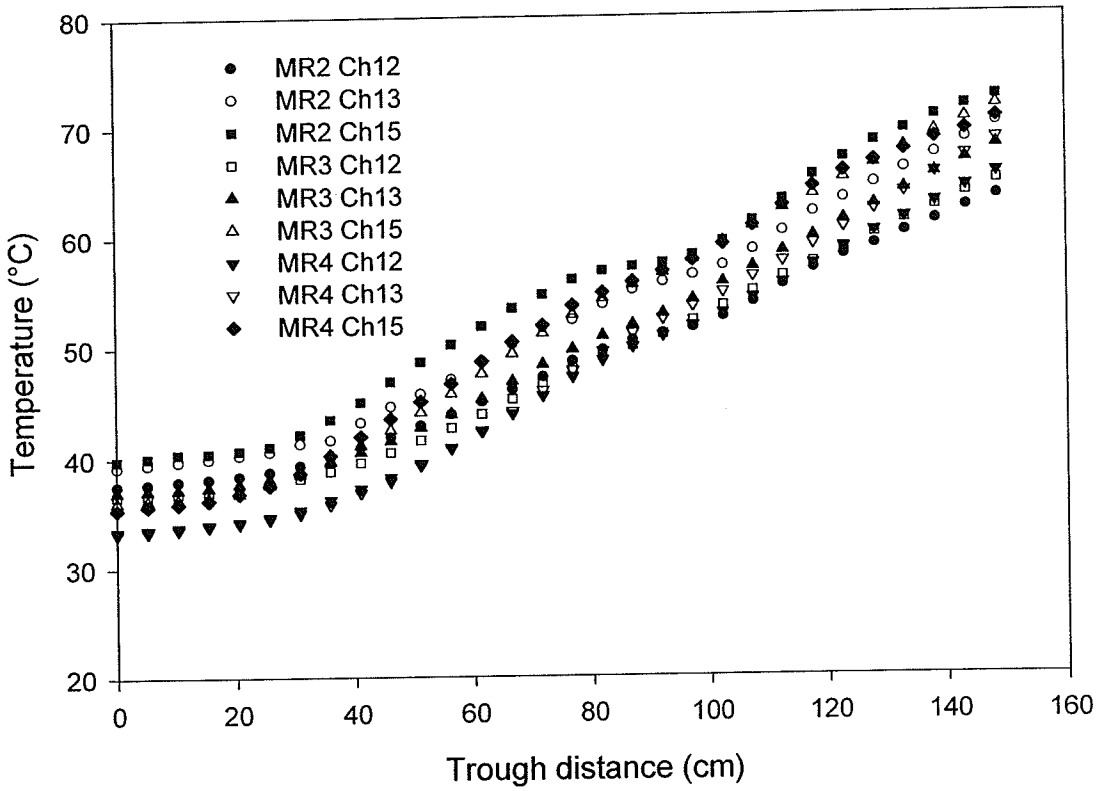

Figure 5.3.5 Temperatures of peas during micronization for a moving-element configuration and tempered to 25% initial moisture content. Data show one run (MR2 to MR4) for pea temperatures measured by thermocouples on channel 12 to 15 (Ch12, Ch13, and Ch15).

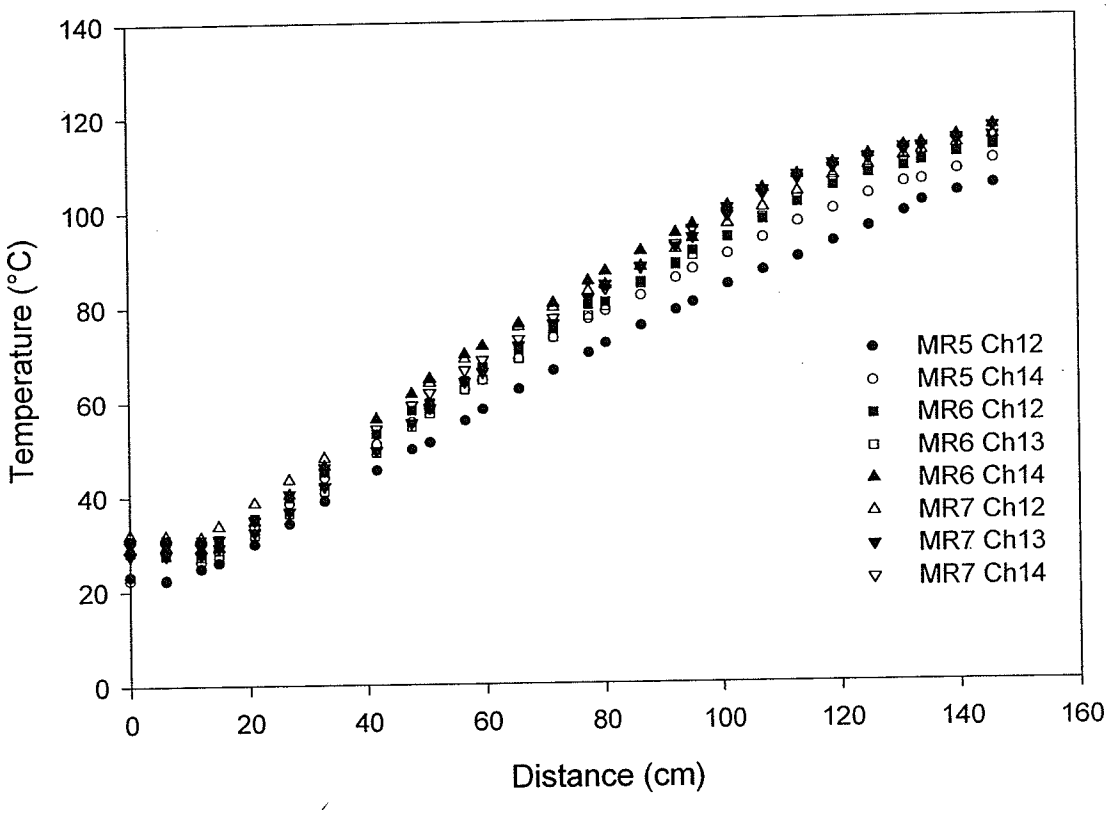

Figure 5.3.6 Temperatures of peas during micronization for a moving-element configuration and tempered to 30% initial moisture content. Data show one run (MR5 to MR7) for pea temperatures measured by thermocouples on channel 12 to 14 (Ch12 to Ch14). Average residence time was 98 s for this condition.

5-4 Measurement of Other Parameters

The proposed mathematical model in Chapter 3 has the form of a non-linear first order differential equation and needs several parameters if it is to be solved. These parameters include coverage, mass flowrate, and average residence time for validation of the model. In this section, the results of these parameter measurements are presented.

5-4-1 Measurement of coverage factor

The coverage of the micronized material on the vibrating trough during IR processing depends on the slope of the vibratory conveyor (vibrating trough) and the mass flowrate of the test material for a given operating condition. The coverage of the test material on the vibratory conveyor was not uniform.

The entrance area of the conveyor was covered with the test material more densely and the exit portion of the trough was covered more loosely. Thus, the average value of the coverage of each operating condition was measured. Table 5.4.1 shows the results of five tests that were carried out to determine the coverage factor. The tests were conducted for the horizontal trough arrangement (slope = 0°). The measured results gave an average coverage of 0.44 with a standard deviation of 0.06.

Table 5.4.1. Coverage values at the slope of zero for the vibratory conveyor.

Run no.	Area covered with the material (=A_S) (cm^2)	Area of the trough (=A_5) (cm^2)	Coverage, Φ (=A_S /A_5) (-)
1	1378	3869	0.36
2	1643	3869	0.42
3	1802	3869	0.46
4	2040	3869	0.53
5	1669.5	3869	0.43
Average			0.44 ± 0.06

5-4-2 Measurement of mass flowrate

A series of measurements of the mass flowrate on wet basis was performed at the exit of the vibratory conveyor and tabulated in Table 5.4.2. The micronizer setup was the same for all experiments. Also, the moisture content of the material was measured at the exit at the same time to calculate dry mass flowrate. Tempering peas of different initial moisture contents affected the movement of the material during micronization. The mass flowrate of the peas decreased as the moisture content of the peas increased. The average values were 0.833 ± 0.065, 0.449 ± 0.043, 0.305 ± 0.024 kg/min for peas entering the micronizer at 20, 25, 30% target moisture content, respectively.

5-4-3 Measurement of residence time

As a result of vibration of the trough, the dynamic behavior of individual whole peas shows quite a complicated pattern. The residence time for individual peas on the vibratory gas-fired micronizer shows a wide distribution in the range of 15 second to 135 second at the zero slope of the vibratory conveyor for peas at 20% initial moisture content and moving at the average mass flowrate of 0.833 kg/min. To obtain an average value for the residence time, 164 samplings for the experiment of residence time measurement was performed and averaged. This wide distribution of the residence time came from the shape of the pea itself and the interference among the peas under the vibration of the trough. The residence time of the peas during micronization has wide distribution as shown in Figure 5.4.1, and approximately 85% of peas had a residence time in the range from 40 to 80 seconds.

Table 5.4.2 Average mass flowrate of whole yellow peas on the micronizer trough at the slope zero.

Initial MC (%)	Mass flowrate (wb) (kg/min)		No. of runs
	Average (kg/min)	Standard deviation	
20	0.831	0.065	6
	0.876	0.021	4
	0.825	0.014	3
	0.833 ± 0.065		
25	0.419	0.025	7
	0.449	0.046	6
	0.480	0.037	7
	0.449 ± 0.043		
30	0.300	0.022	9
	0.317	0.030	6
	0.313	0.012	5
	0.305 ± 0.024		

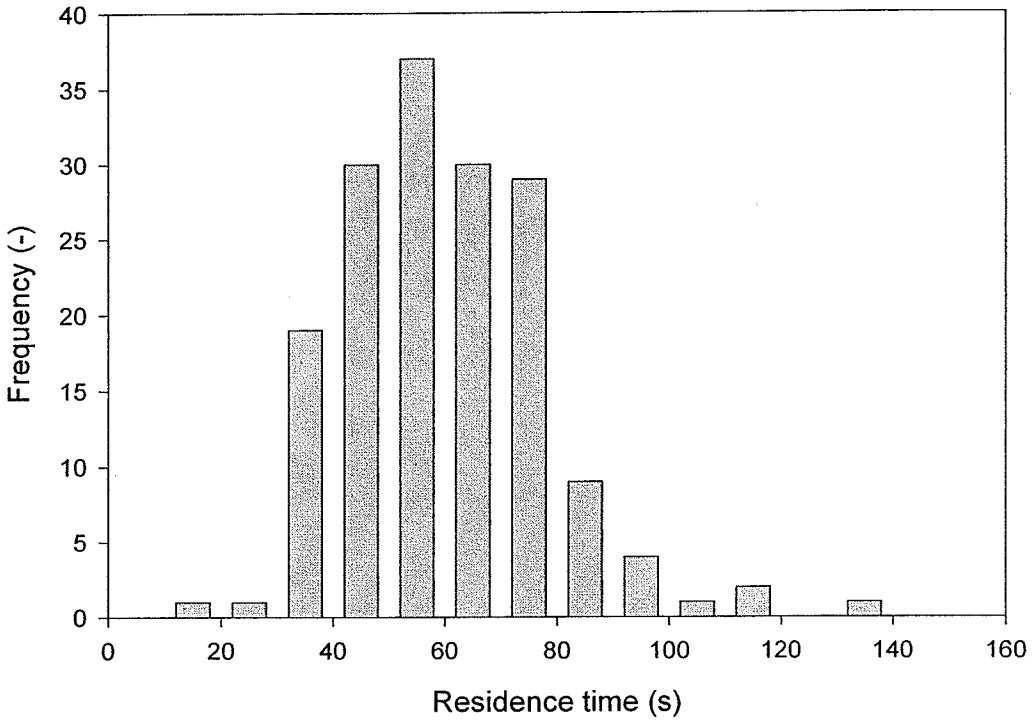

Figure 5.4.1 Residence time distribution for micronized yellow peas at 25% initial MC and at the average mass flowrate of 0.833 kg/min. The slope of the trough was maintained at zero degrees.

CHAPTER 6

ANALYSIS OF IR PROCESSING USING THE PROPOSED MODEL

6-1 Numerical Evaluation of the Configuration Factor

The configuration factor is a unique parameter which occurs only in radiation heat transfer operations and most recent research contributions in radiation heat transfer have been devoted to determining the configuration factor quickly in a convenient manner (Howell, 1982). The fraction of the emitted energy from one surface that directly reaches another surface is determined by this factor. The proposed mathematical models require information on the configuration factor which changes as a differential strip of peas changes its position along the vibratory conveyor. The configuration factor is expressed as the sum of four terms of double line integrations and the Gauss-Quadrature method of numerical integration was used for the evaluation of the integration. Numerical integration was performed using 'Quick Basic'. To evaluate the effect of approximations on numerical integrations, the effect of the number of the approximation points in Gauss-Quadrature integration (Stroud and Secrest, 1966) and the effect of separation distance between the bottom trough and the emitter of the micronizer was analyzed first. Figure 6.1.1 shows the values of the configuration factor along the trough length as the peas move at a separation distance of 12 cm from the IR emitter for three different numbers of approximations in the Gauss-Quadrature numerical integration (N=5, 10, and 20). The micronizer trough (model 'MR2', Micronizing Company Ltd. UK) is 18 cm longer than the length of the emitter (12 cm longer at the inlet and 6 cm at the exit location, Chapter 4). Therefore, the shape of the configuration factor characteristic in Figure 6.1.1

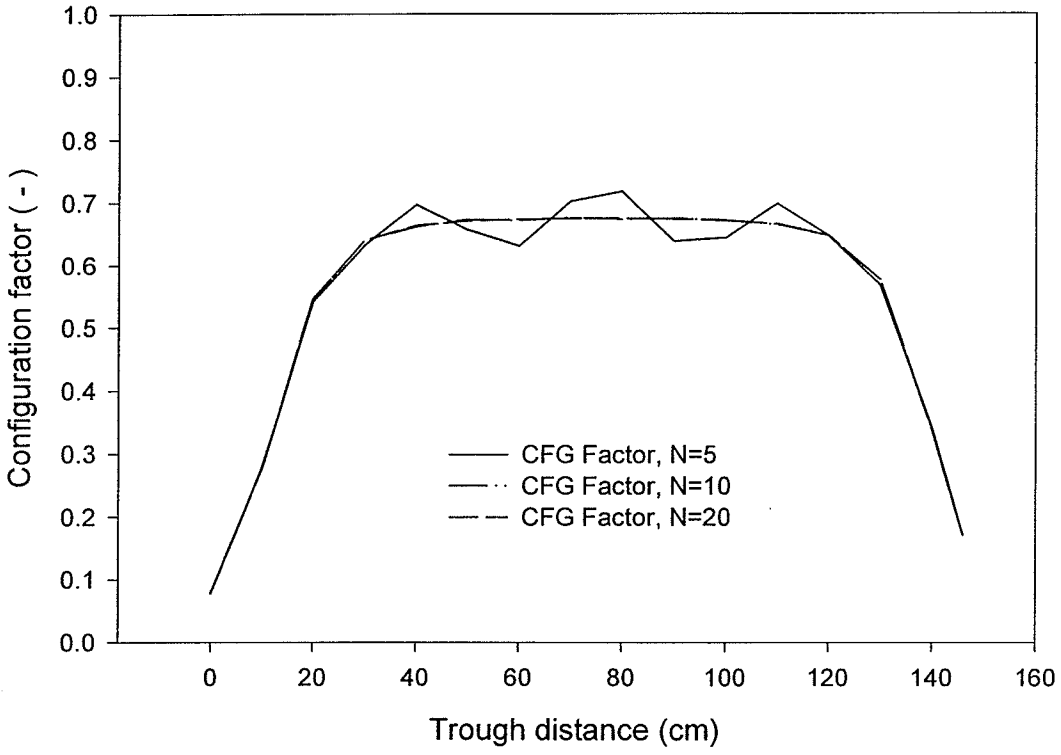

Figure 6.1.1 Configuration factor determined for a 12 cm separation distance from the IR emitter to the trough for three numbers of approximations (N=5, 10, and 20) in the Gauss-Quadrature numerical integration along the trough distance. The configuration factor was calculated when viewed from the differential strip of the bottom trough to the IR emitter.

is not symmetrical. The solid line indicates the configuration factor value when the number of approximation points was assumed N=5, and it shows good agreement in the range between 0 to 30 cm and 120 to 146 cm of the trough length with the values for the configuration factor obtained when the number of approximation [in Eq.(3-57), Eq.(3-58), Eq.(3-59), and Eq.(3-60)] points was chosen to be 10 and 20. But in the range of the trough distance 30 to 120 cm, the factor values oscillated. When the number of approximations increased to 10 and 20, the graph showed a very smooth curve in that range. The calculated value of the configuration factor was very sensitive to the number of approximations and converged to a constant value for the 30 to 120 cm trough length when the number was larger than 10. The values of the factor which were calculated with the approximation number of 20 showed good agreement with the literature values (Siegel and Howell, 1992). To validate the accuracy of the numerical calculations for the configuration factor (Appendix V), the configuration factor was compared with the known configuration geometry (Siegel and Howell, 1992) shown in Figures 6.1.2 (Case1) and 6.1.3 (Case 2). Table 6.1 shows the values calculated analytically and numerically for the two cases of this geometry. In Figure 6.1.2, the diagram denotes the configuration factor from a planar differential element to the coaxial parallel rectangle which is designated as Case 1 in Table 6.1. The analytical mathematical expression of configuration factor ($F_{dl\text{-}2}$) from a differential element dA_1 to A_2 for Figure 6.1.2 is described by Eq.(6-1), (Siegel and Howell, 1992):

Table 6.1 Configuration factor comparison between calculated values and reference values.

Case No.	Calculation results by the program	Reference Value*	% error
1	0.778736	0.778688	0.006
2	0.338374	0.338374	0.000

* (Siegel and Howell, 1992)

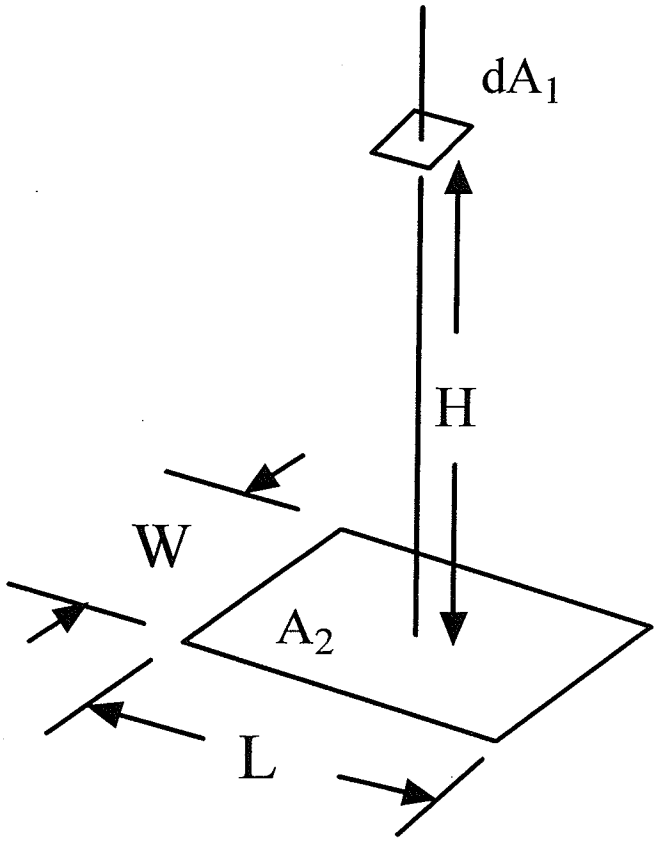

Figure 6.1.2 Diagram of configuration factor from a planar element to a coaxial parallel rectangle.

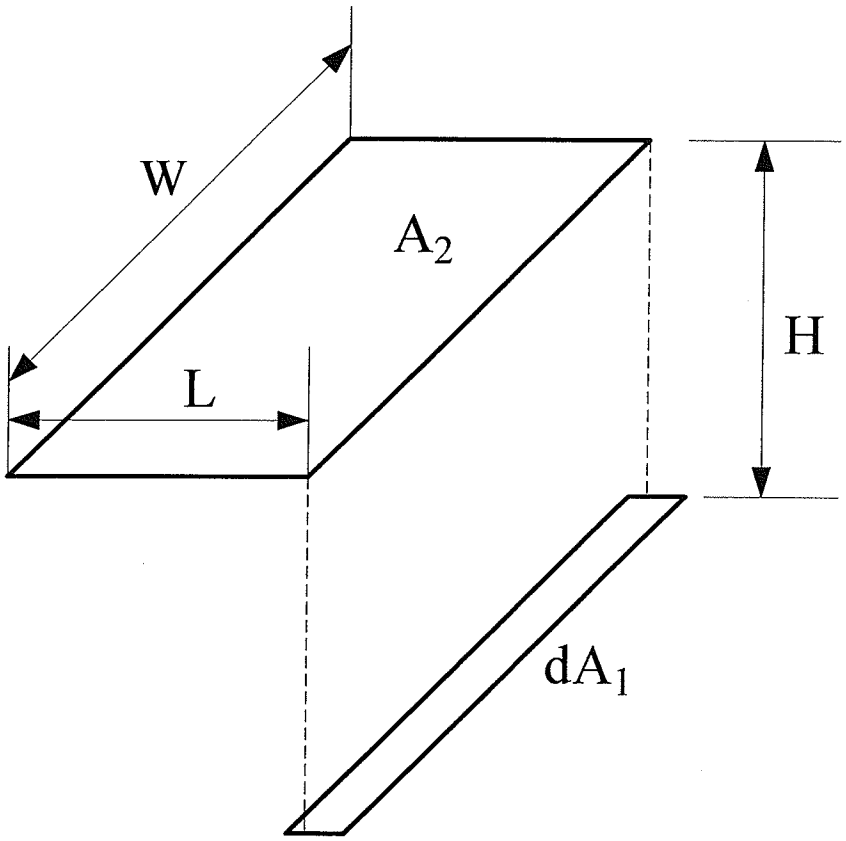

Figure 6.1.3 Diagram of the configuration geometry from a strip (rectngle) element (A_2) to a narrow parallel strip of rectangle (dA_1) that is located beneath the edge of rectangle A_2.

$$F_{d1-2} = \left(\frac{2}{\pi}\right)\left\{\left[\frac{X}{\sqrt{(1+X^2)}}\right]\tan^{-1}\left[\frac{Y}{\sqrt{(1+X^2)}}\right] + \left[\frac{Y}{\sqrt{(1+Y^2)}}\right]\tan^{-1}\left[\frac{X}{\sqrt{(1+Y^2)}}\right]\right\} \quad (6\text{-}1)$$

where, $X = \frac{L}{2H}$, $Y = \frac{W}{2H}$.

For the second geometry for the configuration factor in Figure 6.1.3, the mathematical expression is described as follows (Siegel and Howell, 1992):

$$F_{d1-2} = \frac{1}{\pi Y}\left[\sqrt{(1+Y^2)}\ \tan^{-1}\left(\frac{X}{\sqrt{(1+Y^2)}}\right) - \tan^{-1}X + \frac{XY}{\sqrt{(1+Y^2)}}\tan^{-1}\left(\frac{Y}{\sqrt{(1+X^2)}}\right)\right] \quad (6\text{-}2)$$

where, $X = \frac{L}{H}$, $Y = \frac{W}{H}$.

Eq.(6-2) is a special case of the configuration factor for the moving elemental strip (Chapter 3), and this is the case when the elemental strip is under the emitter at the end location of the trough. As shown in Table 6.1, the percent error was 0.006 % and 0.000 % for Case 1 and Case 2, respectively. The comparison of the results between analytical and numerical solution indicates good accuracy with the literature values. The computer program used to arrive at a numerical solution is listed in Appendix III. For modelling purposes, the factor was calculated with 20 points of approximation and used for the prediction of pea temperatures during micronization.

Figure 6.1.4 shows the effect of separation distance between the bottom trough and the emitter and the configuration factor values were evaluated at separation distances of 8, 12, and 20 cm with 20 points of approximation. In Figure 6.1.4, the "H" symbol denotes separation distance between the

trough and the emitter. The configuration factor decreases as the separation distance increases except for the ends of the trough. In the range from 30 to 120cm of the trough distance, the configuration factor is almost constant and not much difference in configuration factor is observed. The numerical values of the configuration factor for the micronizer along the trough are given in Appendix V (Table 5A-1 and Table 5A-2).

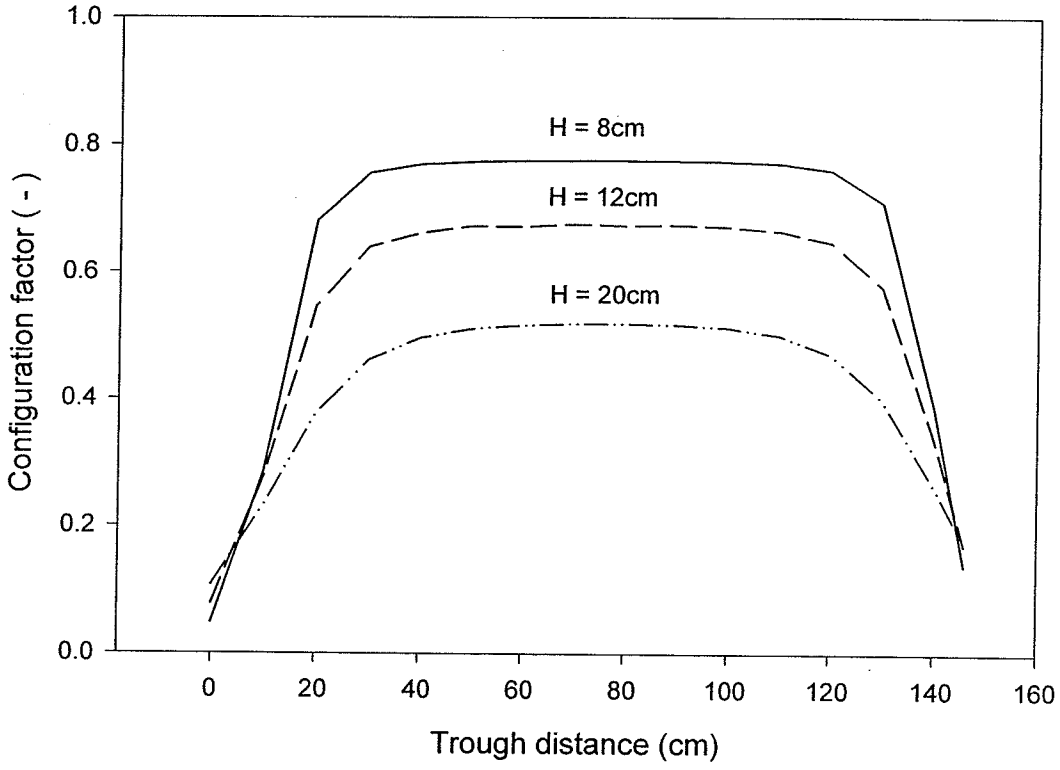

Figure 6.1.4 Configuration factor evaluated for different separation distances (H). Calculations were done at the number of approximation of 20 in the Gauss-Quadrature numerical integration which was done along the trough distance.

6-2 Fitting of the Moisture Content

Moisture content of peas which are exposed to high intensity IR heat decreases as the peas travel along the trough under the IR emitter. During IR processing, each individual pea undergoes moisture loss, and temperature rise (Fasina et al., 1998). Temperature and moisture changes are being affected by configuration factor change, reflectivity changes due to moisture loss, and splitting of peas due to high vapor pressure build-up inside peas caused by the high IR heat intensity. These factors will affect the radiation heat transfer between the pea surface and the emitter, and also affect the optical properties of peas such as reflectivity, emissivity, and absorptivity (Fasina and Tyler, 2001; Siegel and Howell, 1992). Finally, these factors will affect the moisture-temperature gradient as the micronization progresses. In this study, the moisture-temperature gradient was obtained from the experimental data for peas tempered to 20, 25, and 30% initial moisture content. Functional relationships of moisture content during micronization by the regression of the experimental data of moisture content was obtained and the derivative of these functions with respect to time (for a fixed-element configuration model, dM/dt) or the derivative with respect to the distance along the trough (for a moving-element configuration system, dM/dx) was taken. The functional relationship for the temperature of peas during micronization was determined and the derivatives for the average temperature was obtained. By dividing the moisture content derivative by the temperature derivative, the moisture-temperature gradients were determined.

The best fit lines obtained by the regression of the experimental data on the moisture content have the form of polynomials with respect to processing time or trough distance and initial moisture content and are expressed as follows:

For the fixed-element configuration system,

$$M = M_0 + a_1 t + a_2 t^2 + a_3 t^3$$
where, M_0= initial moisture content, a_i = coefficient. (6-3)

For the moving-element configuration system,

$$M = M_0 + a_1' x + a_2' x^2 + a_3' x^3$$
where, M_0 = initial moisture content, a_i' = coefficient. (6-4)

Figure 6.2.1 to 6.2.3 show the best fit lines obtained for the experiments conducted with pea samples exposed to IR processing at the fixed location (Figure 3.7) (fixed-element configuration system) and Figure 6.2.4 to 6.2.6 represent the best fit lines for moisture content for peas moving along the trough (moving-element configuration system). The experiments were conducted with peas tempered to 19.1, 25.2, and 29.8% initial moisture content for the fixed-element configuration and to 19.6, 24.1, and 28.8 % moisture content for the moving-element configuration. In Figure 6.2.4, the regression line indicates the experimental set, runs MMC1 to MMC3 for initial moisture content of 19.6%. All the regression curves for the fixed-element configuration system show a similar pattern but for the moving-element configuration system the pattern of the moisture content during micronization is close to a linear relationship. This might arise from the difference of the configuration factor on the trough between the fixed-element configuration system and the moving-element configuration system experiment. The change in configuration factor means there is a change in heat intensity irradiating on the surface of the peas. For the fixed-element configuration system, the configuration factor is constant and the heat intensity reaching the peas does not change. But for the moving system, the peas travel along the trough and the configuration factor changes as the control volume of peas moves along the trough and consequently, the heat intensity on the pea surface changes as the configuration factor changes.

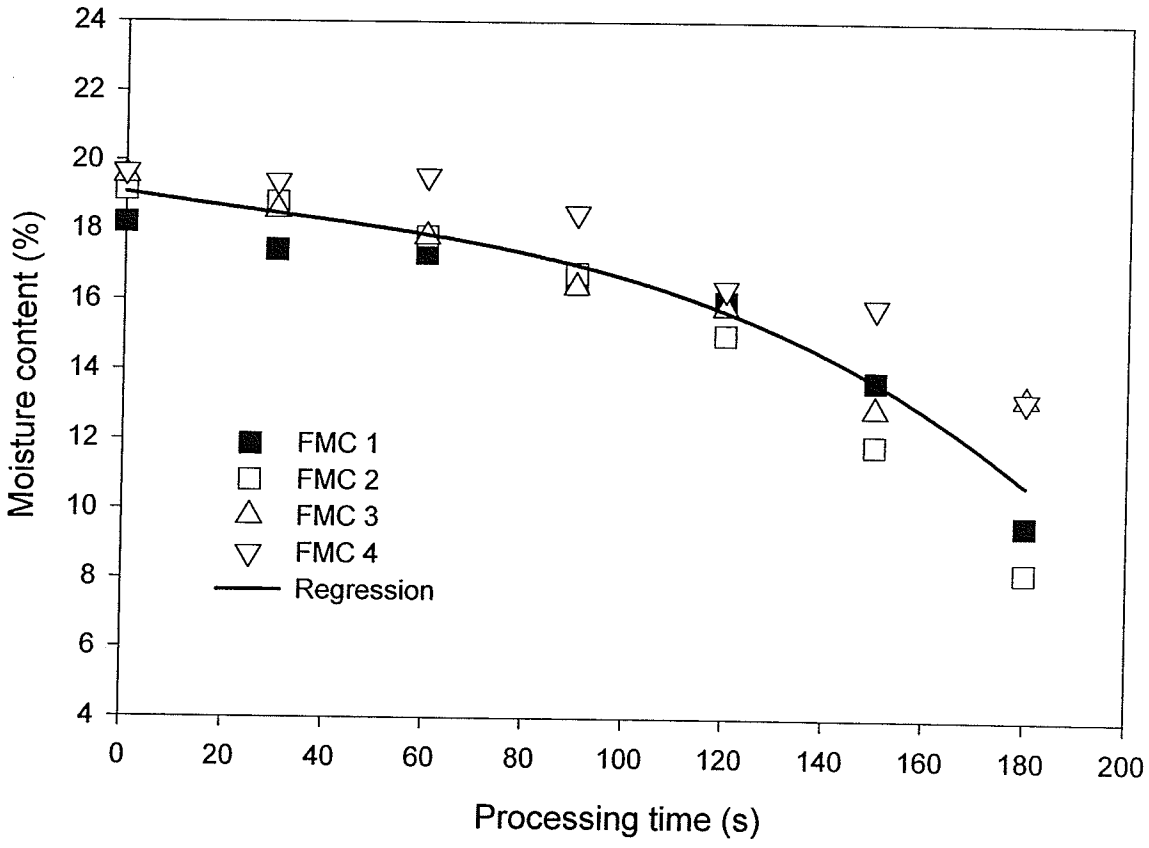

Figure 6.2.1 Curve fitting for moisture content for peas tempered to 19.1% MC and micronized at constant heat intensity (fixed-element configuration) where the configuration factor is 0.67. The data show four tests (FMC1 to FMC4).

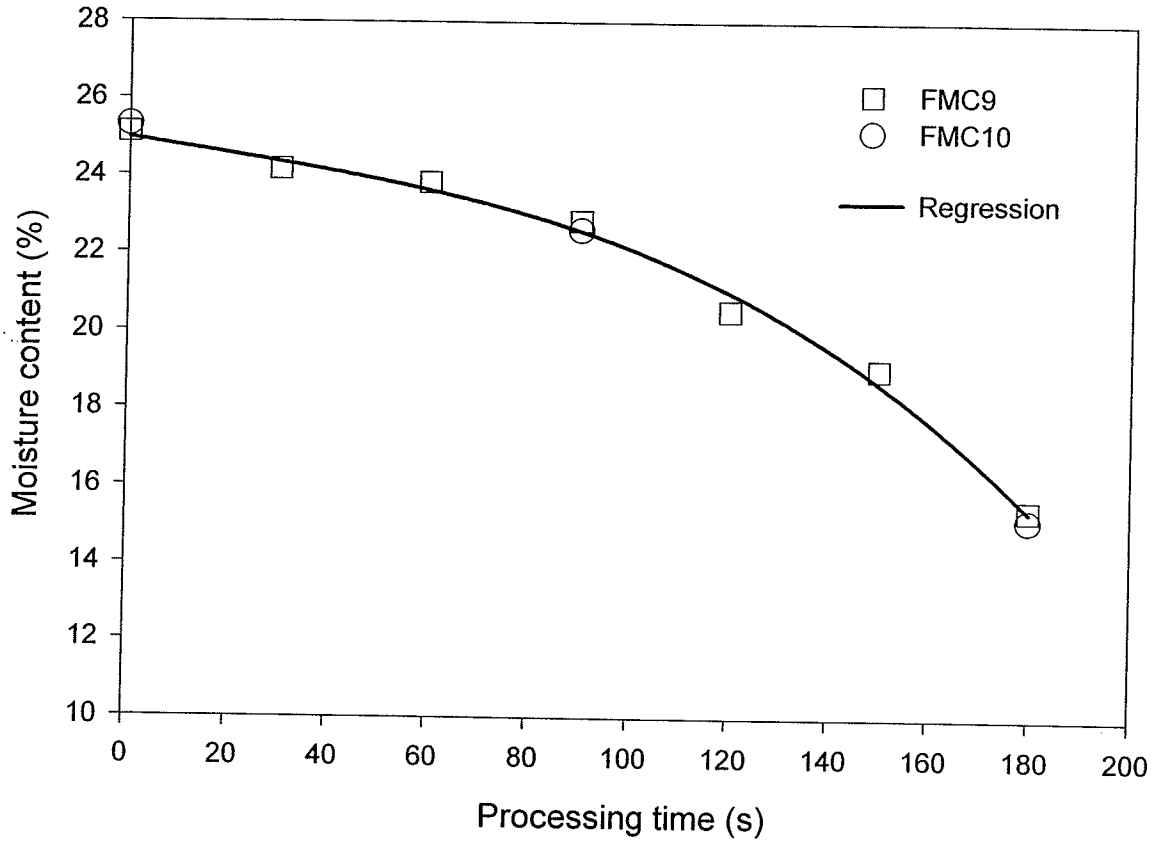

Figure 6.2.2 Curve fitting for moisture content for peas tempered to 25.2% MC and micronized at constant heat intensity (fixed-element configuration) where the configuration factor is 0.67. The data show two tests (FMC9 and FMC10).

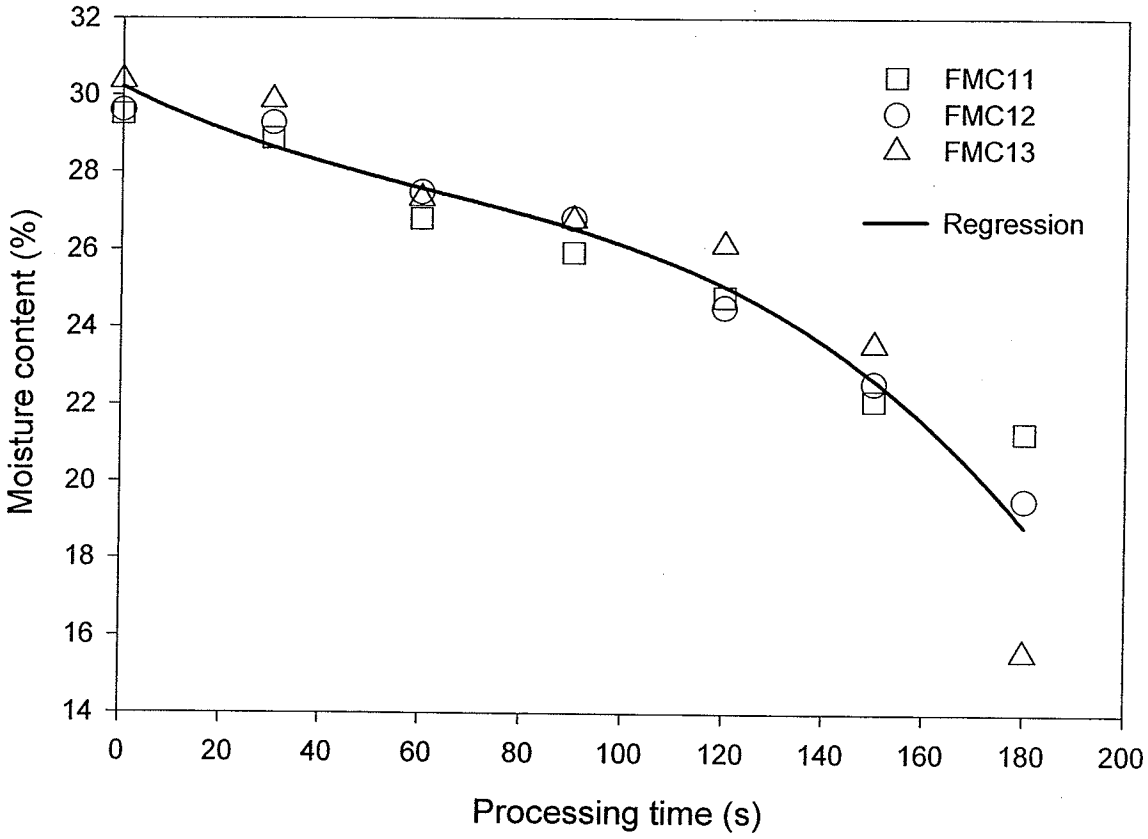

Figure 6.2.3 Curve fitting for moisture content for peas tempered to 29.8% MC and micronized at constant heat intensity (fixed-element configuration) where the configuration factor is 0.67. The data show three tests (FMC11 and FMC13).

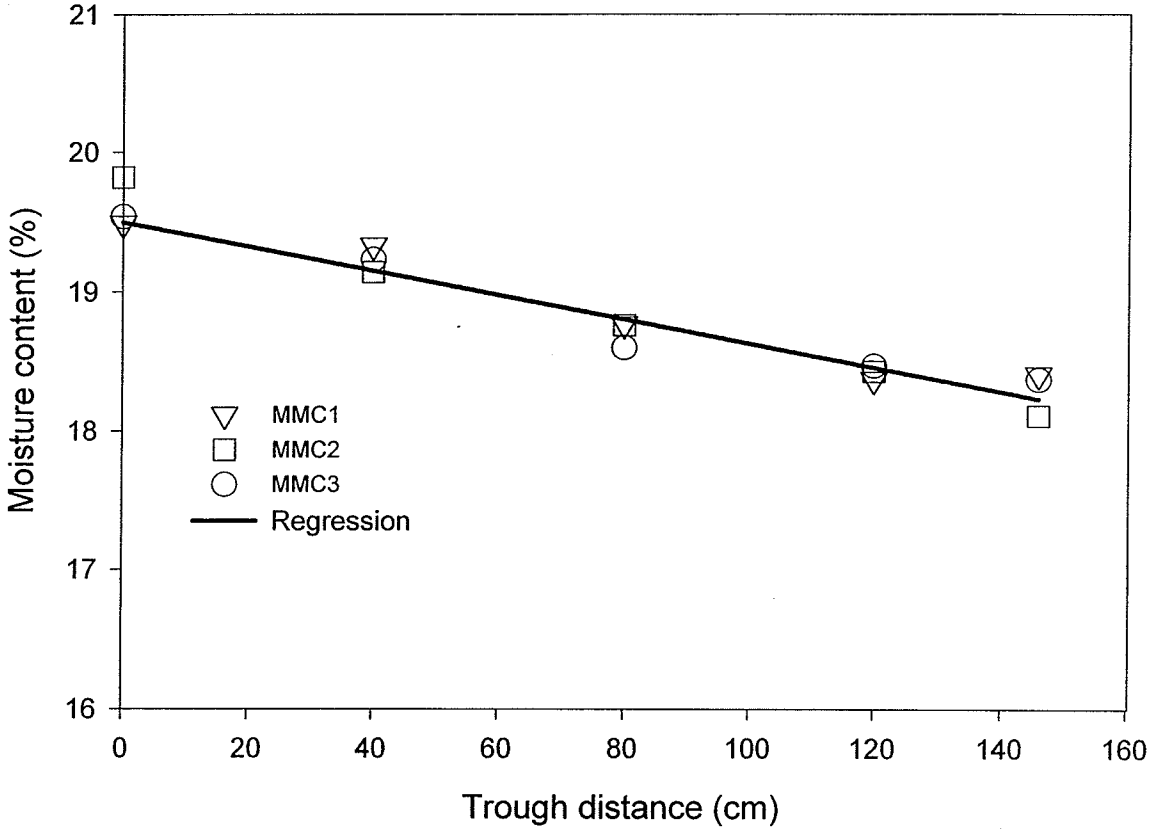

Figure 6.2.4 Curve fitting for moisture content along the trough during micronization of peas tempered to 19.6% MC on a vibratory conveyor for three runs for the moving-element configuration (MMC1 to MMC3). The slope of the trough was zero degrees.

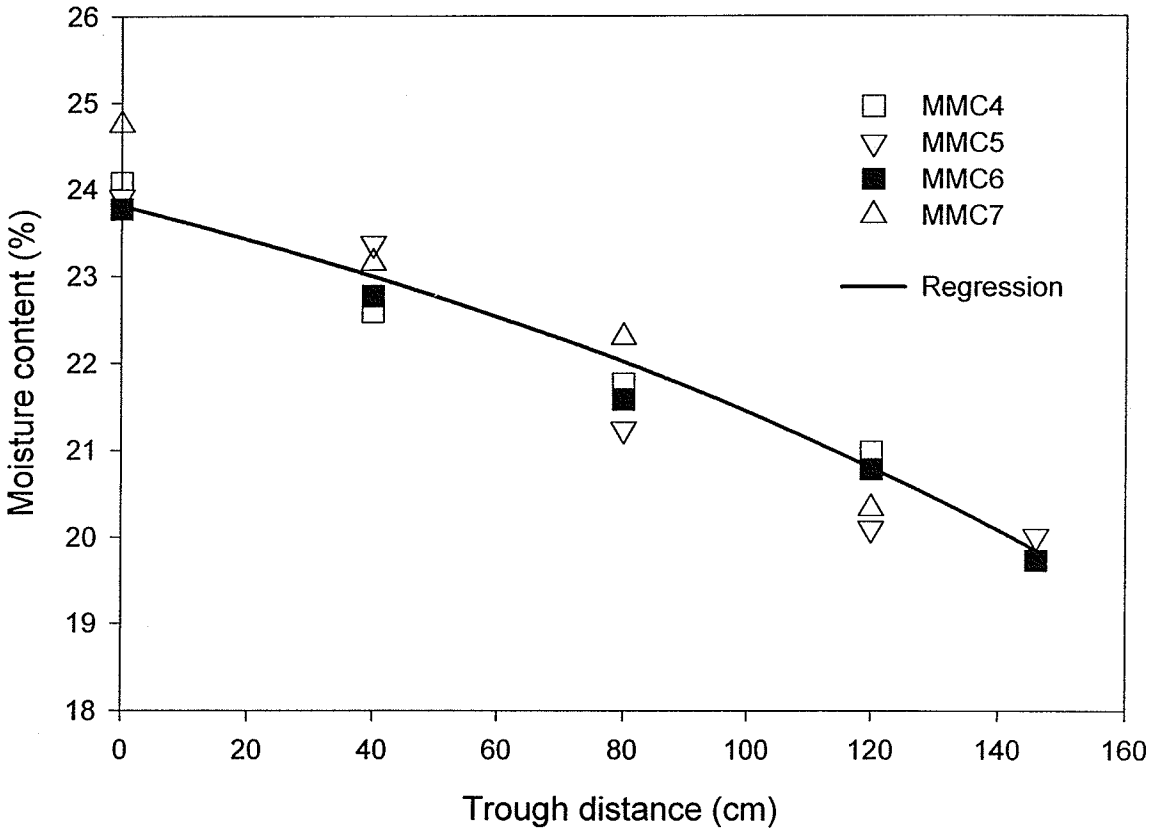

Figure 6.2.5 Curve fitting for moisture content along the trough during micronization of peas tempered to 24.1% MC on a vibratory conveyor for four runs for the moving-element configuration (MMC4 to MMC7). The slope of the trough was zero degrees.

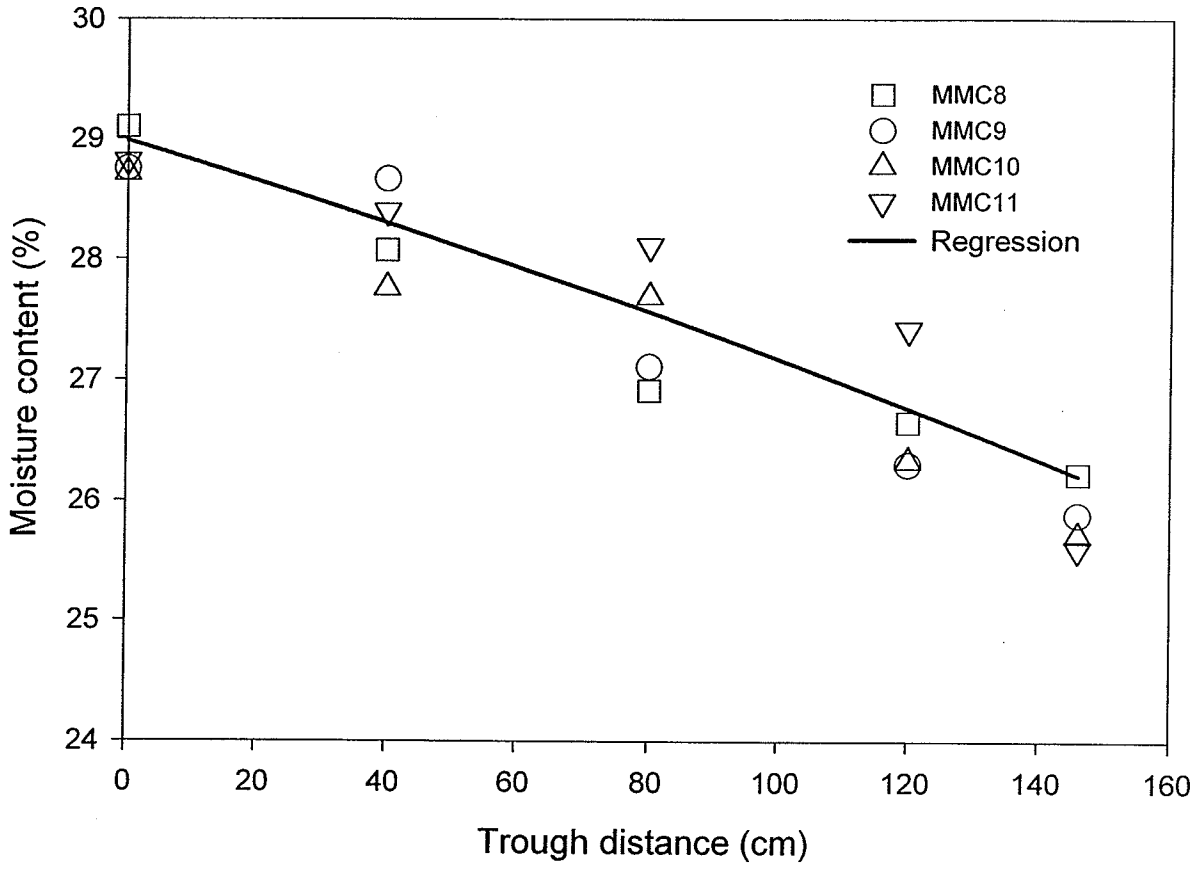

Figure 6.2.6 Curve fitting for moisture content along the trough during micronization of peas tempered to 28.8% MC on a vibratory conveyor for four runs for the moving-element configuration (MMC8 to MMC11). The slope of the trough was zero degrees.

Eq.(6-3) and (6-4) were used to calculate the derivatives of moisture content with respect to time and with respect to distance. All the coefficients of the polynomials are listed in Tables 4A-1 to 4A-6 in Appendix IV.

6-3 Fitting of the Temperature

Figure 6.3.1 to 6.3.6 show the best fit lines for the average temperatures measured in the fixed-element and the moving-element configuration system for the peas tempered to different initial moisture contents. The best fit lines are polynomials of the following form:

For the fixed-element configuration system,

$$T = T_0 + b_1 t + b_2 t^2 + b_3 t^3 \tag{6-5}$$

where,

T_0 = initial temperature of the peas, b_i=coefficients.

For the moving-element configuration system,

$$T = T_0 + b_1' x + b_2' x^2 + b_3' x^3 \tag{6-6}$$

where,

b_i'=coefficients.

The temperature rise in all experiments showed a similar pattern as the fixed-element configuration.

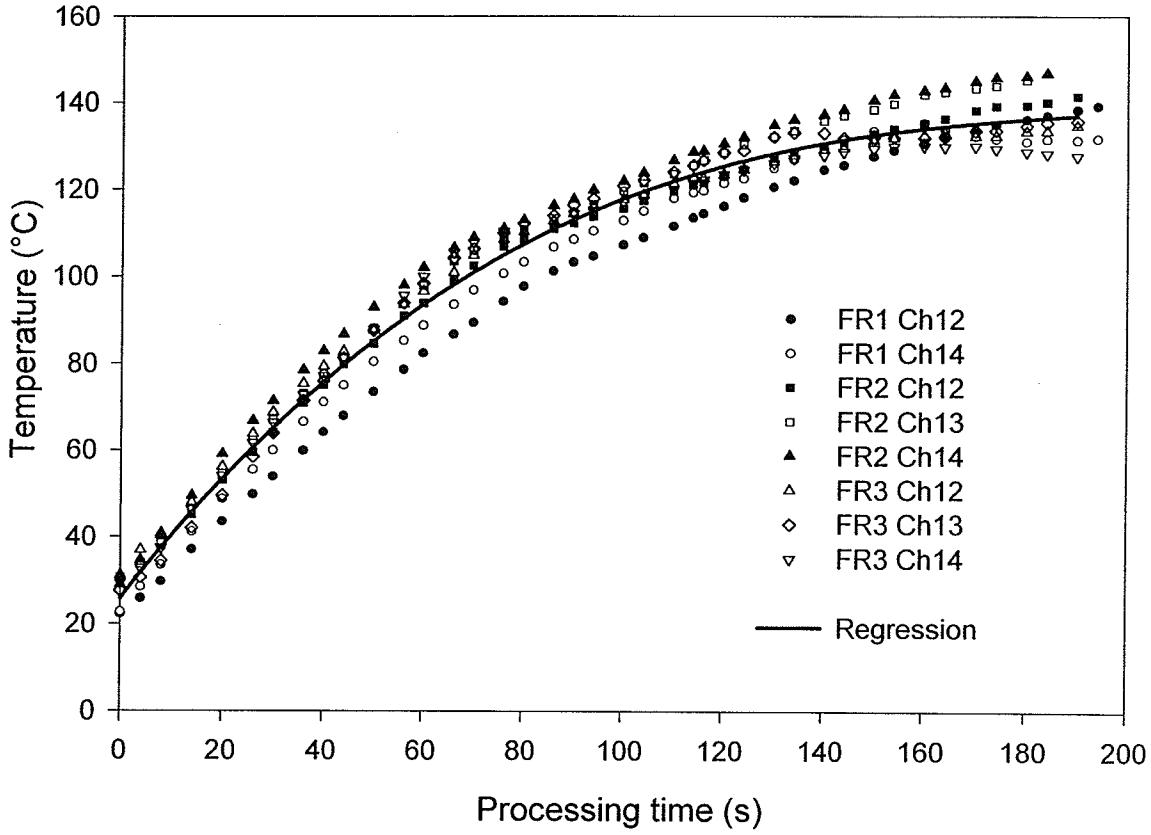

Figure 6.3.1 Curve fitting for the temperature of peas during micronization at a fixed-element configuration and tempered to 19.1% initial MC. The sample was positioned at 40cm from the end of the bottom trough where the configuration factor was 0.67. Data show three runs FR1 to FR3 for peas temperatures measured by thermocouples on channel 12 to14 (Ch12 to Ch14).

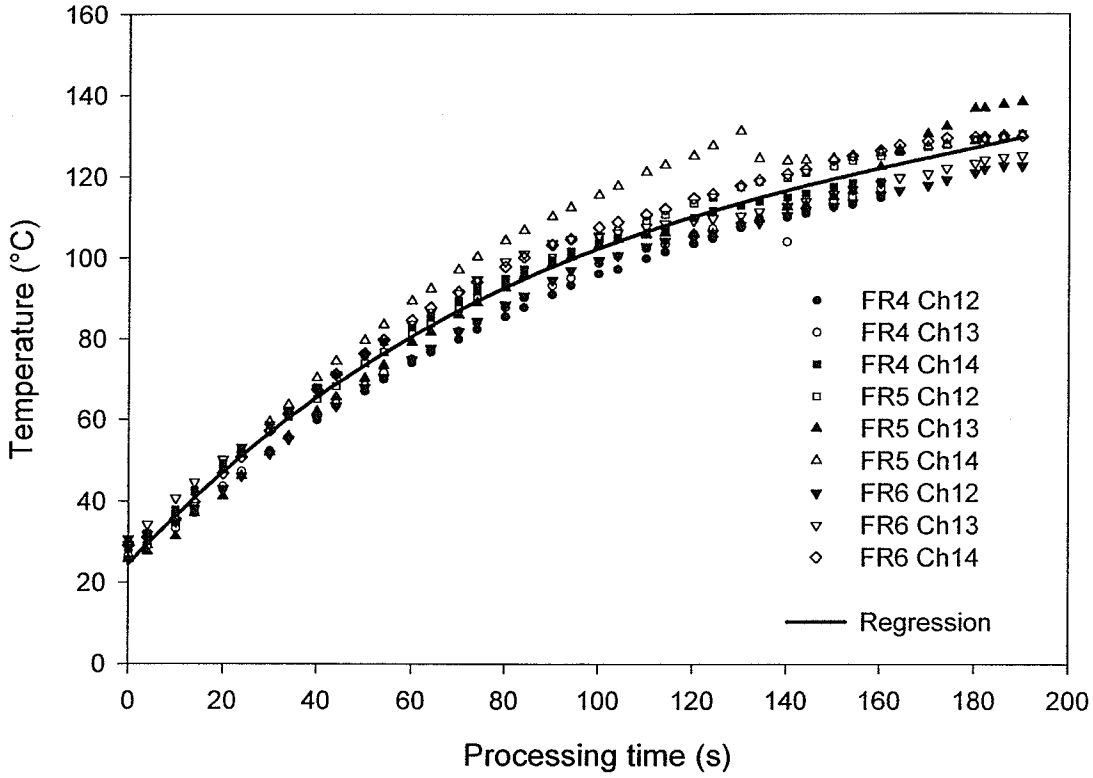

Figure 6.3.2 Curve fitting for the temperature of peas during micronization at a fixed-element configuration and tempered to 25.2% initial MC. The sample was positioned at 40cm from the end of the bottom trough where the configuration factor was 0.67. Data show three runs (FR4 to FR6) for peas temperatures measured by thermocouples on channel 12 to 14 (Ch12 to Ch14).

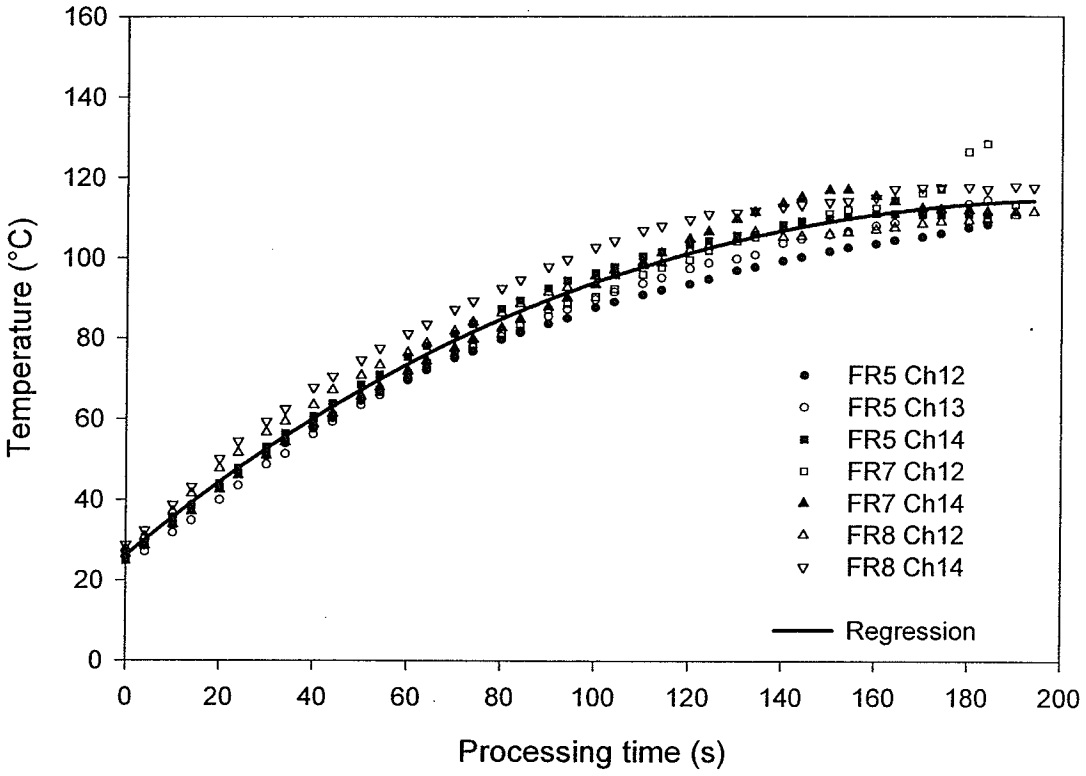

Figure 6.3.3 Curve fitting for the temperature of peas during micronization at a fixed-element configuration and tempered to 29.8% initial MC. The sample was positioned at 40cm from the end of the bottom trough where the configuration factor was 0.67. Data show three runs (FR5 to FR8) for peas temperatures measured by thermocouples on channel 12 to 14 (Ch12 to Ch14).

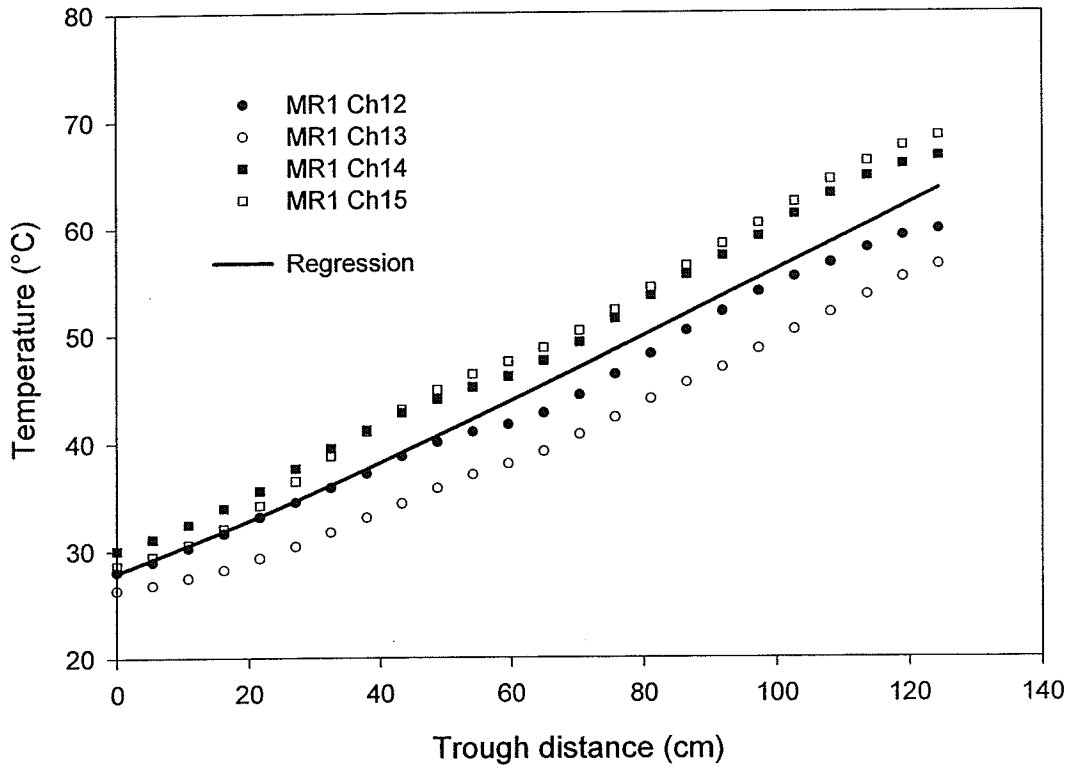

Figure 6.3.4 Curve fitting for the temperatures of peas during micronization for a moving-element configuration and tempered to 19.6% initial MC. Data show one run (MR1) for pea temperatures measured by thermo-couples on channel 12 to 15 (Ch12 to Ch15).

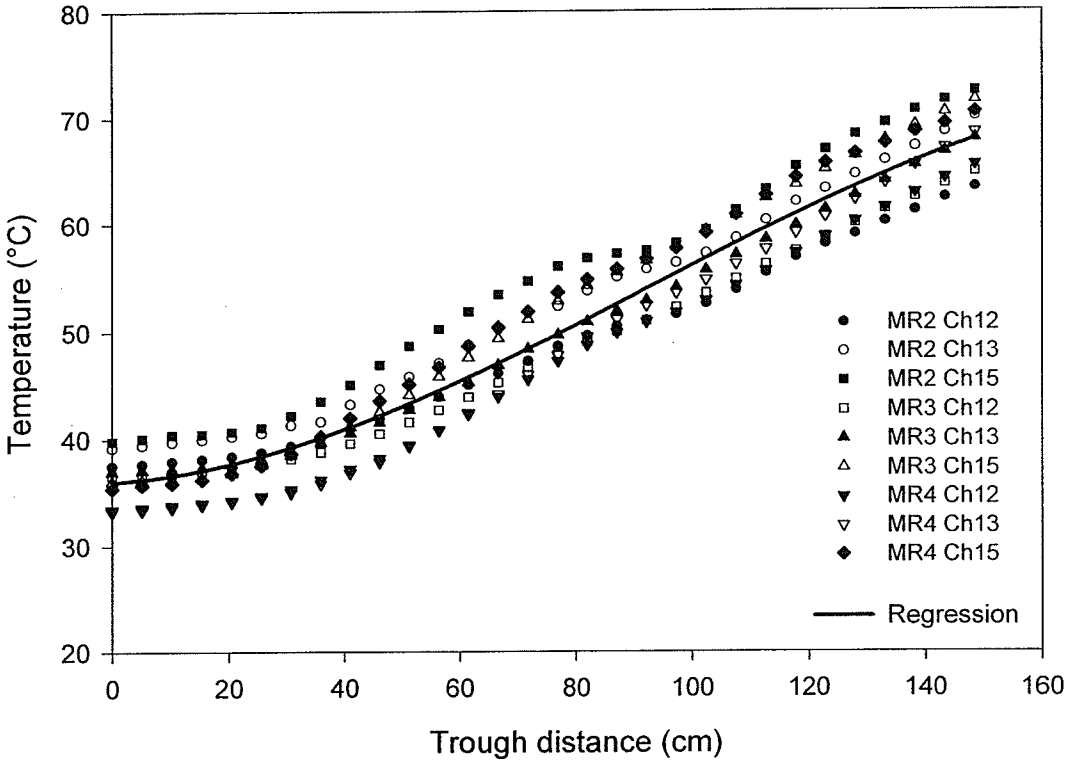

Figure 6.3.5 Curve fitting for the temperatures of peas during micronization for a moving-element configuration and tempered to 24.1% initial MC. Data show three runs (MR2 to MR4) for pea temperatures measured by thermocouples on channel 12 to 15 (Ch12 to Ch15).

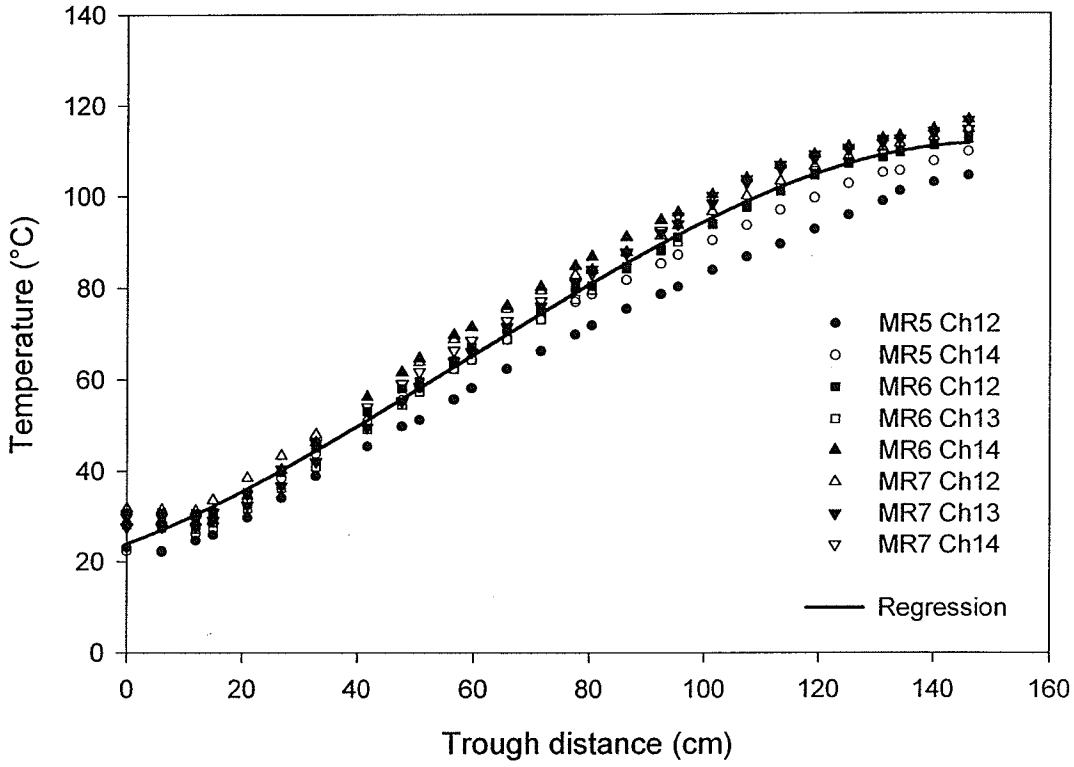

Figure 6.3.6 Curve fitting for the temperatures of peas during micronization for a moving-element configuration and tempered to 28.8% initial MC. Data show three runs (MR5 to MR7) for pea temperatures measured by thermocouples on channel 12 to 15 (Ch12 to Ch15).

The maximum temperature of peas reached at the end of micronization depended on the initial moisture content. For the moving-element configuration system, the regression line for the average temperature rise looks closer to linear compared to the regression line as the fixed-element configuration system. All the data were regressed with the third-order polynomials with satisfactory coefficients of determination, r^2, of 0.95 to 0.99.

6-4 Moisture-Temperature Gradient

The values of the moisture-temperature gradient (dM/dT) were obtained by dividing the moisture derivatives (dM/dt or dM/dx) by the temperature derivatives (dT/dt or dT/dx) over processing time or trough distance for peas tempered to various initial moisture contents (Figures 6.4.1 to 6.4.6). The regression curves have been described mathematically by power functions.

Mohamed et al. (2001) conducted IR processing experiments of peas and showed the mathematical expression for the moisture-temperature gradient by power function as shown in Eq. (6-7). The power index ranged from 3.6 to 3.8 for peas tempered to the moisture content of 25% wb. For the fixed-element configuration system, the processing time is a independent variable and the moisture-temperature gradient can be described as follows (Mohamed, 2003):

$$\frac{dM}{dT} = \left(\frac{dM}{dt}\right) \Big/ \left(\frac{dT}{dt}\right) = -10^{-8} t^{n} \tag{6-7}$$

For the moving-element configuration system, the moisture-temperature gradient was described with the same power function relationship as Eq.(6-7) over the trough distance:

$$\frac{dM}{dT} = \left(\frac{dM}{dx}\right) \Big/ \left(\frac{dT}{dx}\right) = -10^{-8} x^{n'} \tag{6-8}$$

where n and n' are power indices for the fixed-element and moving-element configuration system, respectively.

The power indices of Eq.(6-7) and (6-8) were tabulated in Table 4A-5 in Appendix IV.

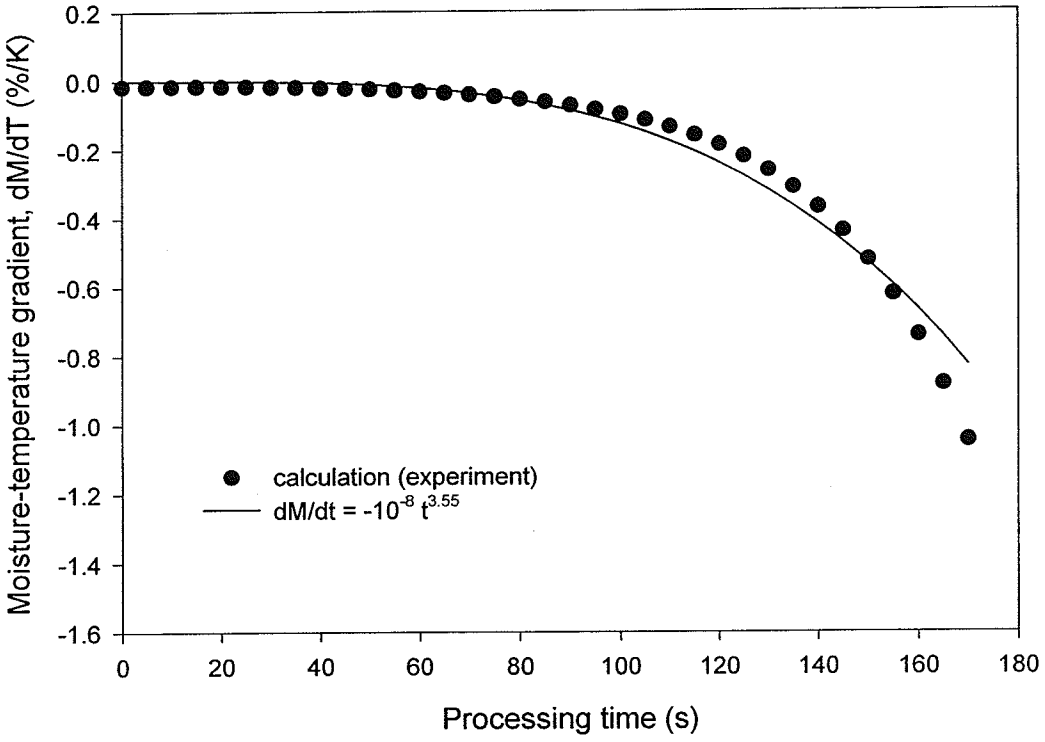

Figure 6.4.1 Moisture-temperature gradient (dM/dT) for peas tempered to 19.1% initial MC and micronized at the fixed-element configuration.

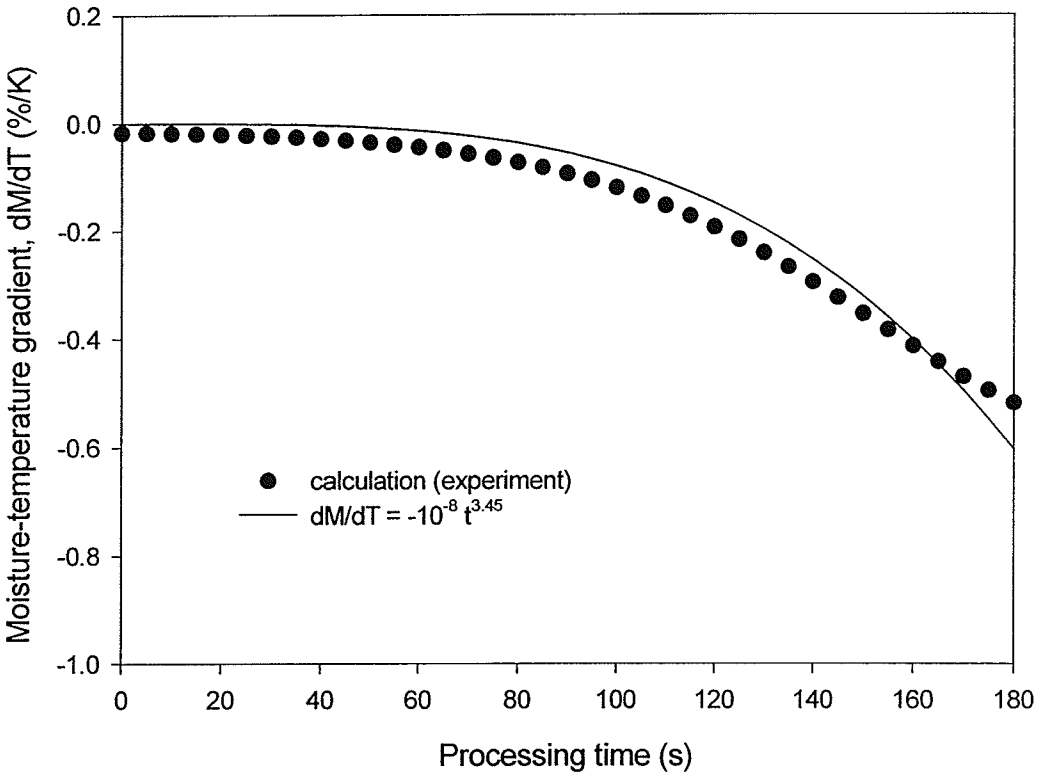

Figure 6.4.2 Moisture-temperature gradient (dM/dT) for peas tempered to 25.2% initial MC and micronized at the fixed-element configuration.

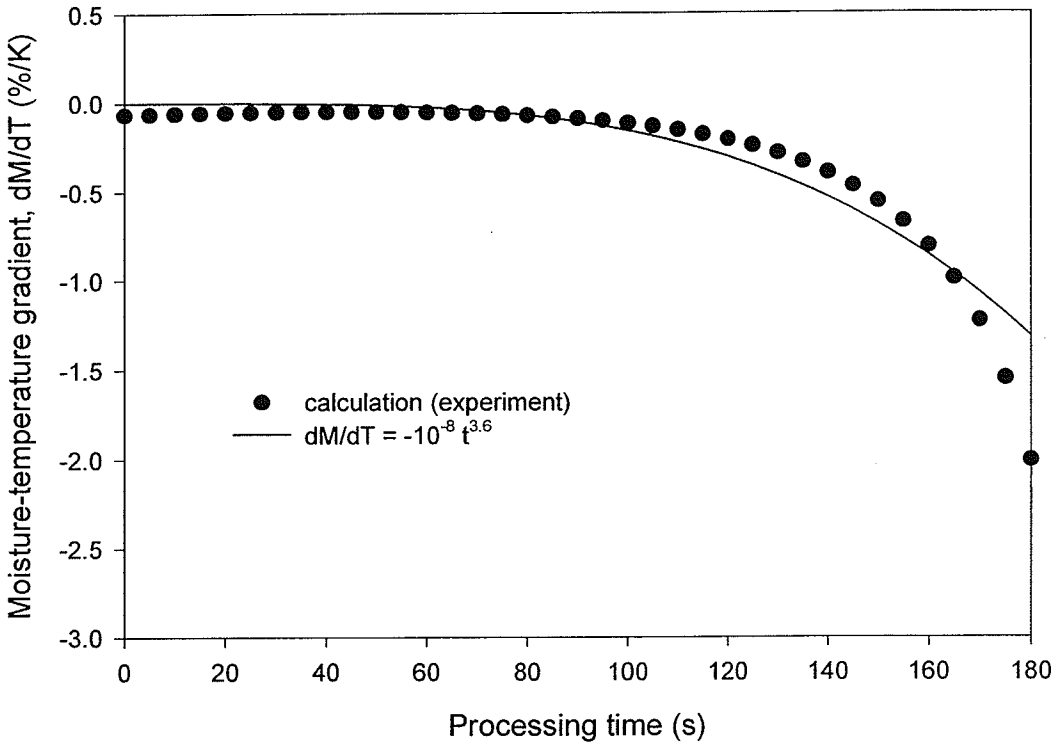

Figure 6.4.3 Moisture-temperature gradient (dM/dT) for peas tempered to 29.8% initial MC and micronized at the fixed-element configuration.

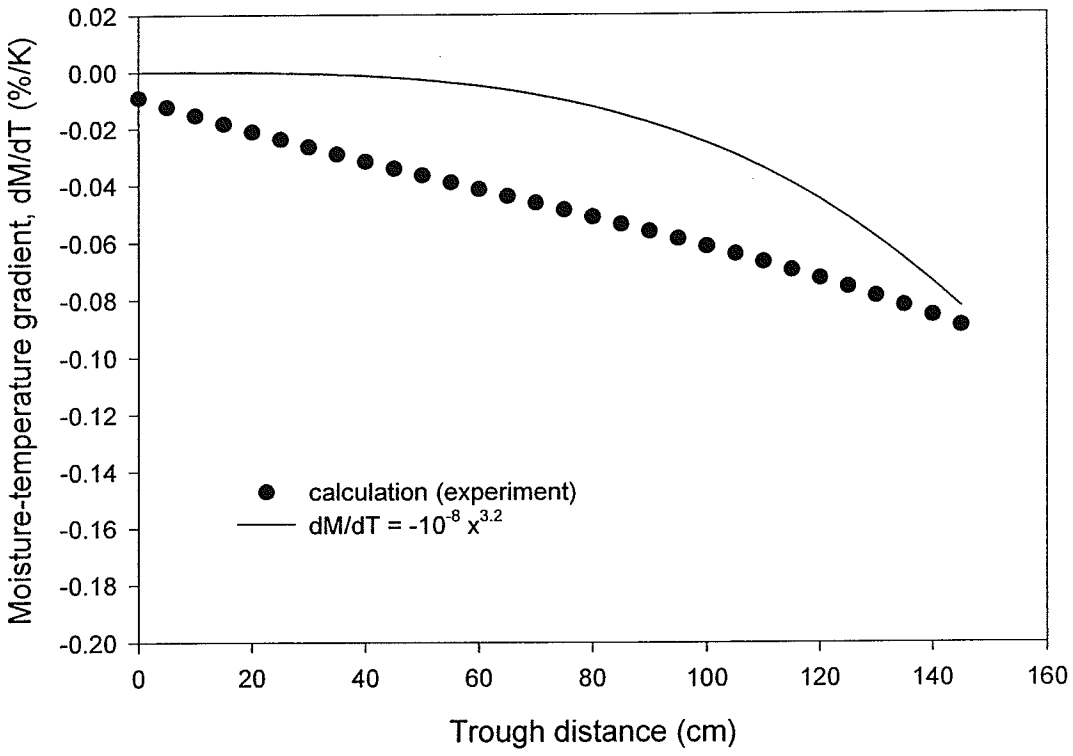

Figure 6.4.4 Moisture-temperature gradient (dM/dT) for peas tempered to 19.6% initial MC and micronized at the moving-element configuration.

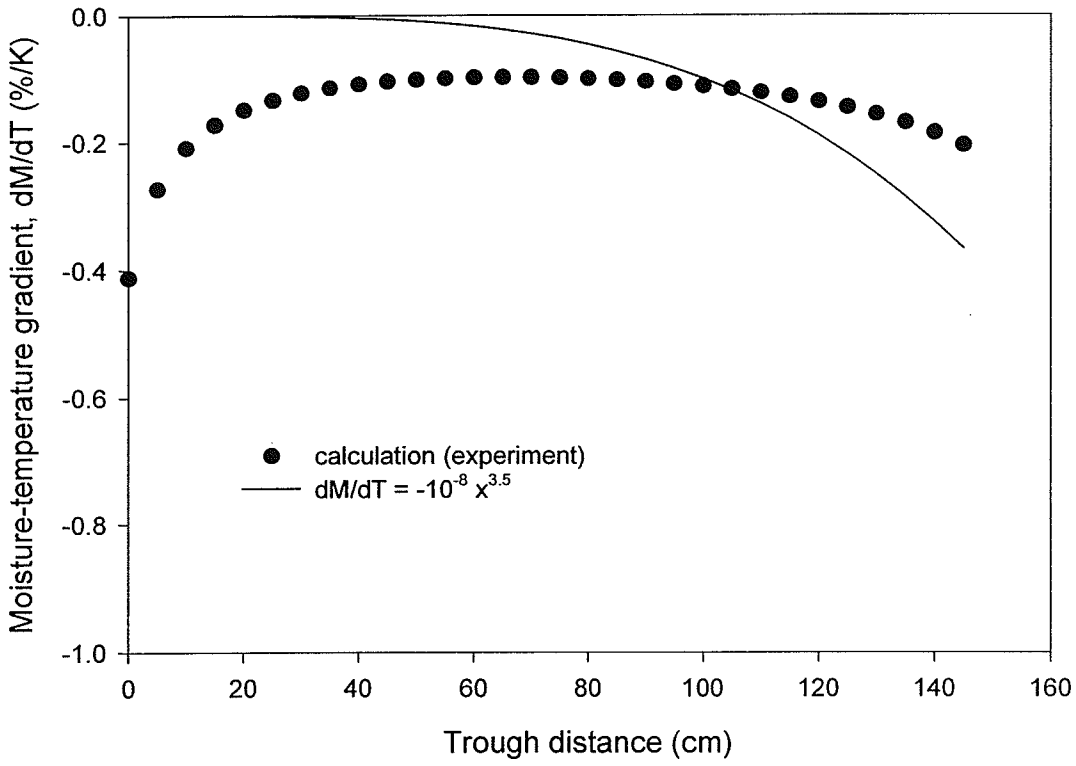

Figure 6.4.5 Moisture-temperature gradient (dM/dT) for peas tempered to 24.1% initial MC and micronized at the moving-element configuration.

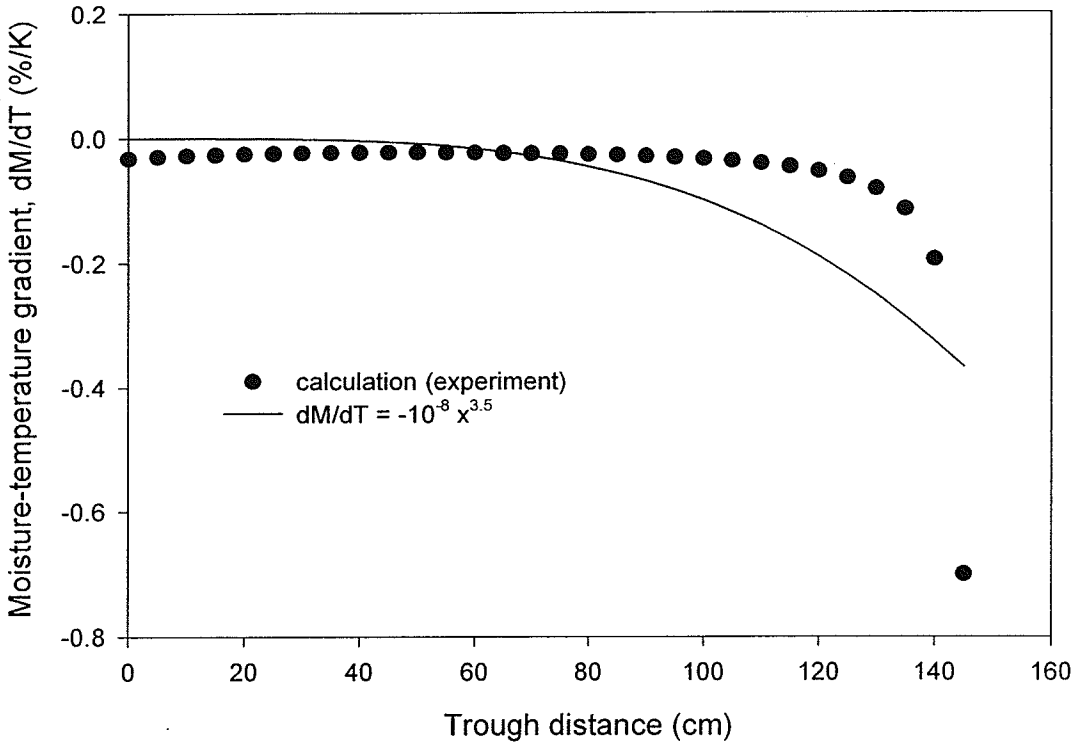

Figure 6.4.6 Moisture-temperature gradient (dM/dT) for peas tempered to 28.8% initial MC and micronized at the moving-element configuration.

The moisture gradient curve is very sensitive to the change of moisture and the temperature of the peas during micronization. Figure 6.4.1 and 6.4.3 show the regression curves of the moisture gradient for the 19.1 and 29.8% initial moisture peas during micronization for the fixed-element configuration experiments at the configuration factor of 0.67. The power index in Eq.(6-7) ranged from 3.45 to 3.60. For the moving-element configuration, the power index in Eq.(6-8) ranged from 3.2 to 3.5 with poor fit. The variability in the calculated results was substantial due to the sensitivity of the dM/dT relationship to the increments in dt or dx. Generally, the moisture increment in dx were very small at the entrance zone to the micronizer whereas the increment of pea temperature in dx is large at the entrance zone compared to the moisture increment. Most absorbed infrared energy into the peas contributes to increase the pea temperature (sensible heat) whereas the moisture evaporation from the peas are very small. This would be reflected in the moisture-temperature ratio giving small values at the entrance zone.

6-5 Inlet and Initial Conditions for the Models

In Chapter 3, heat and mass transfer equations were developed for the continuous IR process of granular materials for the moving-element configuration system and the fixed-element configuration system. The heat transfer equations have the form of a first order non-linear differential equation and require the initial and entrance condition of the micronizer to be solved. For the present study, the feed material is assumed to have a uniform moisture content and temperature at the inlet to the micronizer. Thus, the inlet conditions for the moving-element configuration model is:

$$M=M_0 \quad \text{and} \quad T=T_0 \quad \text{at} \quad x=0 \tag{6-9}$$

At the exit from the vibratory conveyor of the micronizer, the mass flowrate of the feed in wet basis is measured to evaluate the dry mass flowrate of the feed. Therefore, the exit conditions are described as follows:

$$\dot{m} = \dot{m}_L \quad \text{and} \quad M = M_L \quad \text{at} \quad x = L \tag{6-10}$$

where L= length of the vibratory conveyor.

In case of the fixed-element configuration model, initial conditions are needed to solve the first order non-linear differential equation [Eq.(3-39)] for the fixed-element configuration model and can be expressed as:

$$M=M_0 \quad \text{and} \quad T=T_0 \quad \text{at} \quad t=0 \tag{6-11}$$

6-6 Effect of Emissivity on Temperature Prediction

6-6-1 Fixed-element configuration system

The prediction of temperature by the developed models requires several parameters such as emissivity of the materials in the enclosures (peas, emitter surfaces, trough), and other operating parameters, such as, the surface temperature of the emitter and the bottom trough, coverage of the feed material, its average residence time, mass flowrate, and moisture content change during IR operation. Parameters used in the simulation are shown in Table 6.6.1. The emissivity data (hemispherical-total emissivity) for yellow peas are not available in the literature. Due to this reason, the emissivity values for yellow peas were chosen as 0.7, 0.8, 0.9, and 0.95 for the simulation to see the effect of the emissivity variation because biological materials have high emissivity (usually higher than 0.7) compared to metals or other materials (Sala, 1986; Singham, 1962). Also, according to Fasina and Tyler (2001) in IR process calculations when the emissivity of agricultural products is unknown, frequently 0.9 is assigned for the emissivity. The computer simulation of micronization was conducted with two methods of numerical solution for the model [Eq.(3-30) and Eq.(3-39)]: i) The Runge-Kutta 4th order method (the R-K method), and ii) the Euler method. In both methods a programming tool in 'Sigmaplot 5.0' was used (Appendix VI). Figures 6.6.1 to 6.6.3 show that simulation results of temperature and moisture prediction by the model using the Runge-Kutta 4th order method for the emissivity values in the range from 0.7 to 0.95. Figures 6.6.1c, 6.61d, 6.6.2c, 6.6.2d, 6.6.3c, and 6.6.3d show the plots of temperature and moisture content residuals which represent the difference between the predicted results by the fixed-element configuration model and the experimental results. The predicted temperature and moisture content by the model showed good agreement with the experimental results when the emissivity of yellow peas was in the range

between 0.9 and 0.95 with the maximum standard deviation of 6.6°C and 1.9% wb, respectively. The results of standard deviation for the residuals in the fixed-element configuration model for temperature and moisture content predictions are given in Table 6.6.3.

Table 6.6.1 Parameters and operating conditions used in the simulation of a fixed-element configuration.

Parameters	Values	Unit
Φ	0.44	[-]
ε_S	$0.7 \leq \varepsilon_S \leq 0.95$ (1)	[-]
ε_1	0.25 (2)	[-]
ε_2	1.00	[-]
ε_5	0.20 (2)	[-]
σ	5.67×10^{-8} (3)	$W/(m^2 K^4)$
T_1	1003	K
T_2	298	K
T_5	433	K
C_P	2407 (4)	J/(kg K)
h_{fg}	2257×10^3 (5)	J/kg
W	0.265	m
H	0.12	m
F_{d3-1}	0.67	[-]
m_d	0.115	kg

(1) Sala (1986), (2) Singham (1962), (3) Siegel and Howell (1992), (4) Pabis et al. (1998), and (5) Felder and Rousseau (2000).

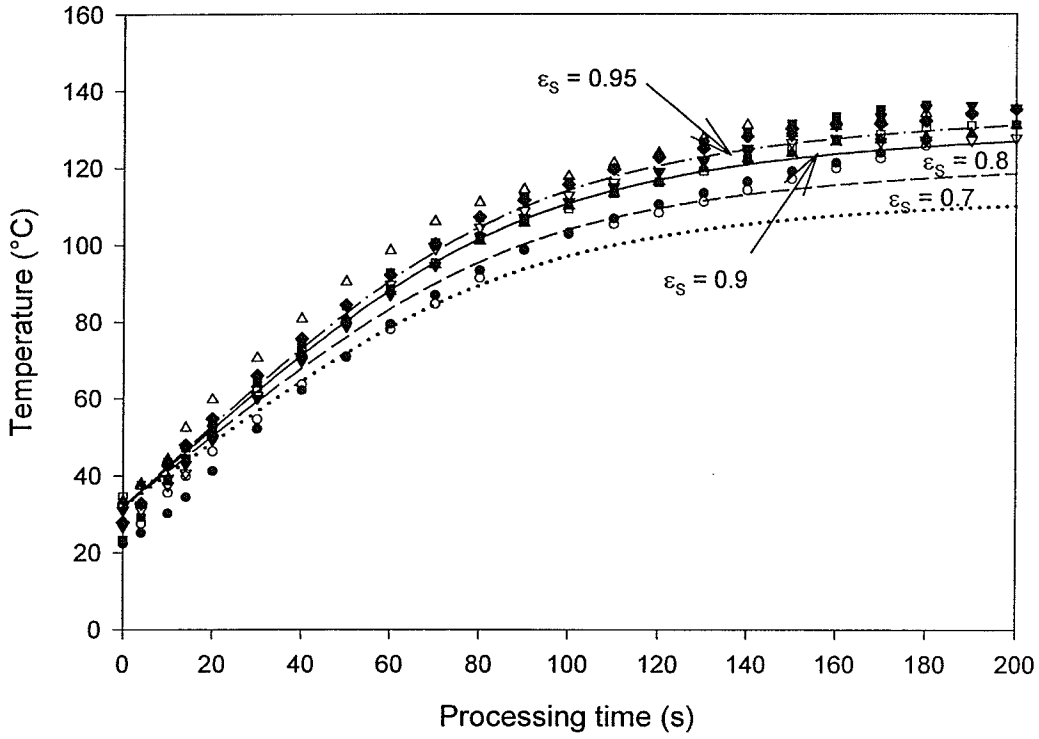

Figure 6.6.1a Validation of the simulation results (lines) by the Runge-Kutta method with experimental data (symbols) for temperatures of peas at 19.1% initial MC and exposed to micronization (fixed-element configuration). The same symbols indicate data obtained from one experiment.

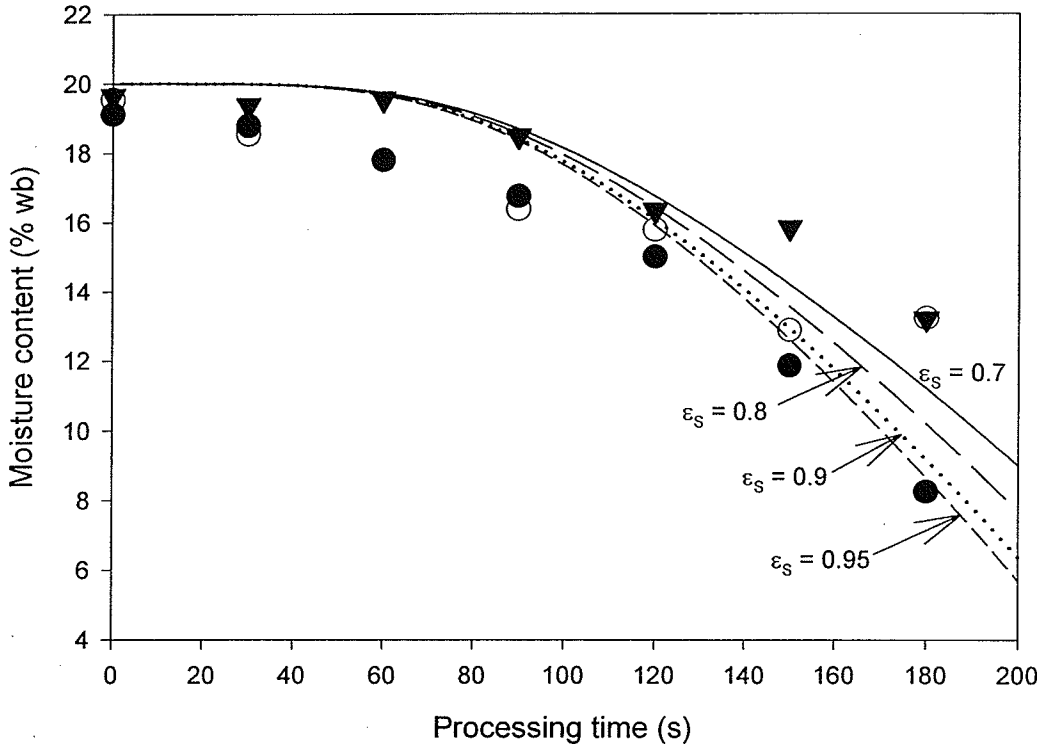

Figure 6.6.1b Validation of the simulation results (lines) by the Runge-Kutta method with experimental data (symbols) for moisture change of peas at 19.1% initial MC and exposed to micronization (fixed-element configuration). The same symbols indicate data obtained from one experiment.

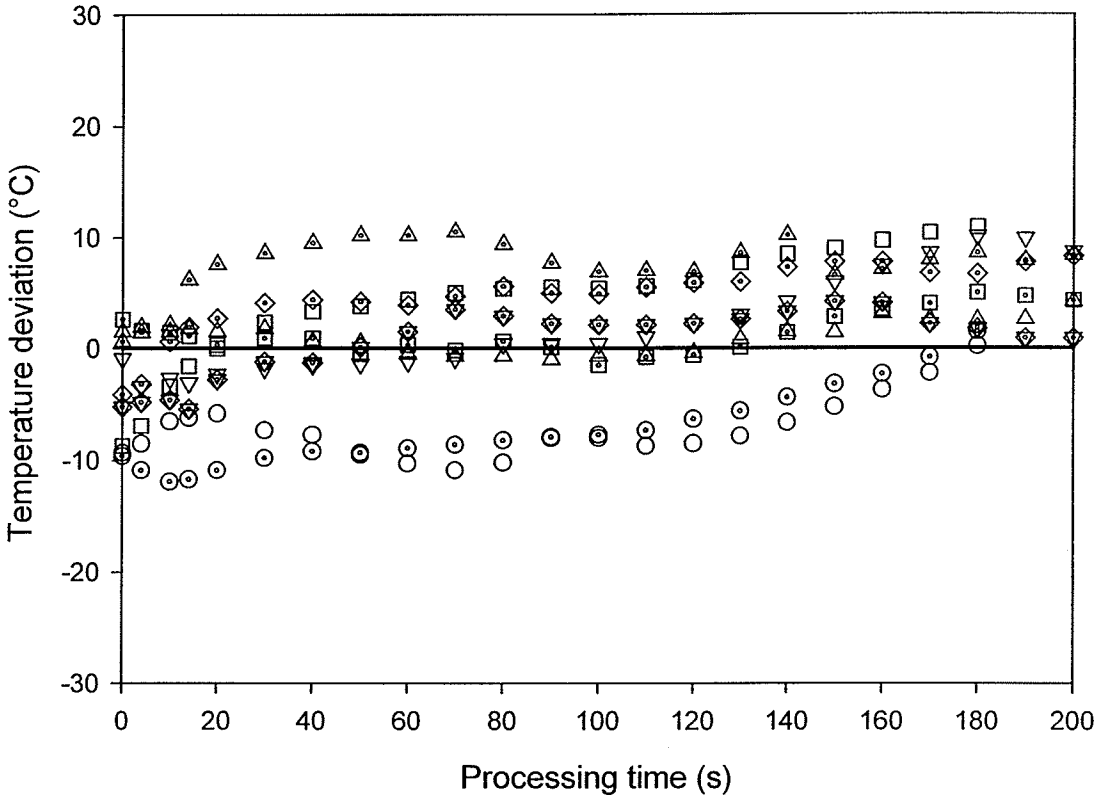

Figure 6.6.1c Temperature deviation of the experimental data of yellow peas tempered to 19.1% initially from the temperature predicted by the fixed-element configuration model. The temperature which was predicted t by the model was set to zero as reference values when the emissivity of yellow peas was set at 0.9 for the calculation of temperature deviation.

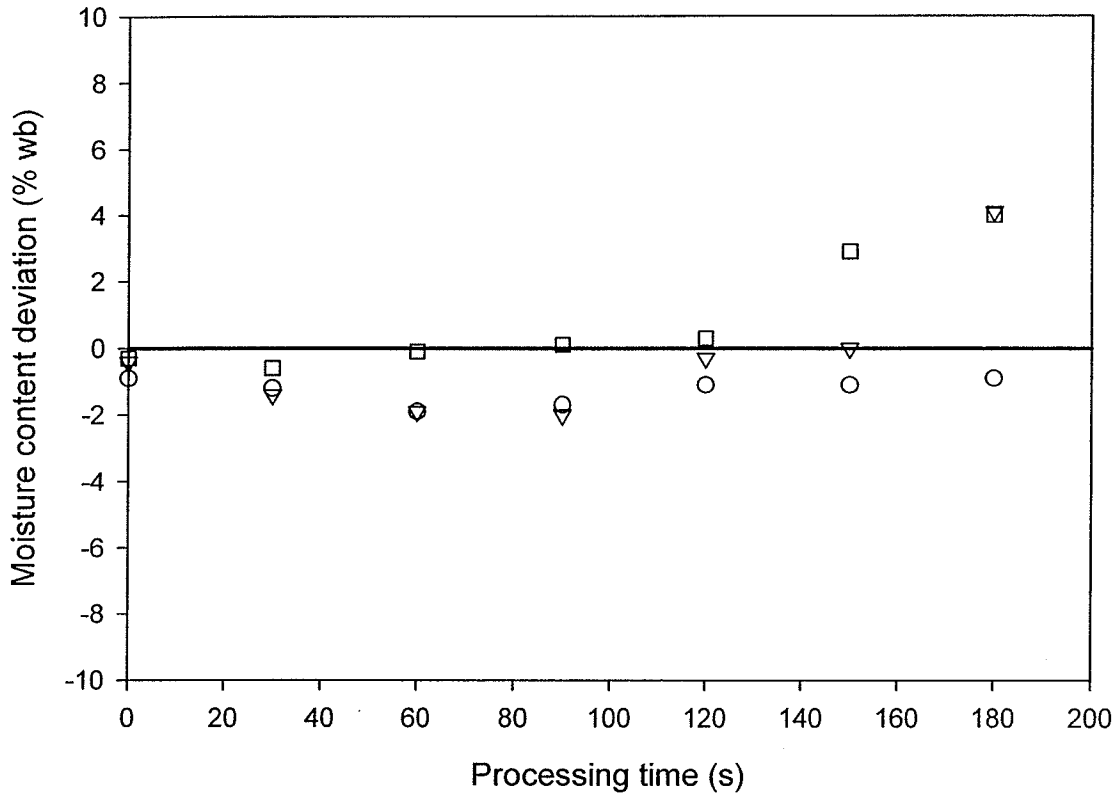

Figure 6.6.1d Moisture content deviation of the experimental data of yellow peas tempered to 19.1% initially from the temperature predicted by the fixed-element configuration model. The moisture content which was predicted by the model was set to zero as reference values when the emissivity of yellow peas was set at 0.9 for the calculation of moisture content deviation.

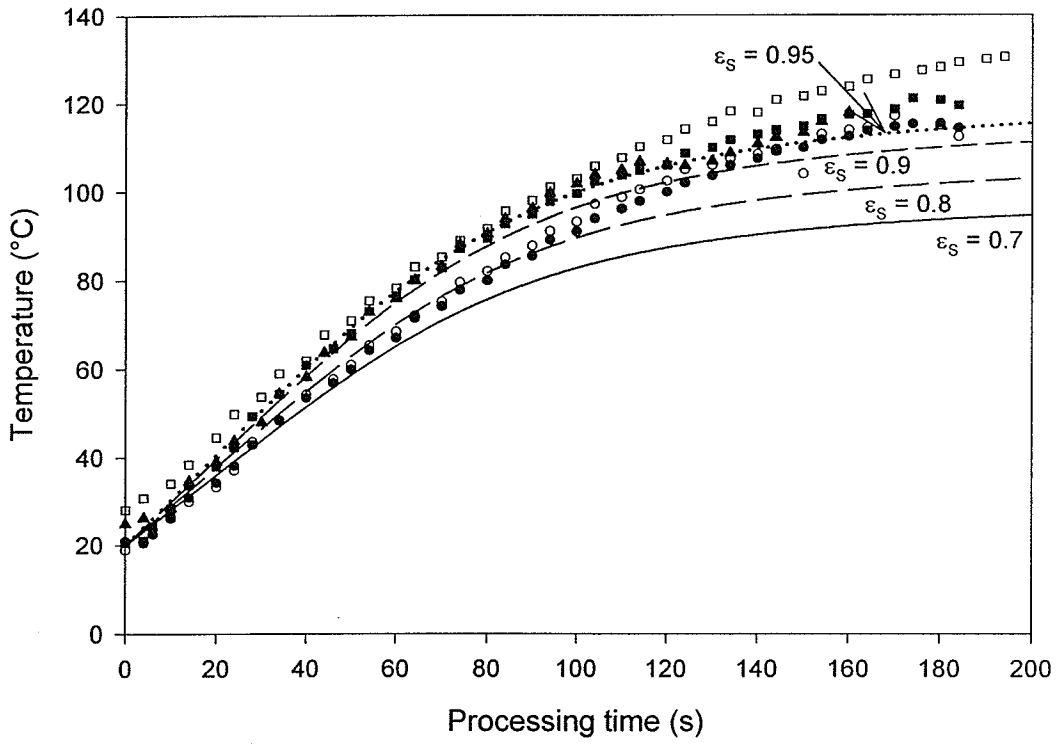

Figure 6.6.2a Validation of the simulation results (lines) by the Runge-Kutta method with experimental data (symbols) for temperatures of peas at 25.2% initial MC and exposed to micronization (fixed-element configuration). The same symbols indicate data obtained from one experiment.

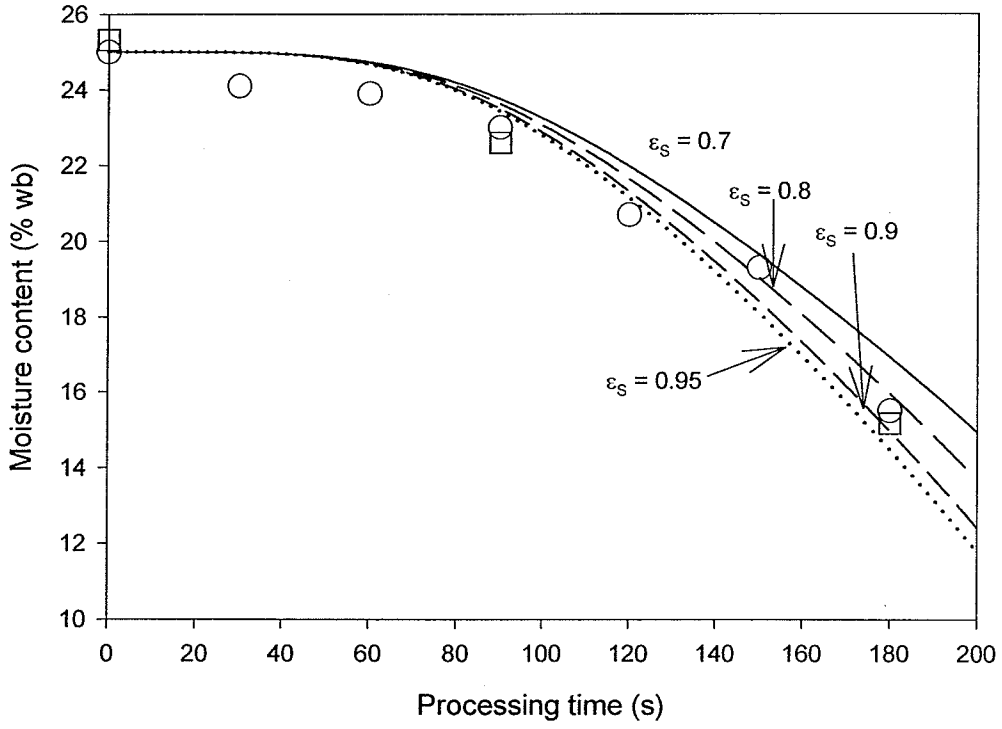

Figure 6.6.2b Validation of the simulation results (lines) by the Runge-Kutta method with experimental data (symbols) for moisture change of peas at 25.2% initial MC and exposed to micronization (fixed-element configuration). The same symbols indicate data obtained from one experiment.

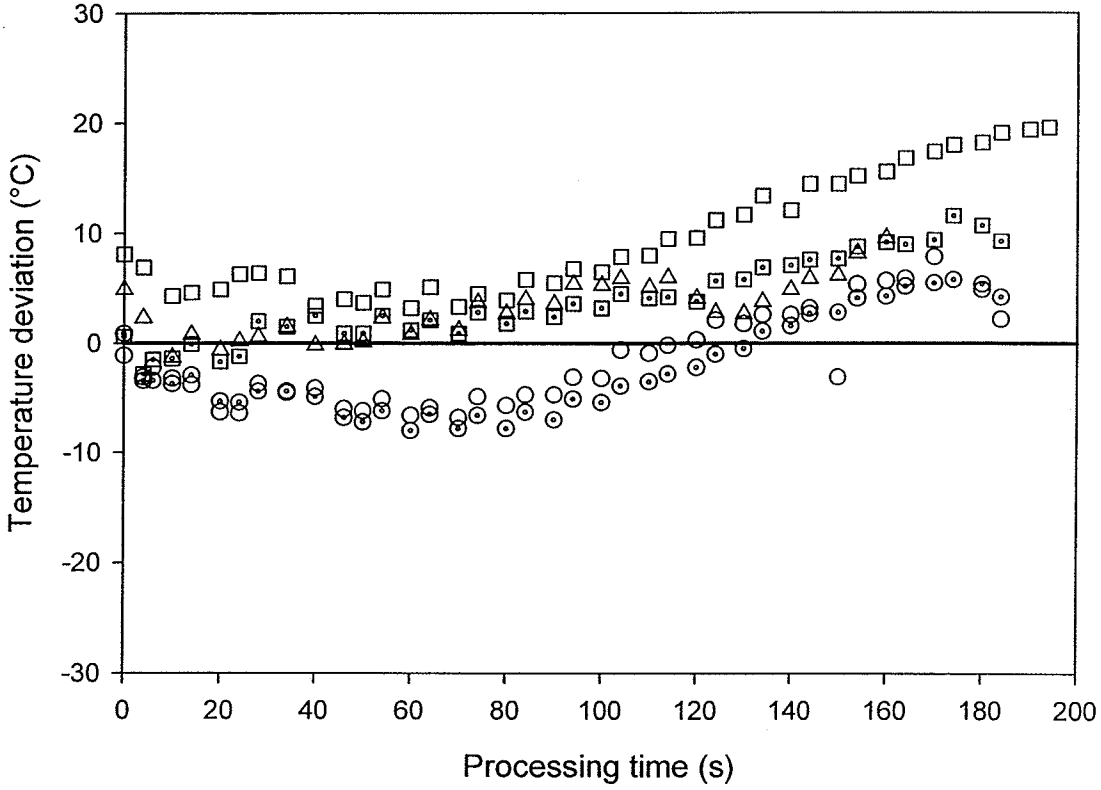

Figure 6.6.2c Temperature deviation of the experimental data of yellow peas tempered to 25.2% initial MC from the temperature predicted by the fixed-element configuration model. The temperature which was predicted by the model was set to zero as reference values when the emissivity of yellow peas was set at 0.9 for the calculation of temperature deviation.

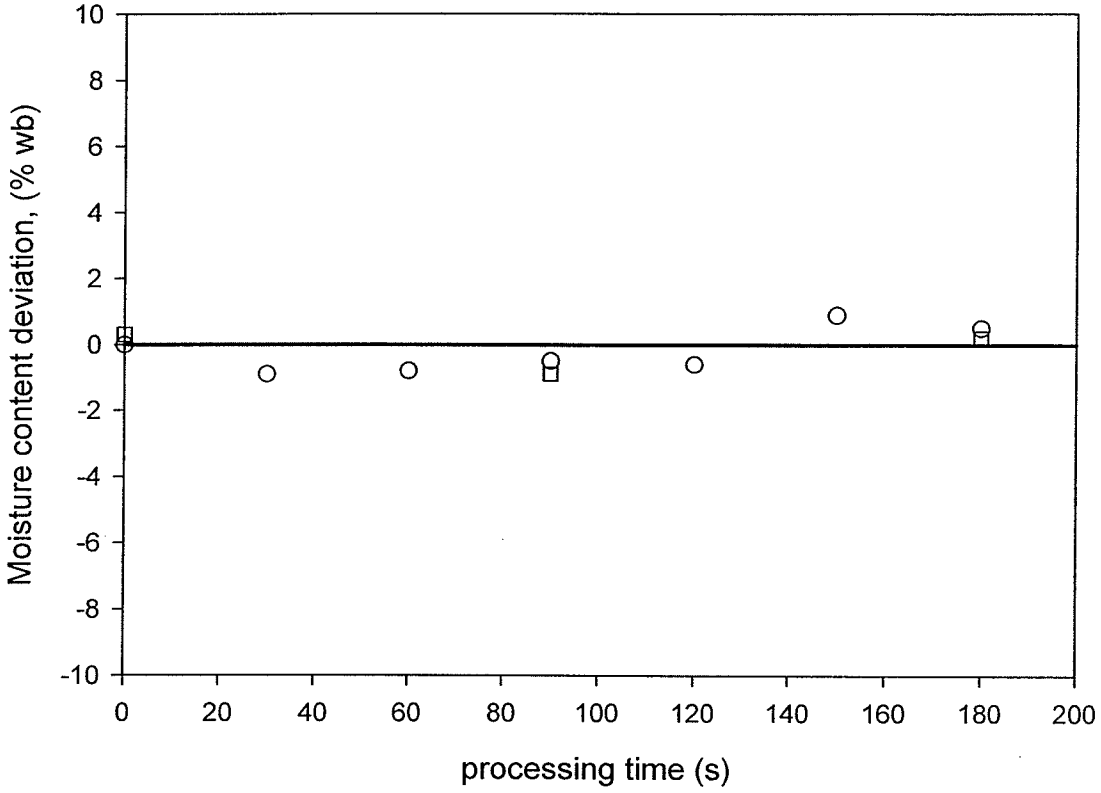

Figure 6.6.2d Moisture content deviation of the experimental data of yellow peas tempered to 25.2% initially from the temperature predicted by the fixed-element configuration model. The moisture content which was predicted by the model was set to zero as reference values when the emissivity of yellow peas was set at 0.9 for the calculation of moisture content deviation.

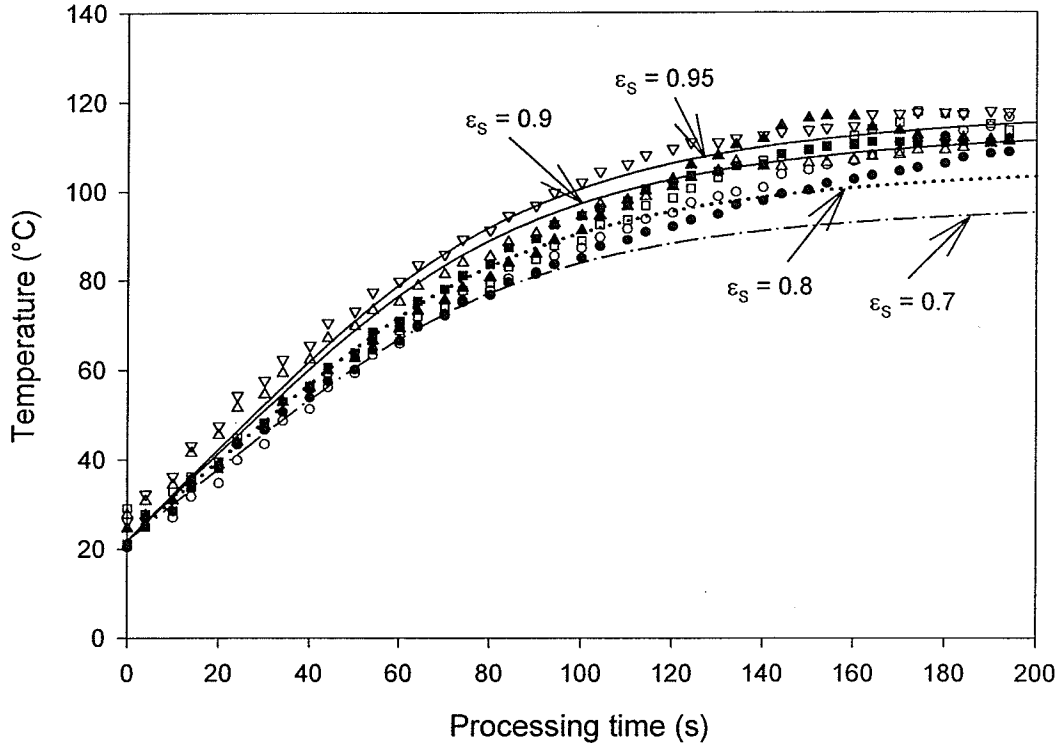

Figure 6.6.3a Validation of the simulation results (lines) by the Runge-Kutta method with experimental data (symbols) for temperatures of peas at 29.8% initial MC and exposed to micronization (fixed-element configuration). The same symbols indicate data obtained from one experiment.

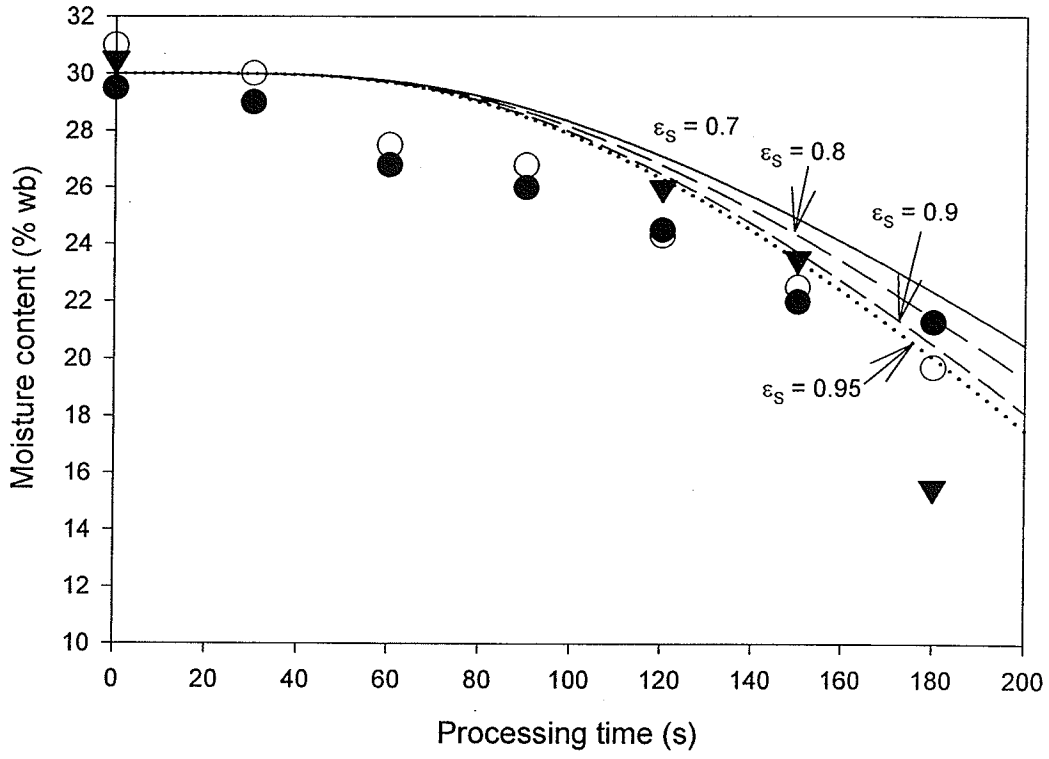

Figure 6.6.3b Validation of the simulation results (lines) by the Runge-Kutta method with experimental data (symbols) for moisture change of peas at 29.8% initial MC and exposed to micronization (fixed-element configuration). The same symbols indicate data obtained from one experiment.

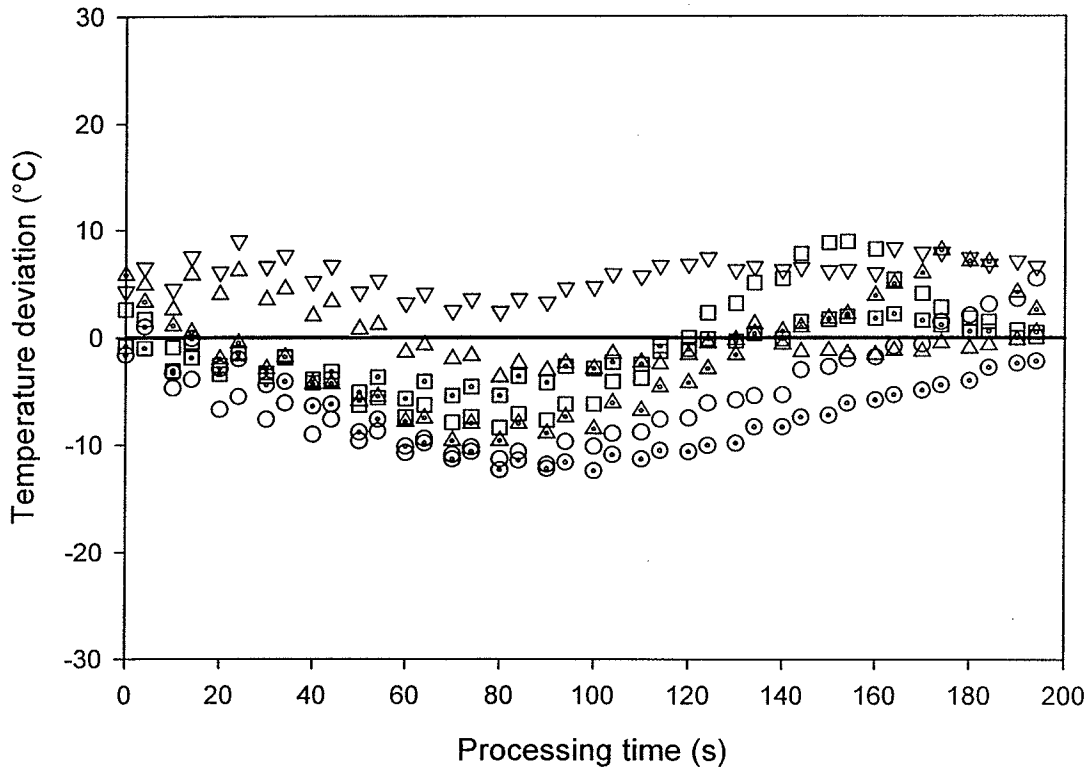

Figure 6.6.3c Temperature deviation of the experimental data of yellow peas tempered to 29.8% initially from the temperature predicted by the fixed-element configuration model. The temperature which was predicted by the model was set to zero as reference values when the emissivity of yellow peas was set at 0.9 for the calculation of temperature deviation.

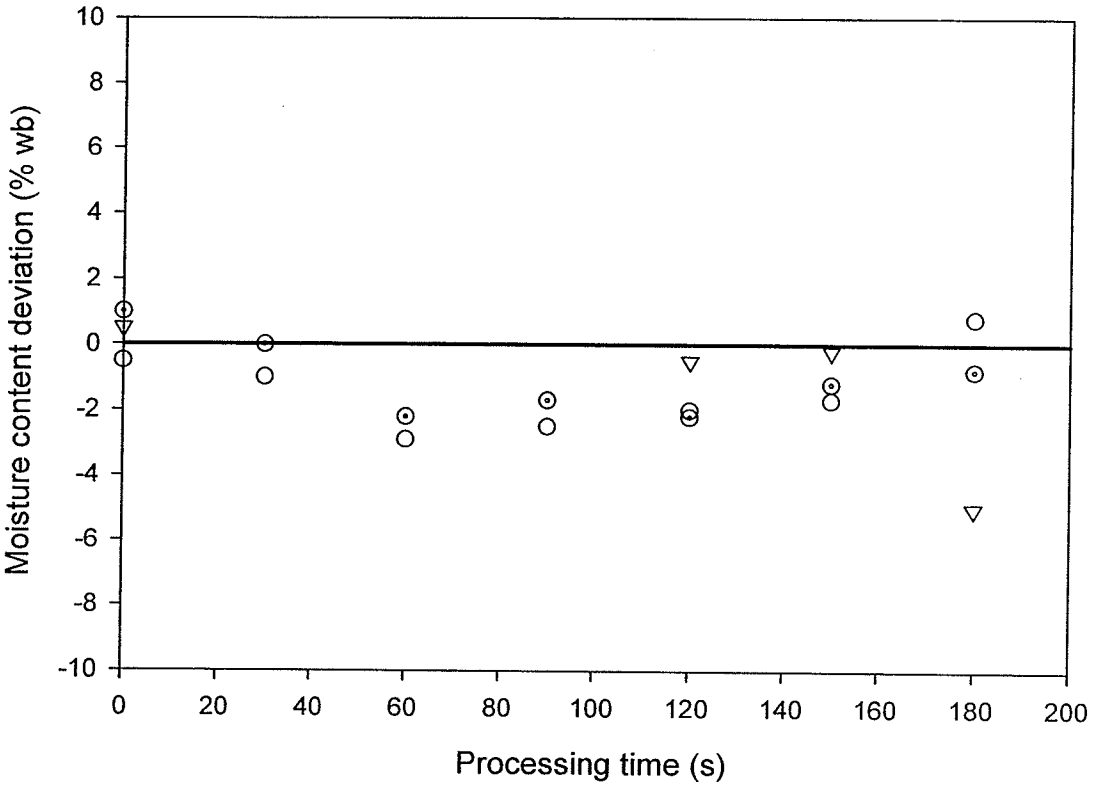

Figure 6.6.3d Moisture content deviation of the experimental data of yellow peas tempered to 29.8% initially from the temperature predicted by the fixed-element configuration model. The moisture content which was predicted by the model was set to zero as reference values when the emissivity of yellow peas was set at 0.9 for the calculation of moisture content deviation.

To see the effect of the numerical analysis algorithm, the temperature results predicted by the Euler method are shown in Figure 6.6.4a. The temperature results with successive simulations showed a big discrepancy with the experimental results for emissivities between 0.7 and 0.95. The Runge-Kutta 4th order method (the R-K method) is well known for its high accuracy in the solution of differential equations compared to the Euler method (Chapra and Canale, 1989). The temperature prediction by the model of the fixed-element configuration system represented good agreement to the experimental results when the emissivity of yellow pea was higher than 0.9 and when it was solved with the R-K method. The predicted moisture by the R-K method showed a little higher values than the experimental results.

6-6-2 Moving-element configuration system

The temperature of peas traveling along the trough during micronization for the moving-element configuration was predicted by the model (Eq.(3-30)) and showed good agreement with the experimental results (Figures 6.6.5a, 6.6.6a, and 6.6.7a). The moisture-temperature gradient was approximated by power functions. In Figure 6.6.6a, the temperature was calculated for moisture-temperature gradients with different emissivity values of peas. The power function approximation of dM/dT did not give a good fit (not shown in Figure 6.6.6a) for the experimental data of the 24.1% initial moisture content. The temperature prediction by the model showed satisfactory results with the experimental results when the emissivity of peas was higher than 0.8. On the contrary, moisture prediction by the model which included the approximation functions of the moisture-temperature gradient was not as good as the temperature prediction by the model and did not change much with the change in the emissivity of peas. The approximation functions of the moisture-temperature gradient are shown in Table 6.6.2 and the power index (n-value in the power function) being in

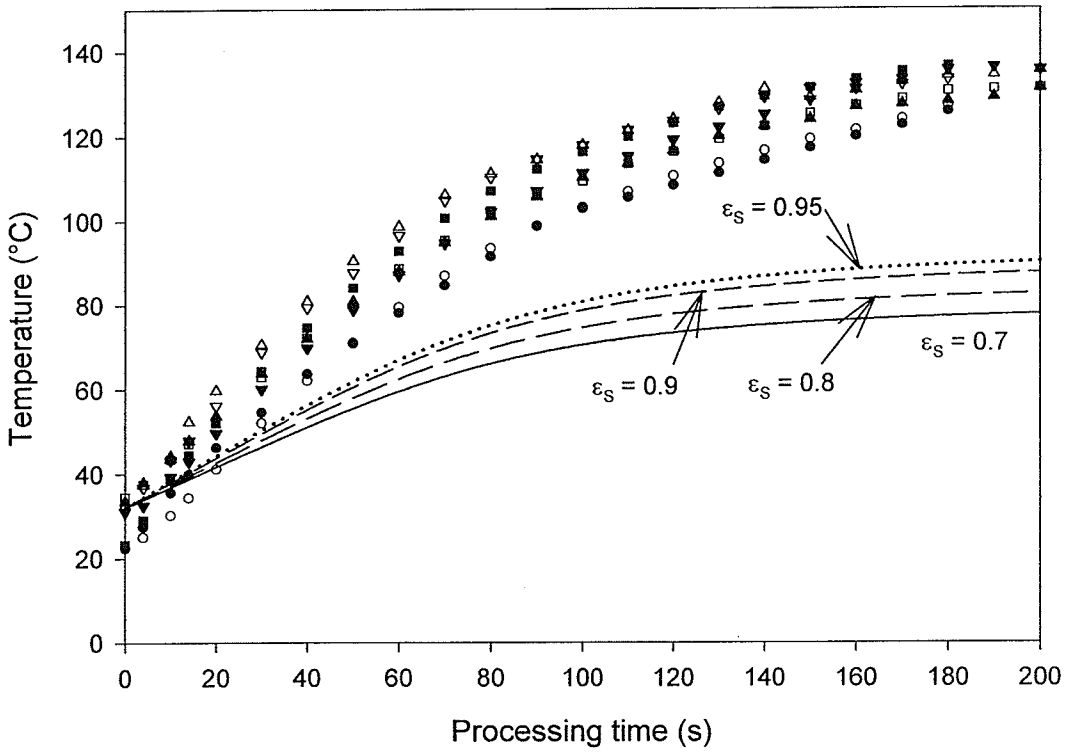

Figure 6.6.4a Validation of the simulation results (lines) by the Euler method with experimental data (symbols) for temperatures of peas at 19.1% initial MC and exposed to micronization (fixed-element configuration). The same symbols indicate data obtained from one experiment.

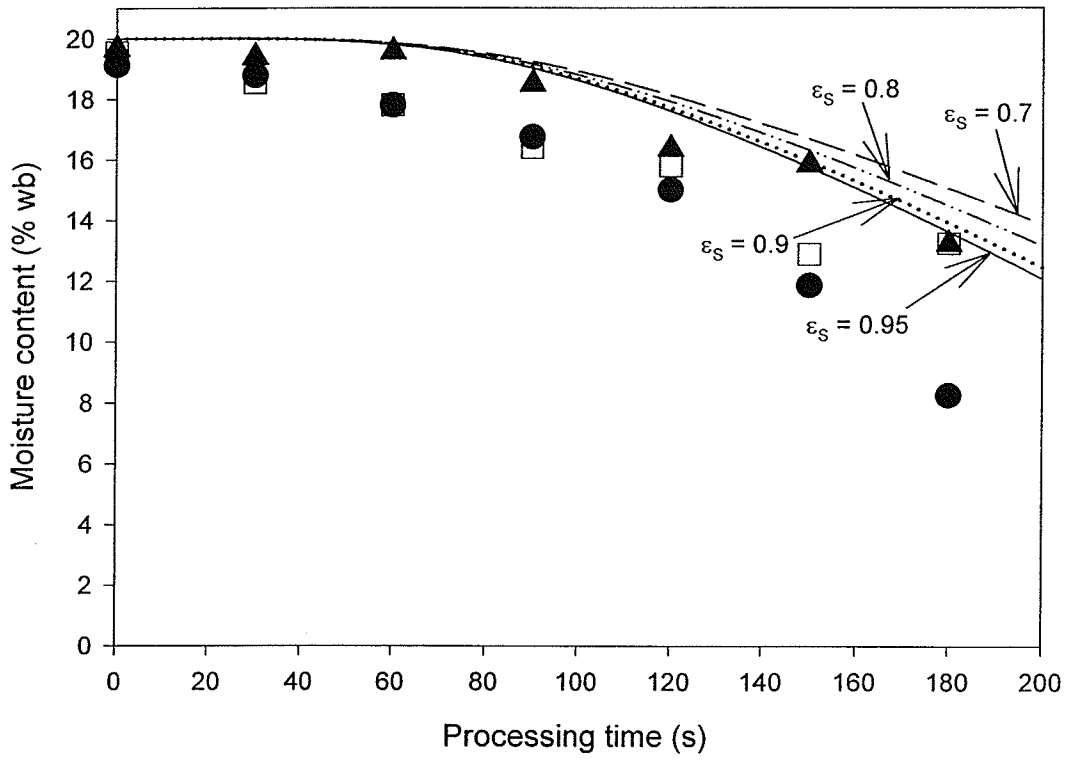

Figure 6.6.4b Validation of the simulation results(lines) by the Euler method with experimental data (symbols) for moisture change of peas at 19.1% initial MC and exposed to micronization (fixed-element configuration). The same symbols indicate data obtained from one experiment.

the range from 3.2 to 3.5 showed a satisfactory temperature prediction by the model. The deviations of the temperature and moisture content predictions from the experimental data for the moving-element configuration model are shown in Figures 6.6.5c, 6.6.5d, 6.6.6c, 6.6.6d, 6.6.7c, and 6.6.7d. Temperature prediction by the model showed good agreement with the experimental results with 7.2°C of standard deviation on temperature residuals whereas the moisture content prediction by the model resulted in the standard deviation with respect to the residual moisture of 0.8% wb. The values of the standard deviations for residual temperatures and moisture contents are shown in Table 6.6.3 for three initial moisture contents of tested yellow peas.

Table 6.6.2 Approximation functions for the moisture-temperature gradient (moving-element configuration).

Moisture content, (% wb)	Approximation function for dM/dT	Power index (n)
19.6	$-10^{-8} x^n$	3.2
24.1	$-10^{-8} x^n$	3.5
28.8	$-10^{-8} x^n$	3.5

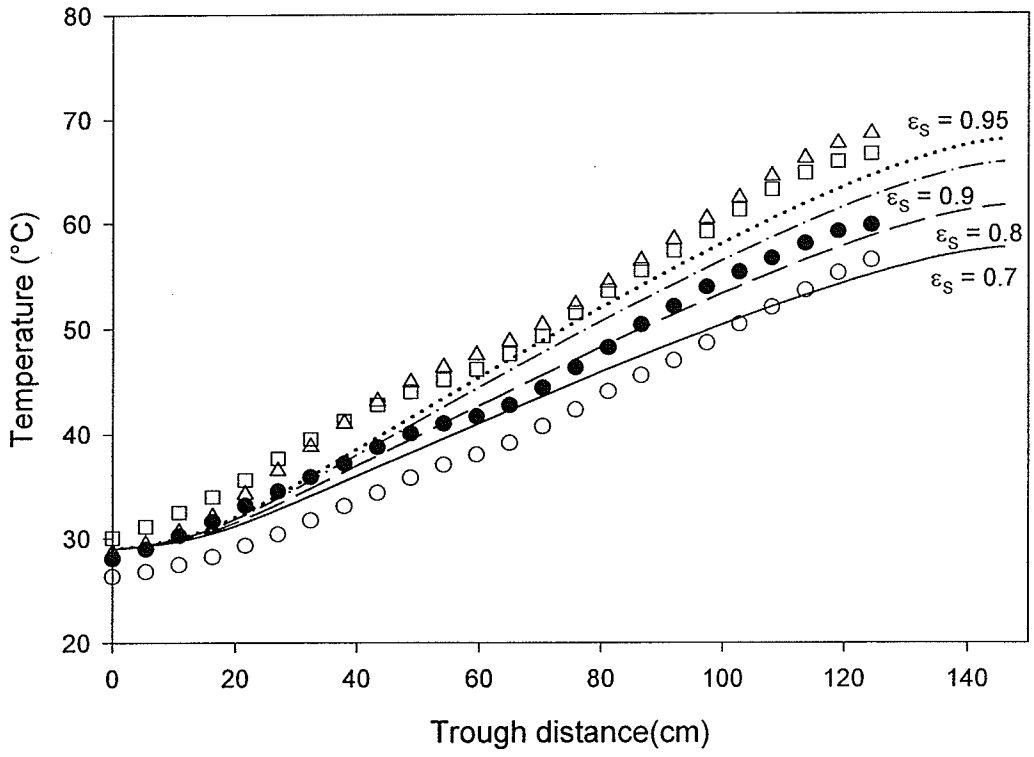

Figure 6.6.5a Validation of the simulation results(lines) by the Runge-Kutta method with experimental data (symbols) for temperatures of peas at 19.6% initial MC and exposed to micronization (moving-element configuration, $dM/dT = -10^{-8} x^{3.2}$). The same symbols indicate data obtained from one experiment.

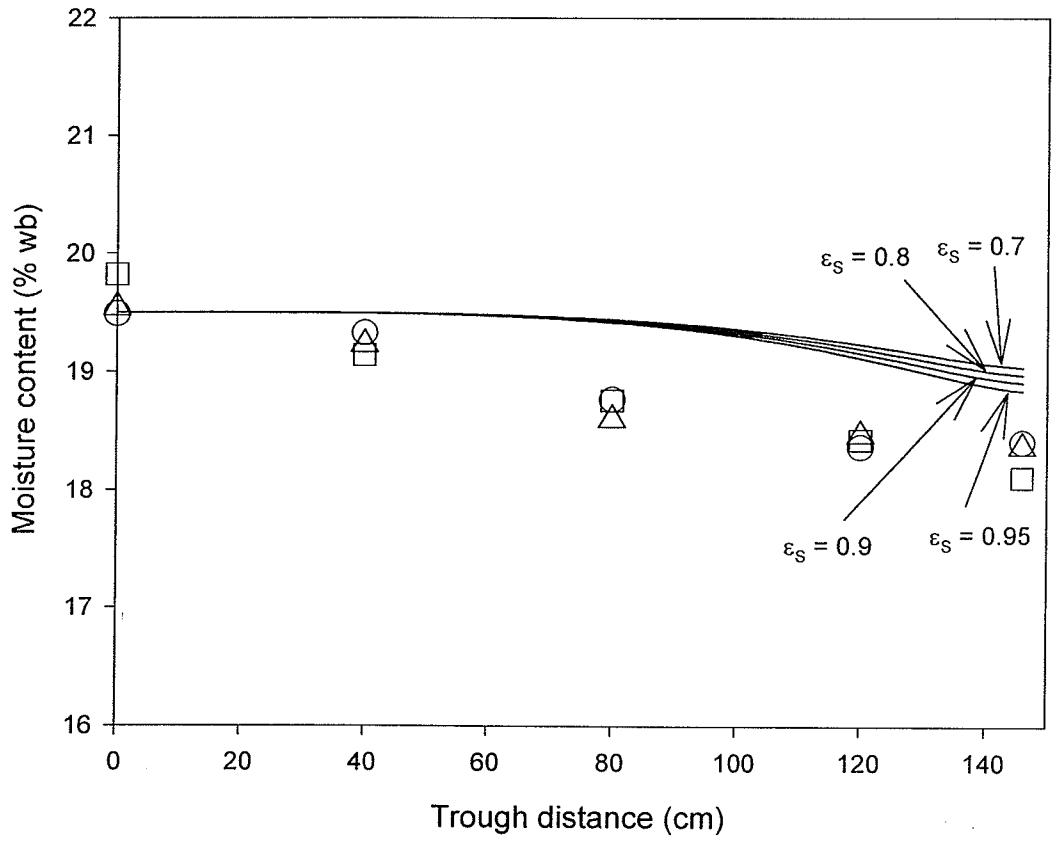

Figure 6.6.5b Validation of the simulation results (lines) by the Runge-Kutta method with experimental data (symbols) for moisture change of peas at 19.6% initial MC and exposed to micronization (moving-element configuration, $dM/dT = -10^{-8} x^{3.2}$). The same symbols indicate data obtained from one experiment.

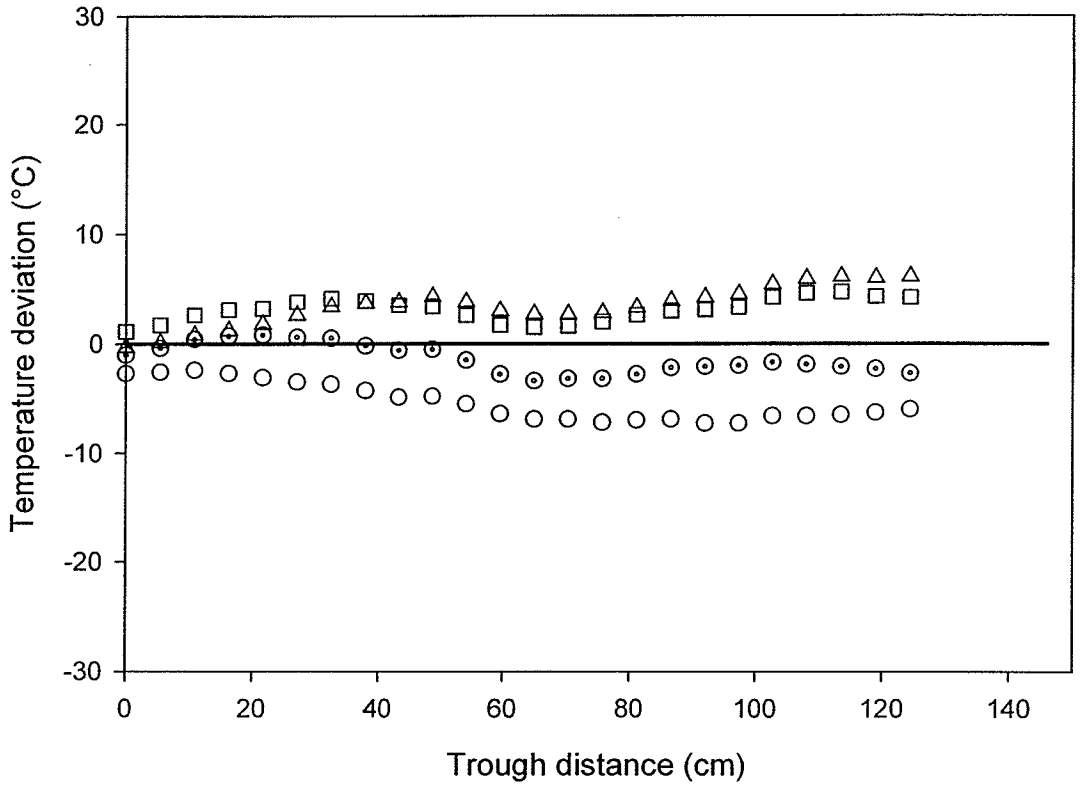

Figure 6.6.5c Temperature deviation of the experimental data of yellow peas tempered to 19.6% initially from the temperature predicted by the moving-element configuration model. The temperature which was predicted by the model was set to zero as reference values when the emissivity of yellow peas was set at 0.9 for the calculation of temperature deviation.

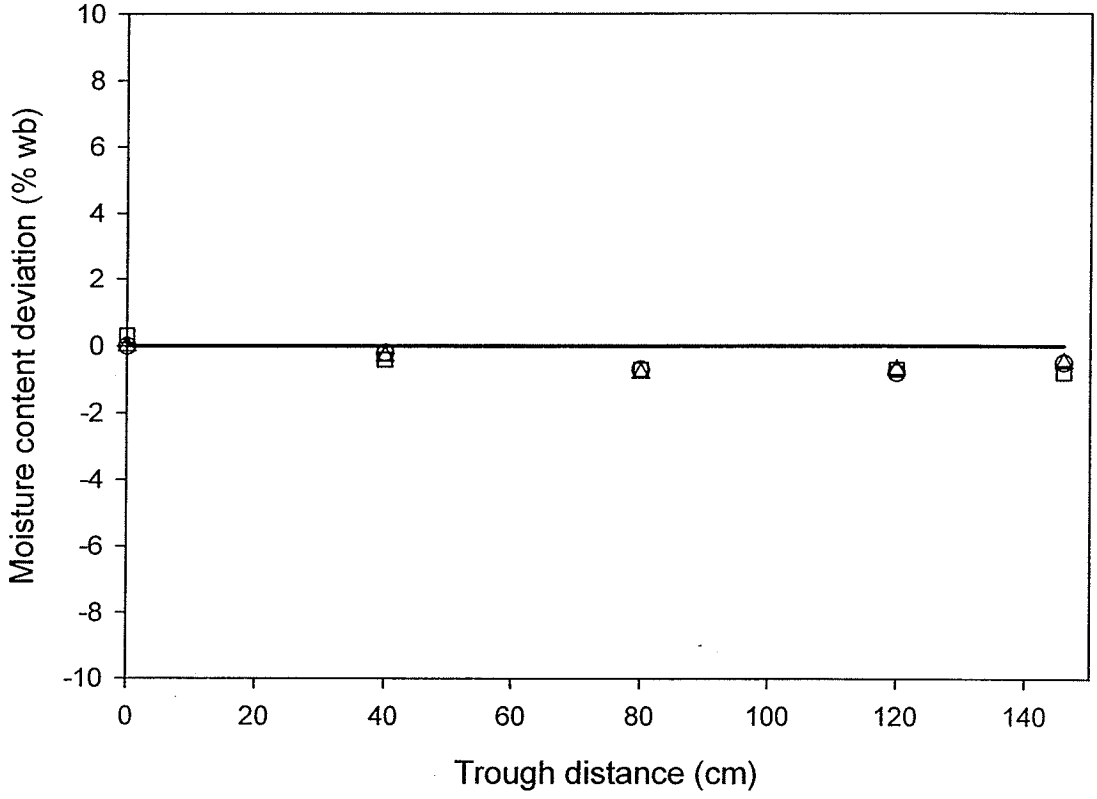

Figure 6.6.5d Moisture content deviation of the experimental data of yellow peas tempered to 19.6% initially from the temperature predicted by the moving-element configuration model. The moisture content which was predicted by the model was set to zero as reference values when the emissivity of yellow peas was set at 0.9 for the calculation of moisture content deviation.

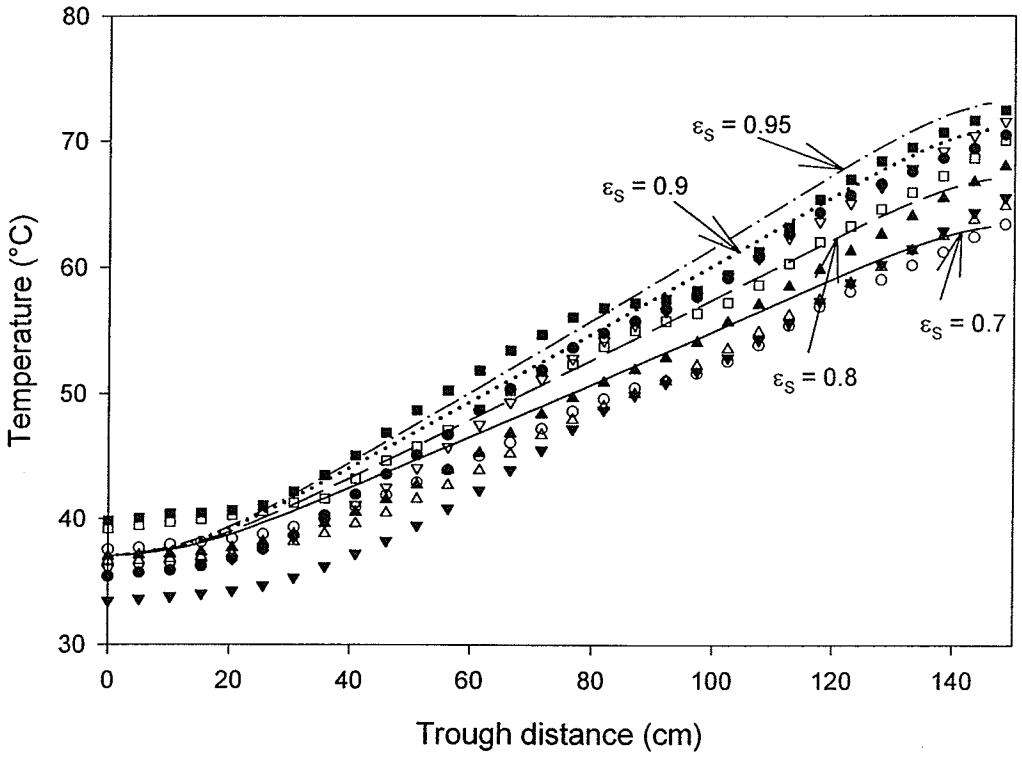

Figure 6.6.6a Validation of the simulation results (lines) by the Runge-Kutta method with experimental data (symbols) for temperatures of peas at 24.1% initial MC and exposed to micronization (moving-element configuration, $dM/dT = -10^{-8} x^{3.5}$). The same symbols indicate data obtained from one experiment.

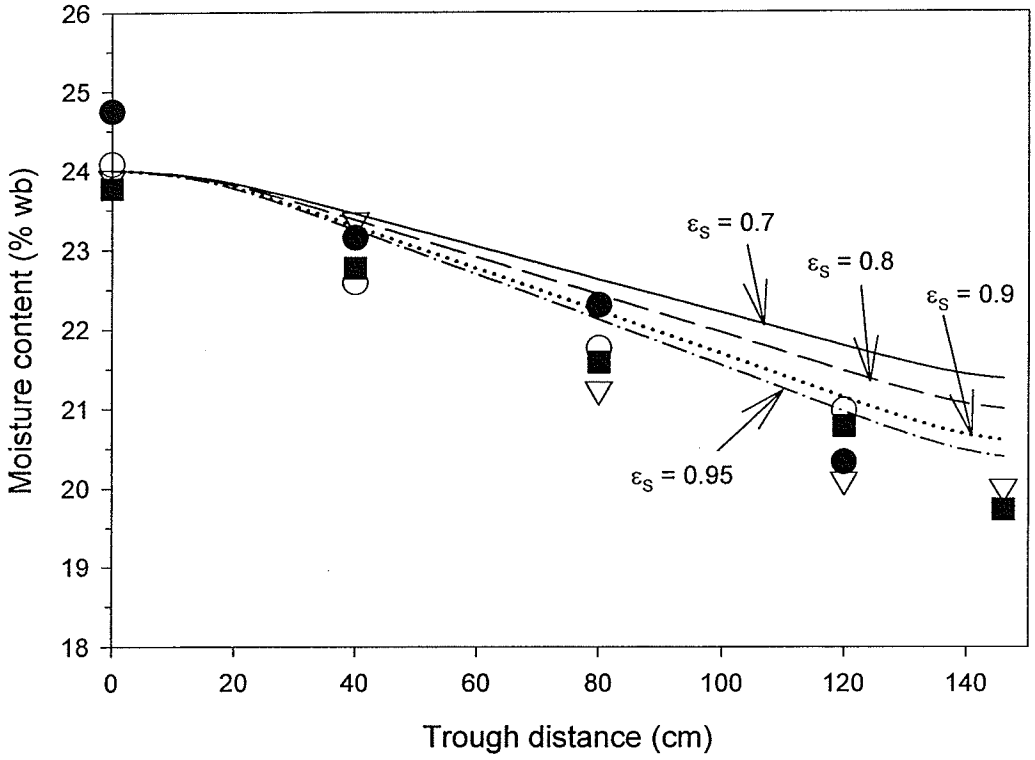

Figure 6.6.6b Validation of the simulation results (lines) by the Runge-Kutta method with experimental data (symbols) for moisture change of peas at 24.1% initial MC and exposed to micronization (moving-element configuration, $dM/dT = -10^{-8} x^{3.5}$). The same symbols indicate data obtained from one experiment.

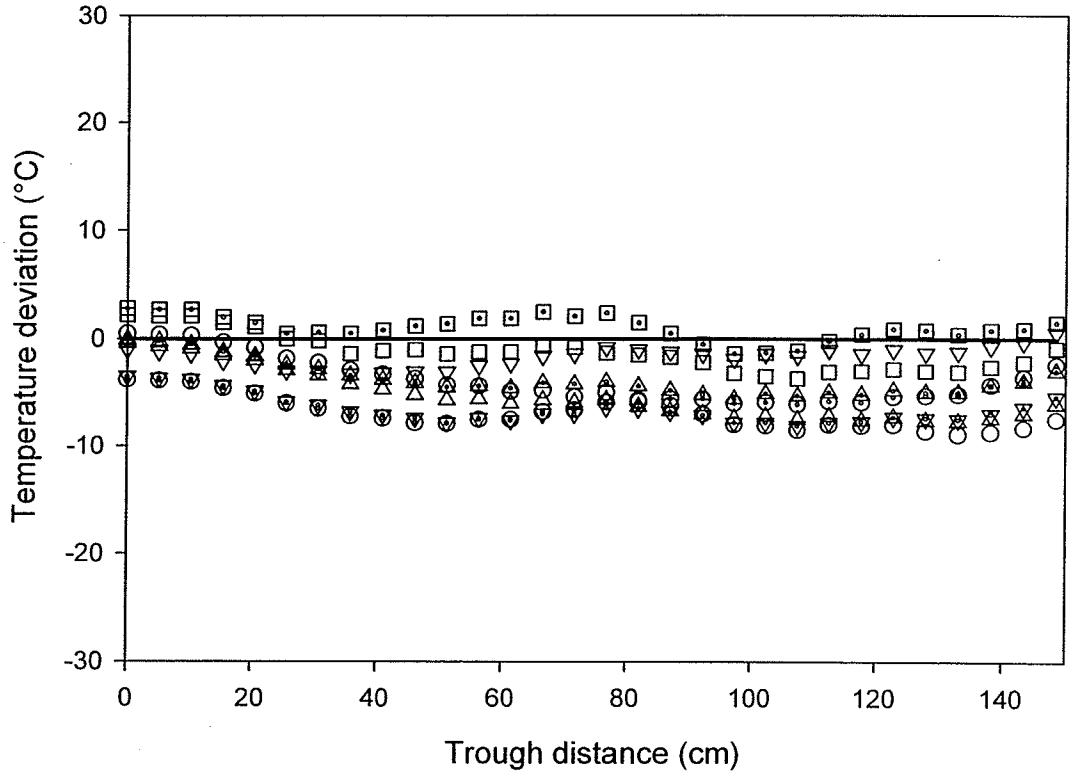

Figure 6.6.6c Temperature deviation of the experimental data of yellow peas tempered to 24.1% initially from the temperature predicted by the moving-element configuration model. The temperature which was predicted by the model was set to zero as reference values when the emissivity of yellow peas was set at 0.9 for the calculation of temperature deviation.

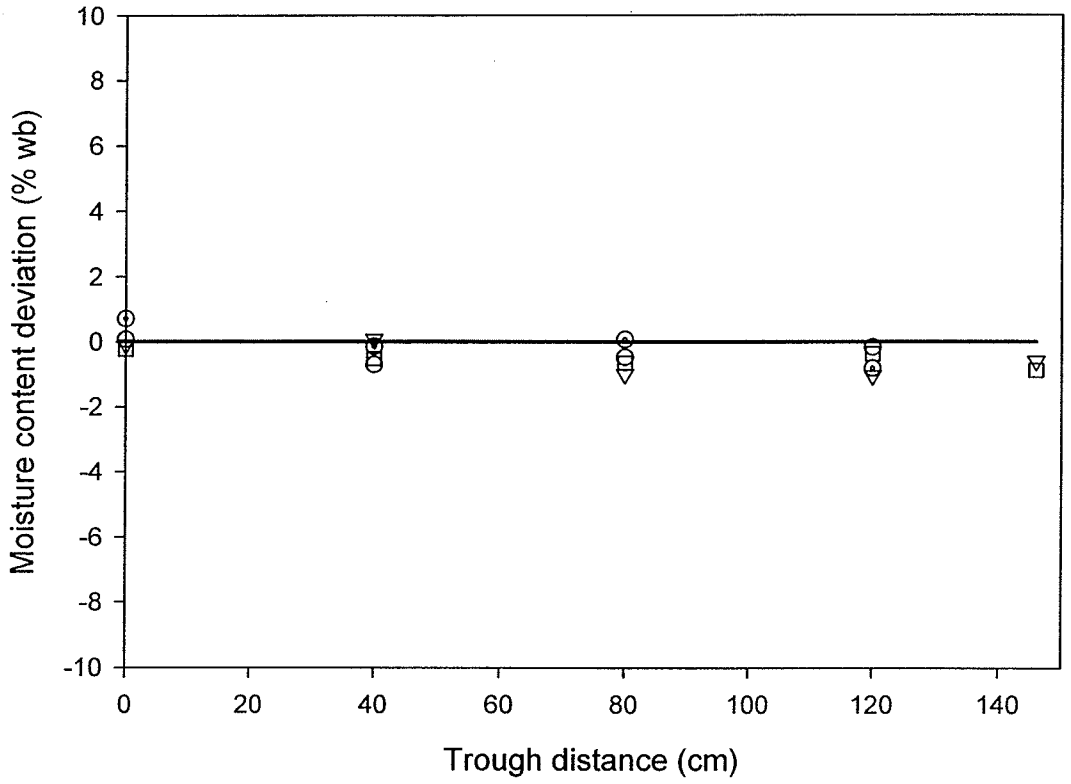

Figure 6.6.6d Moisture content deviation of the experimental data of yellow peas tempered to 24.1% initially from the temperature predicted by the moving-element configuration model. The moisture content which was predicted by the model was set to zero as reference values when the emissivity of yellow peas was set at 0.9 for the calculation of moisture content deviation.

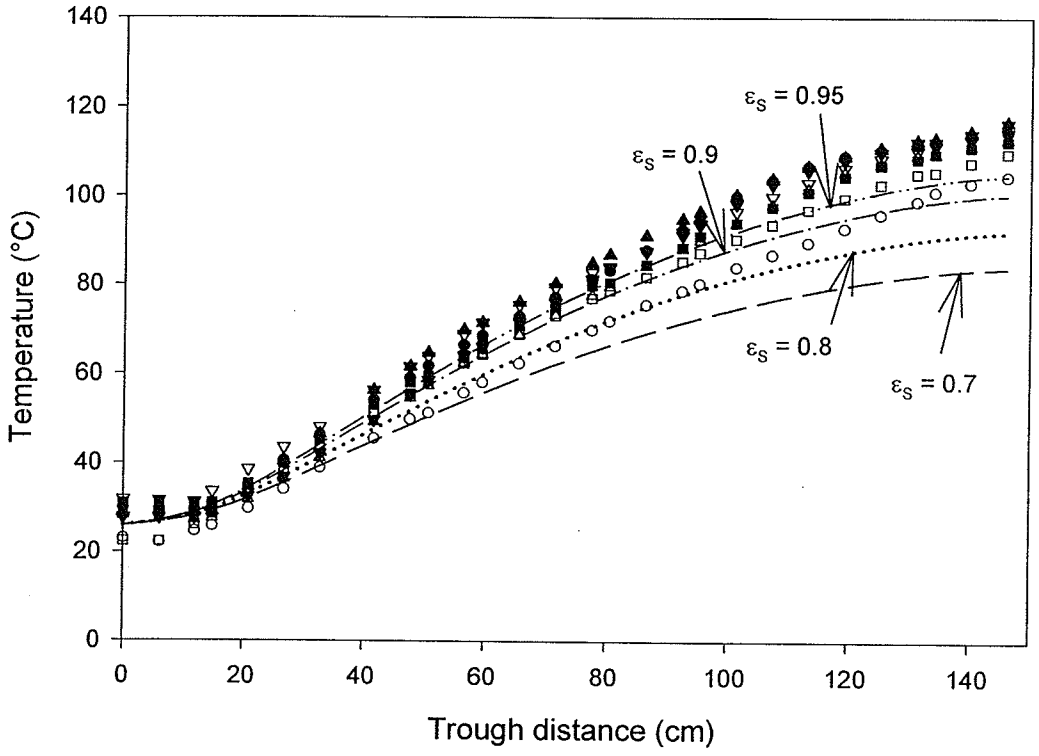

Figure 6.6.7a Validation of the simulation results (lines) by the Runge-Kutta method with experimental data (symbols) for temperatures of peas at 28.8% initial MC and exposed to micronization (moving-element configuration, $dM/dT = -10^{-8} x^{3.5}$). The same symbols indicate data obtained from one experiment.

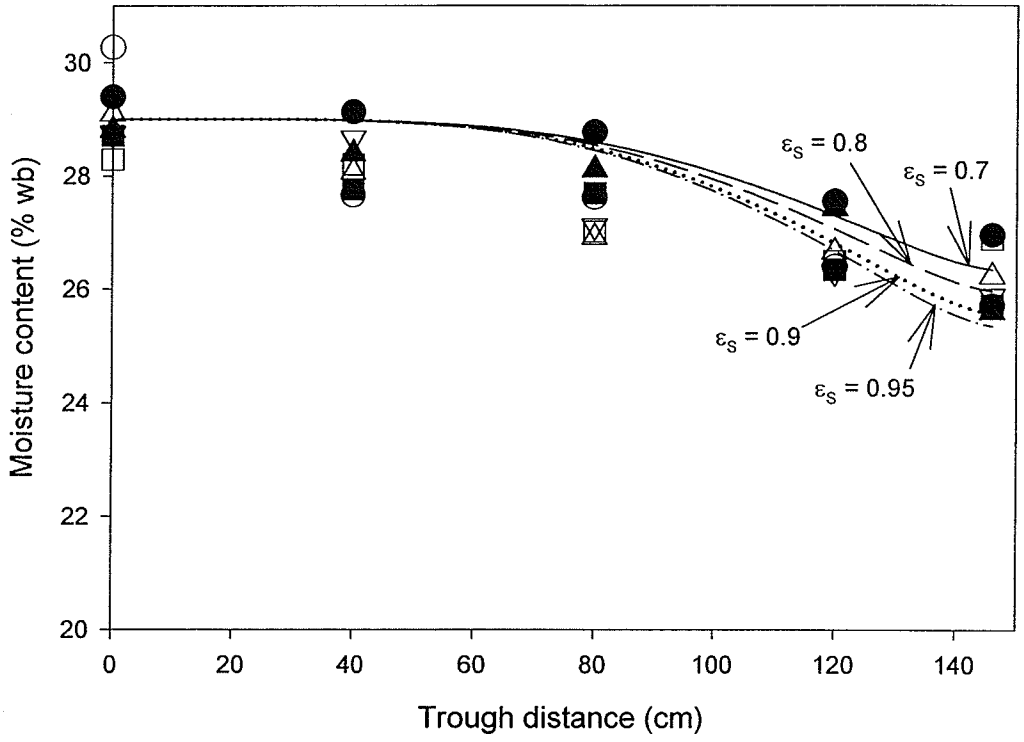

Figure 6.6.7b Validation of the simulation results (lines) by the Runge-Kutta method with experimental data (symbols) for moisture change of peas at 28.8% initial MC and exposed to micronization (moving element-configuration, $dM/dT = -10^{-8} x^{3.5}$). The same symbols indicate data obtained from one experiment.

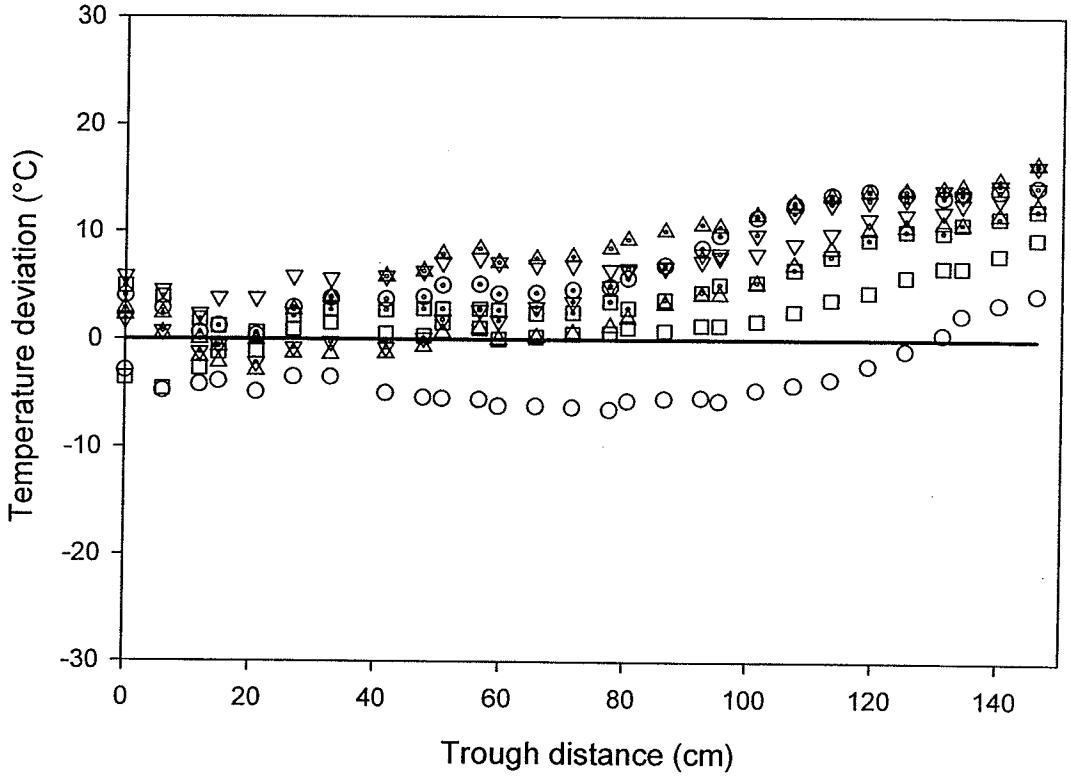

Figure 6.6.7c Temperature deviation of the experimental data of yellow peas tempered to 28.8% initially from the temperature predicted by the moving-element configuration model. The temperature which was predicted by the model was set to zero as reference values when the emissivity of yellow peas was set at 0.9 for the calculation of temperature deviation.

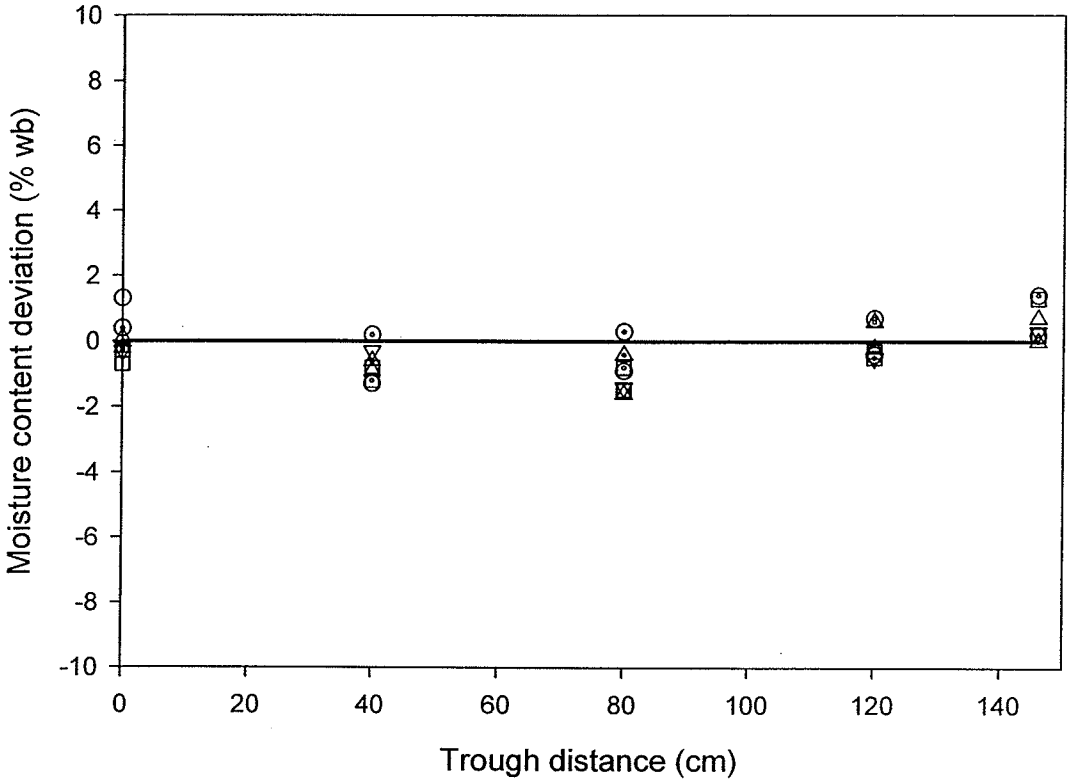

Figure 6.6.7d Moisture content deviation of the experimental data of yellow peas tempered to 28.8% initially from the temperature predicted by the moving-element configuration model. The moisture content which was predicted by the model was set to zero as reference values when the emissivity of yellow peas was set at 0.9 for the calculation of moisture content deviation.

Table 6.6.3 Standard deviations of temperature and moisture content residuals as the difference between the experimental values and the values predicted by the models.

Fixed-element configuration model			Moving-element configuration model		
Initial MC, (% wb)	Standard deviation		Initial MC, (% wb	Standard deviation	
	Temperature, (°C)	MC, (% wb)		Temperature, (°C)	MC, (% wb)
19.1	4.6	1.8	19.6	3.9	0.6
25.2	6.6	0.7	24.1	4.7	0.6
29.8	5.7	1.9	28.8	7.2	0.8

6-7 Effect of Initial Moisture Content on Temperature Rise

The effect of initial moisture content of the micronized peas on their temperature rise for the fixed-element configuration system is shown in Figure 6.7.1. The operating conditions and parameters for the simulations are shown in Table 6.7.1. The emissivity in this computer simulation was set to 0.9 which showed good agreement with the experimental results. The temperature rise for the identical micronization time of 200 s was different as the initial moisture increased. For the peas tempered to 20%, the simulated temperature of the pea increased to 115 °C at 200 s. The maximum temperature differences among the peas tempered to 20%, 25%, and 30% (wb) were 7.2 and 7.3 °C, respectively.

In the moving-element configuration, the simulated temperature of peas of initial moisture content of 25% and 30% at the end of the trough is higher by 3 to 4 °C than the temperature of peas at 20% initial moisture content due to the operating conditions shown in Table 6.7.2. The residence time was approximately one minute and the configuration factor changed with the movement of peas along the trough. The initial moisture content affected the final temperature of peas during micronization. The final temperature which was obtained at the end of the trough or at a desired micronization time decreased as the initial moisture content increased.

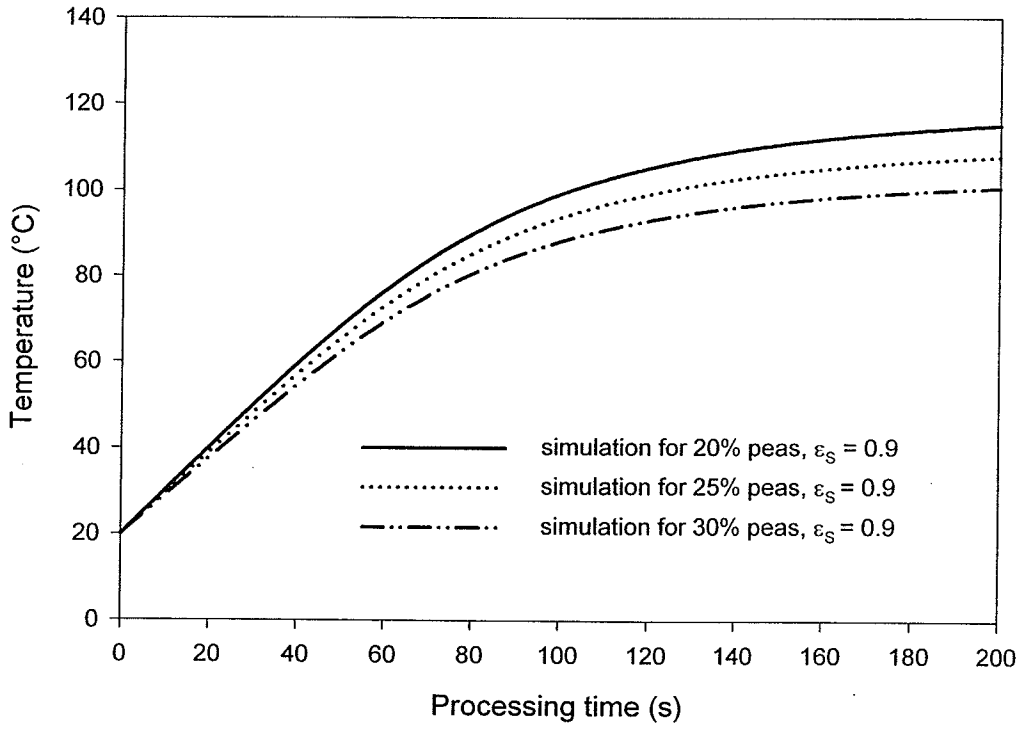

Figure 6.7.1 Temperature prediction by the fixed-element configuration model for the peas of 20, 25, and 30% initial MC when the emissivity of peas was set to 0.9.

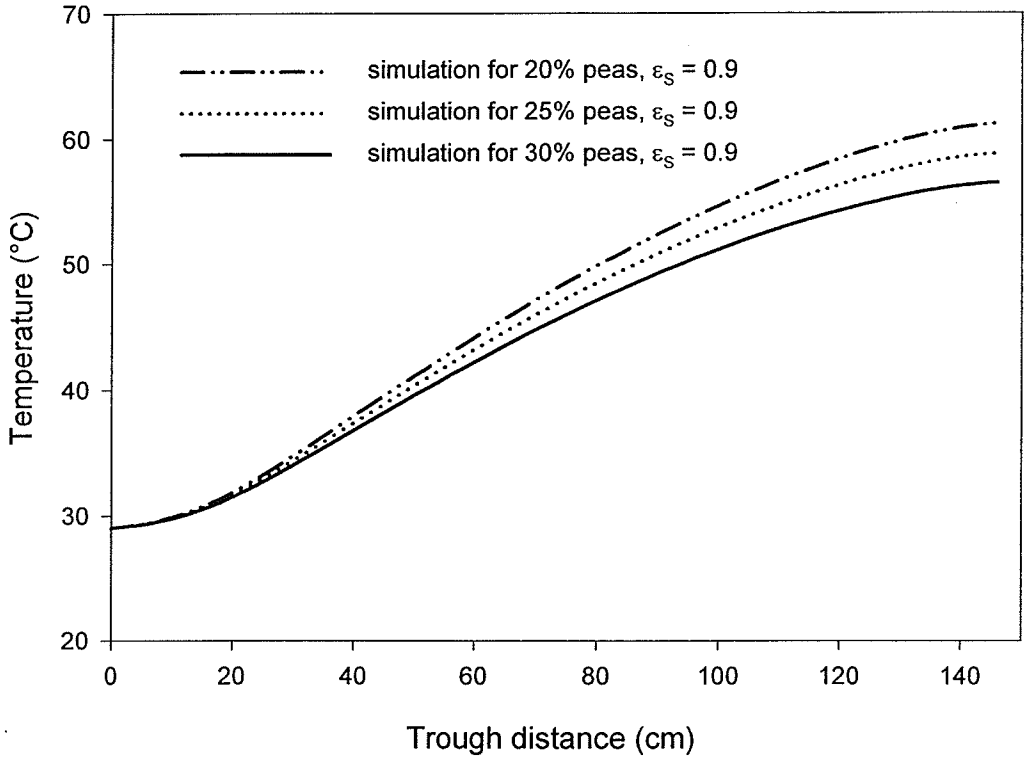

Figure 6.7.2 Temperature prediction by the moving-element configuration model for the peas of 20, 25, and 30% initial MC when the emissivity of peas was set to 0.9.

Table 6.7.1 Parameters and operating conditions for the simulation (fixed-element configuration).

Parameters	Values	Unit
Φ	0.44	[-]
ε_S	0.9	[-]
ε_1	0.25	[-]
ε_2	1.00	[-]
ε_5	0.20	[-]
σ	5.67×10^{-8}	$W/(m^2 K^4)$
T_1	978	K
T_2	294	K
T_5	383	K
C_P	2407	J/(kg K)
h_{fg}	2257×10^3	J/kg
W	0.265	m
H	0.12	m
$F_{d3\text{-}1}$	0.67	[-]
m_d	0.115	kg

Table 6.7.2 Parameters and operating conditions for the simulation (moving-element configuration).

Parameters	Values	Unit
Φ	0.44	[-]
ε_S	0.9	[-]
ε_1	0.25	[-]
ε_2	1.00	[-]
ε_5	0.20	[-]
σ	5.67×10^{-8}	$W/(m^2 K^4)$
T_1	978	K
T_2	293	K
T_5	384	K
C_P	2407	J/(kg K)
h_{fg}	2257×10^3	J/kg
W	0.265	m
H	0.12	m
$F_{d3\text{-}1}$	variable (Fig. 6.1.1, H=12cm)	[-]
n	3.4	[-]
$\dot{m}_d$	0.011	kg/s

6-8 Summary of the Chapter

In this chapter, the effects of various operating parameters on the temperature prediction of peas by the developed models during micronization have been shown. The temperature with respect to micronization time (fixed-element configuration) or the distance along the trough (moving-element configuration) was affected by several parameters, such as configuration factor, initial moisture content of peas, the emissivity of pea and the approximation function for the moisture-temperature gradient. This gradient was expressed in the form of power functions for the fixed-element configuration model, and for the moving-element configuration model. With a reasonable assumption of pea emissivity, the temperature prediction by the models gave satisfactory results and fitted the experimental data well.

CHAPTER 7

CONCLUSIONS

To study IR processing of agricultural products, mathematical models using a parallel tray-type gas-fired micronizer were developed and were validated against some experimental results. In the developed models, 'enclosure theory' was applied to the models by using 'net-radiation method' to include all the surfaces which participated in IR exchanges in the micronizer. When the processed materials (yellow peas) are moving along the vibratory conveyor, the configuration factor from the emitter to the moving yellow peas are changing along the location of the peas. To include the proper IR heat intensity on the surfaces of the peas from all the other enclosure surfaces, a mathematical expression of the configuration factor from the elemental control surface to the emitter was developed using the Contour-Integration method. The configuration factor was calculated numerically by Gauss-Quadrature integration method and the factor was sensitive to the number of approximation points. The calculated configuration factor showed good agreement with the literature values for two cases of analytical expressions from the literature up to four decimals when the integration was performed with the number of approximation points higher than 10.

The proposed IR models need information of the moisture-temperature gradient (dM/dT) during micronization to validate the models as an additional parameter. The moisture-temperature data were obtained experimentally to evaluate the moisture-temperature gradient which was approximated by power functions. The power functions approximated well the fixed-element configuration system whereas they showed a discrepancy between the experimental results with the approximation functions for the moving-element configuration system.

The temperature prediction by the model simulations showed good agreement with the experimental results when the emissivity of yellow peas was set to 0.9 and 0.95 for the moving-element and the fixed-element configuration system. Also, the results of moisture prediction by the models represented good agreement with the experimental results of the fixed-element configuration system. For the moving-element configuration system, the moisture prediction by the model was poor and it is believed that it came from the error sources in experimental handling of the moving-element configuration system and from the poor approximation of the moisture-temperature gradient for the moving-element configuration system.

The proposed mathematical models of the micronization of yellow peas can also be extended to other granular agricultural products and, therefore, can provide useful information on operating conditions of a gas-fired micronizers between the surfaces within the enclosures in which heat transfer phenomena occur.

RECOMMENDED FUTURE WORK

The developed models of IR processing require information on radiative properties of the material processed. Data with respect to these properties for biological materials are scarce and a reliable data bank needs to be developed. Also, the emissivity coefficient for the heat source needs to be determined precisely as this coefficient can greatly affect the amount of radiative energy available at the source. The effects of moisture content and physicochemical property changes on radiative properties of biological materials during IR processing need to be determined to validate more accurately the models under broad range of micronization conditions.

REFERENCES

AACC.1995. 9th ed. Moisture-Air-Oven Methods. *Approved Methods of the American Association of Cereal Chemists*. St. Paul, Minnesota: AACC.

Abe, T. and M.A.Tabassum. 1997. A mathematical model to predict temperature rise of radiant heated rice. *Agricultural Engineering Journal.* 6(1): 29-36.

Afzal,T.M. and T. Abe. 1997. Thin-layer drying of rough rice. *Journal of Agricultural Engineering Research.* 67(4): 289-297.

Afzal,T.M. and T. Abe. 1998. Diffusion in potato during far-infrared radiation drying. *Journal of Food Engineering.* 37(4): 353-365.

Afzal,T.M. and T. Abe. 1999. Some fundamental attributes of far-infrared radiation drying of potato. *Drying Technology.* 17(1&2): 137-155.

Afzal,T.M. and T. Abe. 2000. Simulation of moisture changes in barley during far-infrared radiation drying. *Computers and Electronics in Agriculture.* 26(2): 137-145.

Arntfield, S.D., M.G. Scanlon, L.J. Malcolmson, B. Watts, D. Ryland, and V. Savoie. 1998. Effect of tempering and end moisture content on the quality of micronized lentils. *Food Research International.* 30(5): 371-380.

Arinze, E.A., G.J. Schoenau, and F.W. Bigsby. 1987. Determination of solar energy absorption and thermal radiative properties of some agricultural products. *Transactions of the ASAE.* 30(1): 259-267.

Babenko, V.E. and T.A. Shipulina. 1995. Calculation of drying in vibrating fluidized beds heated by thermal radiation. *Theoretical Foundations of Chemical Engineering.* 29(2): 200-202.

Belitz, H.D. and W. Grosch. 1999. *Food Chemistry,* 2nd edition. Springer-Verlag: 296-308.

Billiaderis, C.G. June, 1992. Structures and phase transitions of starch in food system. *Food Technology*: 98-110.

Billiaderis, C.G., D.R. Grant, and J.R. Vose. 1981. Structural characterization of legume starches.II. Studies on acid-treated starches. *Cereal Chemistry*. 58(6): 502-507.

Blenford, D.E. 1980. Potential applications of micronizing in food processing. *Food Trade Review*. 50: 6-8.

Cenkowski, S., J.-T. Hong, S.D. Arntfield, and M.G. Scanlon. 2000. Determination of the temperature profile during micronization of peas. *CSAE* Paper No. AFL 121. Mansonville, QC: CSAE/SCGR.

Cenkowski, S. and F.W. Sosulski. 1998. Cooking characteristics of split peas treated with infrared heat. *Transactions of the ASAE*. 41(3): 715-720.

Cenkowski, S. and F.W. Sosulski. 1997. Physical and cooking properties of micronized lentils. *Journal of Food Process Engineering*. 20(2): 249-264.

Chapra, S.C. and R.P. Canale. 1989. *Numerical Methods for Engineers,* 2nd edition. New York, NY: McGraw-Hill Book Company: 459-609.

Chung, B.T.F. and M.M. Kermani. 1989. Radiation view factors from a finite rectangular plate. *Journal of Heat Transfer*. 111(4): 1115-1117.

Comer, F.W. and M.K. Fry. 1978. Purification, modification, and properties of air classified pea starch. *Cereal Chemistry*. 55(6): 818-829.

Deshpande, S.S. and S. Damodaran. 1990. Food legumes - chemistry and technology. In *Advances in Cereal Science and Technology. Vol.10,* ed. Y. Pomeranz, 147-241. St. Paul, Minnesota. American Association of Cereal Chemists, Inc.

Donovan, J.W. 1979. Phase transitions of the starch-water system. *Biopolymers*. 18(2): 263-275.

Donovan, J.W. and C.J. Mapes. 1980. Multiple phase transitions of starches and Nageli amylodextrins. *Starch*. 32(6): 190-193.

Dostie, M., J.-N. Séguin, O. Maure, Q.-A. Ton-That, and R.Châtigny. 1989. Preliminary measurement on the drying of thick porous materials by combination of intermittent infrared and

continuous convection heating. In *Drying* '89, eds. A.S. Mujumdar and M.A. Roques, 513-519. New York, NY: Hemisphere Publishing Corp., 1990.

Eu, M.T. 1997. Reflectance characteristics of bulk grains using a spectrophotometer. M.Sc. thesis. Department of Biosystems Engineering, University of Manitoba. Winnipeg, MB.

Fasina, O., R.T. Tyler, and M.D. Pickard. 1997a. Infrared heating of legume seeds - effects on physical and mechanical properties. *ASAE* Paper No. 976013. St. Joseph, MI: ASAE.

Fasina, O., R.T. Tyler, and M.D. Pickard. 1997b. Adaptation of micronization to the development of functional food ingredients from waxy barley and pulses, including the adaptation and testing of a small scale, gas-fired micronizer unit. Final Report to the NRCC (the National Research Council of Canada) and IRAP (Industrial Research Assistance Program).

Fasina, O., R.T. Tyler, and M.D. Pickard. 1998. Modeling the infrared radiative heating of agricultural crops. *Drying Technology*. 6(9&10): 2065-2082.

Fasina, O. and R.T. Tyler. 2001. Infrared heating of biological materials. In *Food Processing Operations Modeling*, ed. J. Irudayaraj, 189-224. New York, NY: Marcel Dekker, Inc.

Felder, R.M. and R.W. Rousseau. 2000. *Elementary Principles of Chemical processes,* 3rd ed. New York, NY: John Wiley and Sons, Inc.: 313-337, 646.

Fernandez, M.L. and J.R. Howell. 1996. Drying model of porous materials using infrared radiation. In *1996 National Heat Transfer Conference*. AIAA 96-3962, Houston, TX. August 3-6.

Ginzburg, A.S. 1969. *Application of Infra-red Radiation in Food Processing,* London: Leonard Hill Books: 77-305.

Hall, C. W. 1962. Theory of infrared drying. *Transaction of the ASAE*. 5(1): 14-16.

Hasatani, M., Y. Itaya, and K. Miura. 1988. Hybrid drying of granular materials by combined radiative and convective heating. *Drying Technology*. 6(1): 43-68.

Hasatani, M., Y. Itaya, and K. Miura. 1991. Drying of granular materials in an inclined vibrated fluidized bed by combined radiative and convective heating. *Drying Technology*. 9(2): 349-366.

Hashimoto, A., Y. Yamazaki, M. Shimizu, and S. Oshita. 1994. Drying characteristics of gelatinous materials irradiated by infrared radiation. *Drying Technology*. 12(5): 1029-1052.

Headley, V.E. and C.W. Hall. 1963. Drying of shelled corn vibrated in an infrared source. *Transactions of the ASAE*. 6(2):148-150.

Hebbar, H.U. and N.K. Rastogi. 2001. Mass transfer during infrared drying of cashew kernel. *Journal of Food Engineering*. 47(1): 1-5.

Hottel, H.C. 1954. Radiant-heat transmission. In *Heat Transmission*, 3rd edition, 55-125. ed. W.H. McAdams. New York, NY: McGraw-Hill Book Company.

Howell, J.R. 1982. *A Catalogue of Radiation Configuration Factors,* New York, NY: McGraw Hill, Book Company: 32-75.

Hsu, C.-J. 1967. Shape factor equations for radiant heat transfer between two arbitrary sizes of rectangular planes. *The Canadian Journal of Chemical Engineering*. 45(1): 58-60.

Il'yasov, S.G. and V.V. Krasinikov. 1991. *Physical Principles of Infrared Irradiation of Foodstuffs*, New York, NY: Hemisphere Publishing Co.: 397-412.

Incropera, F.P. and D.P. DeWitt. 1985. *Fundamentals of Heat and Mass Transfer*, 2nd edition. New York, NY: John Wiley & Sons Inc.: 545-662.

Kadam, S.S., S.S. Deshpande and N.D. Jambhale. 1989. Seed structure and composition. In *Handbook of World Food Legumes: Nutritional Chemistry, Processing Technology and Utilization. Vol.1*. eds. D.K. Salunkhe and S.S. Kadam, 23-50. Raton, FL.: CRC Press, Boca.

Kuang, H.-D., J. Thibault, and B.P.A. Grandjean. 1994. Study of heat and mass transfer during IR drying of paper. *Drying Technology*. 12(3): 545-575.

Lai, C.C. and E. Variano-Marston. 1979. Studies on the characteristics of black bean starch. *Journal of Food Science*. 44(2): 528-530, 544.

Lii, C.Y. and S.M. Chang. 1981. Characterization of red bean (*Phaseolus vulgaris var aurea*) starch and its noodle quality. *Journal of Food Science*. 46(1): 78-81.

Lorenz, K.J. 1979. The starch of the faba bean (*Vicia faba*). *Starch.* 31(6): 181-184.

McCurdy, S.M. 1992. Infrared processing of dry peas, canola, and canola screenings. *Journal of Food Science*. 57(4): 941-944.

Massie, D.R. and K.H. Norris. 1965. Spectral reflectance and transmittance properties of grain in the visible and near infrared. *Transactions of the ASAE.* 8(4): 598-600.

Meyer, L.H. 1960. *Food Chemistry,* New York, NY: Reinhold Pub., Corp.: 104-107.

Modest, M.F. 1993. *Radiative Heat Transfer*, New York, NY: McGraw-Hill, Inc.: 1-227.

Mohamed, M., S. Cenkowski, S.D. Arntfield, and M.G. Scanlon. 2001. Moisture and temperature characteristics during infrared processing of peas. *ASAE* Paper No. SD01-101. St. Joseph, MI: ASAE.

Mohamed, M. 2003. Emissivity and moisture –temperature response of yellow peas in the mid-infrared region. unpublished MSc. thesis. Department of Biosystems Engineering. University of Manitoba. Winnipeg, MB.

Nelson, S.O., 1962. Radiation processing in agriculture. *Transactions of the ASAE.* 5(1): 20-30.

Norris, K.H. 1958. Measuring light transmittance properties of agricultural commodities. *Agricultural Engineering.* 39(10): 640-643.

Norris, K.H. 1962. Instrumentation of infrared radiation. *Transactions of the ASAE.* 5(1): 17-20.

Özisik, M.N. 1973. *Radiative Transfer*, New York, NY: John Wiley & Sons Inc.: 121-177.

Pabis, S., D.S. Jayas and S. Cenkowski. 1998. *Grain Drying ; Theory and Practice,* New York, NY: John Wiley & Sons Inc.: 21-115, 148-228.

Parrouffe, J. - M.. 1992. Combined convective and infrared drying of a capillary porous body. PhD. thesis. Dept. of Chemical Engineering. McGill University. Montreal, Quebec.

Person, N.K. Jr. and J.W. Sorenson Jr. 1962. Drying hay with infrared radiation. *Agricultural Engineering* 43(4): 204-227.

Poljak, G.1935. Analysis of heat interchange by radiation between diffuse surfaces. *Tech. Phys. USSR*. 1(5&6): 555-590. Cited in *Thermal Radiation Heat Transfer*, 3rd ed. R. Siegel and J. R. Howell. 1992. Taylor & Francis Publishing Co., Washington D.C.: 189- 242.

Ratti, C. and A.S. Mujumdar. 1995. Infrared Drying. In *Handbook of Industrial Drying*, 2nd edition, ed. A.S. Mujumdar, 567-588. NewYork, NY: Marcel Dekker, Inc.

Reddy, N.R., S.K. Sathe, and D.K. Salunkhe. 1989. Carbohydrates. In *Handbook of World Food Legumes: Nutritional Chemistry, Processing Technology and Utilization. Vol.1*. eds. D.K. Salunkhe and S.S. Kadam., 51-74. Raton, FL.: CRC Press, Boca.

Ready, N.R., M.D. Pierson, S.K. Sathe, and D.K. Salunkhe. 1984.Chemical, nutritional and physiological aspects of dry bean carbohydrates - a review. *Food Chemistry*. 13(1): 25-68.

Roos, Y.H. 1995. *Phase Transitions in Foods*, New York, NY: Academic Press, Inc.: 119-142.

Sala, A. 1986. *Radiant Properties of Materials - Tables of Radiant Values for Black Body and Real Materials*, New York, NY: Elsevier Science Publishing Co. Inc.: 377-383.

Sandu, C. 1986. Infrared radiative drying in food engineering: A process analysis. *Biotechnology Progress*. 2(30): 109-119.

Saravacos, G.D. and Z.B. Maroulis. 2001. *Transport Properties of Foods,* New York, NY: Marcel Dekker, Inc.: 130-132.

Sathe, S.K. and D.K. Salunkhe. 1984. Technology of removal of unwanted components of dry beans. *CRC Critical Reviews in Food Science and Nutrition*. 21(3): 263-287.

Sathe, S.K., P.D. Rangnekar, S.S. Deshpande, and D.K. Salunkhe. 1982. Isolation and partial characterization of black gram (*Phaseolus mungo L.*) starch. *Journal of Food Science*. 47(5): 1524-1527.

Scanlon, M.G., K.I. Segall, and S. Cenkowski. 1999. The stiffness versus porosity relationship for infrared-heat treated (micronized) durum wheat grains. In *Bubbles in Food*, eds. G.M. Cambell, C. Webb, S.S. Pandiella, and K. Niranjan, 283-290. St. Paul, MI: Eagan Press.

Schoch, T.J. and E.C. Maywald. 1968. Preparation and properties of various legume starches. *Cereal Chemistry*. 45(6): 564-573.

Shuman, A.C. and C.H. Staley. 1950. Drying by radiation. *Food Technology*. 4(12): 481-484.

Siegel, R. and J. R. Howell. 1992. *Thermal Radiation Heat Transfer,* 3rd edition. Bristol, PA: Taylor & Francis Inc.: 11-444.

Shiau, S.Y. and S.P. Yang. 1982. Effect of micronizing temperature on the nutritive value of sorghum. *Journal of Food Science*. 47(3): 965-968.

Singham, J.R. 1962. Tables of emissivity of surfaces. *International Journal of Heat and Mass Transfer*. 5: 67-76.

Sosulski, F.W. and A.R. McCurdy. 1987. Functionality of flours, protein fractions and isolates from field peas and Faba bean. *Journal of Food Science*. 52(4): 1010-1014.

Sokhansanj, S. and D.M. Bruce. 1987. A conduction model to predict grain temperatures in grain drying simulation. *Transactions of the ASAE*. 30(4): 1181-1184.

Sparrow, E.M. 1963. A new and simple formulation for radiative angle factors. *Journal of Heat Transfer. 85*: 81-88.

Stroud, A.H. and D. Secrest. 1966. *Gaussian Quadrature Formulas,* Prentice-Hall, Inc.: 100-102.

Strumillo, C. and T. Kudra. 1986. *Drying: Principles, Applications and Design*, New York, NY: Gordon and Breach Science Publishers: 371-376.

van der Poel, A.F.B. 1990. Effect of processing on antinutritional factors and protein nutritional value of dry beans (*Phaseolus vulgaris* L.) - a review. *Animal Feed Science and Technology*. 29(1&2): 179-208.

van Zuilichem, D. J., K. van't Riet, and W. Stolp. 1985. An overview of new infrared radiation processes for various agricultural products. In *Food Engineering and Process Applications. Vol.1. Transport Phenomena,* eds. M. Le Maguer and P. Jelen, 595-610. New York, NY: Elsevier Applied Science Publishers.

van Zuilichem, D. J. and A.F.B. van der Poel. 1989. Effect of HTST treatment of pisum sativum on the inactivation of antinutritional factors. In *Proceedings of the First International Workshop on Antinutritional Factors (ANF) in Legume Seeds,* eds. J. Huisman, T.F.B. van der Poel, and I.E. Liener, 263-267. Wageningen, the Netherlands. November 23-25.

Welty, J. R., C. E. Wicks, and R. E. Wilson. 1984. *Fundamentals of Momentum, Heat, and Mass Transfer*, 3rd edition. New York, NY: John Wiley and Sons Inc.: 30-88.

Wilson, L.A., V.A. Birmingham, D.P. Moon, and H.E. Snyder. 1978. Isolation and characterizationof starch from immature soybeans. *Cereal Chemistry*. 55(5): 661-670.

Wray, S.L. 1999. Thermo-physical and nutritional changes of dehulled yellow peas during infrared processing (micronization). MSc. thesis. Department of Biosystems Engineering. University of Manitoba. Winnipeg, MB.

APPENDIX I. Derivation of the Heat Flux, q_b.

In the derivation of the net radiation heat flux from the bottom tray, q_b, onto the lower surface of the feed layer (surface 4), only the radiation heat transfer mode was included because there was no forced air movement by any equipment, thus any convective heat transfer mode was neglected. Also, due to the vibration of the trough, the peas has very short contact time with the trough. Thus the conduction heat transfer from the heated trough was neglected.

Consider Figure A-1, the rate of outgoing radiation heat from the control volume, surface 4, to the bottom trough, surface 5, can be expressed as follows:

$$\begin{aligned} dQ_{o,d4} = dA_4 \cdot q_{o,d4} &= \Phi \cdot dA_4 \cdot \varepsilon_S \cdot \sigma \cdot T^4 + (1-\Phi) dA_4 \cdot q_{i,d3} + dA_4 \cdot \Phi \cdot \rho_S \cdot q_{o,d5} \\ &= \Phi \cdot dA_4 \cdot \varepsilon_S \cdot \sigma \cdot T^4 + (1-\Phi) dA_4 \cdot q_{i,d3} + dA_4 \cdot \Phi \cdot (1-\varepsilon_S) \cdot q_{o,d5} \end{aligned} \tag{A1-1}$$

By dividing Eq.(A1-1) by dA_4, the average heat flux, $q_{o,d4}$, is:

$$q_{o,d4} = \Phi \cdot \varepsilon_S \cdot \sigma \cdot T^4 + (1-\Phi) q_{i,d3} + \Phi \cdot (1-\varepsilon_S) q_{o,d5} \tag{A1-2}$$

Rearranging Eq.(A1-2),

$$q_{o,d4} - \Phi (1-\varepsilon_S) q_{o,d5} = \Phi \cdot \varepsilon_S \cdot \sigma \cdot T^4 + (1-\Phi) q_{i,d3} \tag{A1-3}$$

Also, the heat outgoing from the surface 5 is:

$$\begin{aligned} dQ_{o,d5} = dA_5 \cdot q_{o,d5} &= dA_5 \cdot \left[\varepsilon_5 \cdot \sigma \cdot T_5^4 + \rho_5 \cdot q_{o,d4} \right] \\ &= dA_4 \cdot \left[\varepsilon_5 \cdot \sigma \cdot T_5^4 + (1-\varepsilon_5) q_{o,d4} \right] \end{aligned} \tag{A1-4}$$

where, $dA_5 = dA_4 = W \cdot dx$.

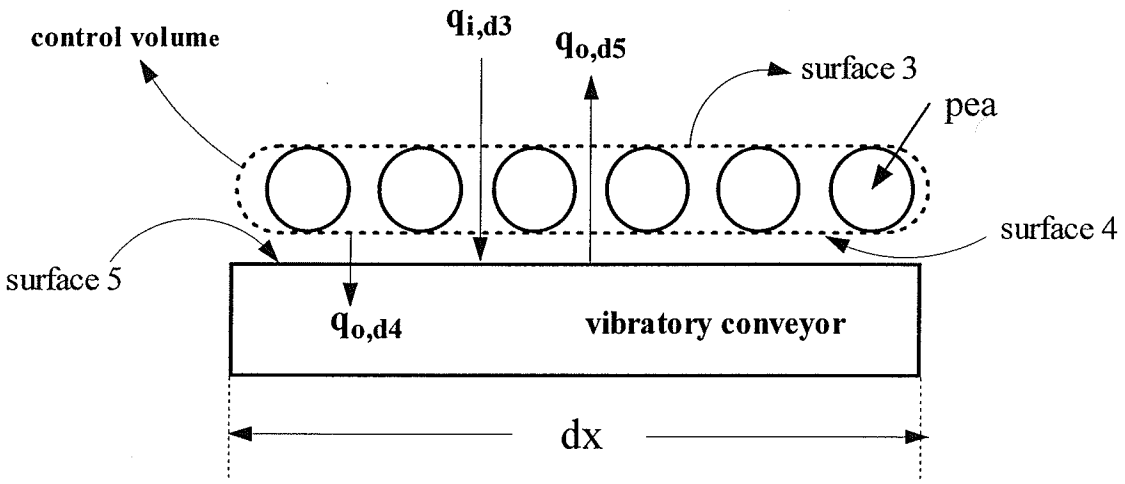

Figure A-1 Schematic diagram of the radiative heat exchange between a control volume of a pea layer and the bottom trough (vibratory conveyor) of the micronizer.

By manipulating and rearranging Eq.(A1-4),

$$(1-\varepsilon_5)q_{o,d4} - q_{o,d5} = -\varepsilon_5 \cdot \sigma \cdot T_5^4 \tag{A1-5}$$

The rate of incoming radiation heat from surface 5 to surface 4 can be expressed as follows:
From Eq.(A1-3) and (A1-5), let

$$\begin{aligned} \xi_1 &= \Phi \cdot \varepsilon_S \cdot \sigma \cdot T^4 + \beta \ , \\ \xi_2 &= -\varepsilon_5 \cdot \sigma \cdot T_5^4 \ , \\ \beta &= (1-\Phi) q_{i,d3} \end{aligned} \tag{A1-6}$$

Eq.(A1-3) and (A1-5) can be rewritten as:

$$q_{o,d4} - \Phi(1-\varepsilon_S)q_{o,d5} = \xi_1 \tag{A1-7}$$

$$(1-\varepsilon_5)q_{o,d4} - q_{o,d5} = \xi_2 \tag{A1-8}$$

Let D be the determinant of the coefficient matrix of Eq.(A1-7) and (A1-8) as follows:

$$D = \begin{vmatrix} 1 & -\Phi(1-\varepsilon_S) \\ (1-\varepsilon_5) & -1 \end{vmatrix} = -1 + \Phi(1-\varepsilon_S)(1-\varepsilon_5) \tag{A1-9}$$

Equating Eq.(A1-7) and Eq.(A1-8) by Cramer's Rule gives:

$$q_{o,d4} = \frac{1}{D}\begin{vmatrix} \xi_1 & -\Phi(1-\varepsilon_S) \\ \xi_2 & -1 \end{vmatrix} = \frac{\xi_1 - \xi_2 \cdot \Phi(1-\varepsilon_S)}{1-\Phi(1-\varepsilon_S)(1-\varepsilon_5)} \tag{A1-10}$$

$$q_{o,d5} = \frac{1}{D}\begin{vmatrix} 1 & \xi_1 \\ (1-\varepsilon_5) & \xi_2 \end{vmatrix} = \frac{\xi_1(1-\varepsilon_5)-\xi_2}{1-\Phi(1-\varepsilon_S)(1-\varepsilon_5)} \tag{A1-11}$$

By the definition of q_b, final equation is obtained as follows:

$$q_b = q_{o,d5} - q_{o,d4} = \frac{\xi_2\left[\Phi(1-\varepsilon_S)-1\right]-\varepsilon_5\xi_1}{1-\Phi(1-\varepsilon_5)(1-\varepsilon_S)} \tag{A1-12}$$

where,

$$\begin{aligned} \xi_1 &= \Phi\cdot\varepsilon_S\cdot\sigma\cdot T^4+\beta, \\ \xi_2 &= -\varepsilon_5\cdot\sigma\cdot T_5^4, \\ \beta &= (1-\Phi)q_{i,d3} = (1-\Phi)\left[F_{d3-1}\cdot\varepsilon_1\cdot\sigma\cdot T_1^4+(1-F_{d3-1})\varepsilon_2\cdot\sigma\cdot T_2^4\right] \end{aligned} \tag{A1-13}$$

APPENDIX II. Derivation of $(d\dot{m}/dx)$, $(d\dot{H}/dx)$, (dm/dt), and (dH/dt)

For the moving-element configuration system, the mass flowrate is expressed as a function of dry mass flowrate [Eq. (3-27)] and moisture content in wet basis as follows:

$$\dot{m} = \left(\frac{100}{100 - M}\right)\left(\dot{m}_d\right) \tag{A2-1}$$

where,

M= moisture content in wet basis, (%)

$\dot{m}_d$= dry mass flowrate of the feed, $\left(\text{kg solid/s}\right)$

The dry mass flowrate is constant and only the moisture content is changing during IR processing. Also, the dry mass flowrate is a function of distance 'x' from the bottom tray inlet position. By differentiating Eq. (A2-1) with respect to 'x', Eq. (A2-1) is reduced to the following equation:

$$\frac{d\dot{m}}{dx} = \frac{100 \cdot \dot{m}_d}{(100 - M)^2}\frac{dM}{dT}\frac{dT}{dx} \tag{A2-2}$$

In a similar manner, the enthalpy of the feed is differentiated with respect to 'x' , and then:

$$\frac{d\dot{H}}{dx} = \frac{d}{dx}\left(\dot{m} \cdot C_P \cdot T\right) = C_P \cdot T\frac{d\dot{m}}{dx} + \dot{m} \cdot T\frac{dC_P}{dx} + \dot{m} \cdot C_P\frac{dT}{dx} \tag{A2-3}$$

Also,

$$\frac{dC_P}{dx} = \frac{dC_P}{dM}\frac{dM}{dT}\frac{dT}{dx} \tag{A2-4}$$

By introducing Eq. (A2-1), (A2-2) and (A2-4) into Eq. (A2-3), finally one can obtain:

$$\frac{d\dot{H}}{dx} = \left(\frac{100 \cdot \dot{m}_d}{100 - M}\right)\left(\frac{dT}{dx}\right)\left[\left(\frac{C_P}{100 - M} + \frac{dC_P}{dM}\right)\frac{dM}{dT}T + C_P\right] \tag{A2-5}$$

For the fixed-element configuration system, same as above, the mass change is expressed as:

$$m = \frac{100 \cdot m_d}{100 - M} \tag{A2-6}$$

and,

$$\frac{dm}{dt} = \frac{100 \cdot m_d}{(100 - M)^2}\frac{dM}{dT}\frac{dT}{dt} \tag{A2-7}$$

The enthalpy change is expressed as:

$$\frac{dH}{dt} = \frac{d}{dt}\left(m \cdot C_P \cdot T\right) = C_P \cdot T\frac{dm}{dt} + m \cdot T\frac{dC_P}{dt} + m \cdot C_P\frac{dT}{dt} \tag{A2-8}$$

Also, the specific heat change with time is:

$$\frac{dC_P}{dt} = \frac{dC_P}{dM} \cdot \frac{dM}{dT} \cdot \frac{dT}{dt} \tag{A2-9}$$

By incorporating Eq.(A2-6), (A2-7), and (A2-9) into Eq.(A2-8), then the final expression of the enthalpy change is:

$$\frac{dH}{dt} = \left(\frac{100 \cdot m_d}{100 - M}\right)\frac{dT}{dt}\left[C_P + \left(\frac{C_P \cdot T}{100 - M}\right)\frac{dM}{dT}\right] \tag{A2-10}$$

Appendix III. Computer Program for the Configuration Factor in Gauss-Quadrature Method.

Configuration Factor for Figure 6.1.2

```
REM ------------------------------------------------------------------------------
2000 ' SUBROUTINE FOR CONFIGURATION FACTOR CALCULATION
   ' by GAUSS-QUADRATURE METHOD from dA1 to A2
REM ------------------------------------------------------------------------------
DIM WFI(100), WFJ(100), SPI(100), SPJ(100)

READ P1, Q1, P3, Q3, W1, HDIST, PI, STEPSIZE 'W1 is half of the width of the top trough.

DATA 0.0,1.5,0.0,1.5,0.15,0.12,3.141592,0.01
NPOINT = 1

2500 ON NPOINT GOSUB 5, 10, 20



3000   CFG1 = 0
     CFG3 = 0
     CFG2 = 0


     FOR I = 1 TO NITER


      REM  PRINT "SPI("; I; ")="; SPI(I); "SPJ("; J; ")="; SPJ(J)


          X1X3 = ((Q1 + P1) + (Q1 - P1) * SPI(I)) / 2 - X3
          Y1 = W1 * (1 + SPI(I)) / 2


          UA1 = W1 * X3 / (2 * PI)
          UA2 = X3 ^ 2
          UA3 = Y1 ^ 2
          UA4 = HDIST ^ 2
          S1 = UA1 / (UA2 + UA3 + UA4)


          UB1 = W1 * (Q1 - X3) / (2 * PI)
          UB2 = (Q1 - X3) ^ 2
          UB3 = Y1 ^ 2
          UB4 = HDIST ^ 2
          S2 = UB1 / (UB2 + UB3 + UB4)

          UC1 = (Q1 - P1) * W1 / (2 * PI)
          UC2 = X1X3 ^ 2
```

```
        UC3 = W1 ^ 2
        UC4 = HDIST ^ 2
        S3 = UC1 / (UC2 + UC3 + UC4)


    REM  PRINT "SPI("; I; ")="; SPI(I); "SPJ("; J; ")="; SPJ(J)
    REM  PRINT "S1="; S1; "S2="; S2; "S3="; S3
    REM  END

        CFG1 = CFG1 + WFI(I) * S1
        CFG2 = CFG2 + WFI(I) * S2
        CFG3 = CFG3 + WFI(I) * S3

    REM   PRINT "CFG1="; CFG1; "CFG2="; CFG2; "CFG3="; CFG3; "CFG4="; CFG4

      NEXT I


     REM  END


REM  'CONFIGURTION FACTOR '


     VFACTOR = CFG1 + CFG2 + CFG3


PRINT "X3="; X3; "VFACTOR="; VFACTOR

IF NDATA > 150 THEN GOTO 5000

   X3 = X3 + STEPSIZE
   NDATA = NDATA + 1
   GOTO 3000

5000 IF NPOINT > 3 THEN GOTO 6000
     NPOINT = NPOINT + 1
     GOTO 2500

6000 END


5 REM SAMPLING POINT = 5
NITER = 5

PRINT "SAMPLING POINTS ="; NITER

    X3 = 0
    NDATA = 1
```

```
    FOR I = 1 TO NITER
    READ SPI(I)
    READ WFI(I)
    NEXT I

    FOR J = 1 TO NITER
    READ SPJ(J)
    READ WFJ(J)
    NEXT J


REM DATA INPUT,   SPI(I), WFI(I)
DATA -.90618,.23693,-.53847,.47863,0.0,.56889,.53847,.47863,.90618,.23693


REM DATA INPUT  SPJ(J), WFJ(J),
DATA -.90618,.23693,-.53847,.47863,0.0,.56889,.53847,.47863,.90618,.23693

RETURN

10 REM SAMPLING POINT = 10
 NITER = 10
 PRINT
 PRINT "SAMPLING POINTS ="; NITER

    X3 = 0
    NDATA = 1


    FOR I = 1 TO NITER
    READ SPI(I)
    READ WFI(I)
    NEXT I

    FOR J = 1 TO NITER
    READ SPJ(J)
    READ WFJ(J)
    NEXT J


REM DATA INPUT,   SPI(I), WFI(I)
DATA -.97391,.06667,-.86506,.14945,-.67941,.21909,-.43339,.26927,-.14887,.29552
DATA .14887,.29552,.43339,.26927,.67941,.21909,.86506,.14945,.97391,.06667


REM DATA INPUT  SPJ(J), WFJ(J),
DATA -.97391,.06667,-.86506,.14945,-.67941,.21909,-.43339,.26927,-.14887,.29552
DATA .14887,.29552,.43339,.26927,.67941,.21909,.86506,.14945,.97391,.06667

RETURN
```

```
20 REM SAMPLING POINT = 20
 NITER = 20
 PRINT
 PRINT "SAMPLING POINTS ="; NITER

      X3 = 0
      NDATA = 1


      FOR I = 1 TO NITER
      READ SPI(I)
      READ WFI(I)
      NEXT I

      FOR J = 1 TO NITER
      READ SPJ(J)
      READ WFJ(J)
      NEXT J


REM DATA INPUT,   SPI(I), WFI(I)
DATA -.99313,.01761,-.96397,.0406,-.91223,.06267,-.83912,.08328,-.74633,.10193
DATA -.63605,.11819,-.51087,.13169,-.37371,.14210,-.22778,.14917,-.07653,.15275
DATA .07653,.15275,.22778,.14917,.37371,.14210,.51087,.13169,.63605,.11819
DATA .74633,.10193,.83912,.08328,.91223,.06267,.96397,.0406,.99313,.01761


REM DATA INPUT  SPJ(J), WFJ(J),
DATA -.99313,.01761,-.96397,.0406,-.91223,.06267,-.83912,.08328,-.74633,.10193
DATA -.63605,.11819,-.51087,.13169,-.37371,.14210,-.22778,.14917,-.07653,.15275
DATA .07653,.15275,.22778,.14917,.37371,.14210,.51087,.13169,.63605,.11819
DATA .74633,.10193,.83912,.08328,.91223,.06267,.96397,.0406,.99313,.01761

RETURN
```

Configuration Factor for Figure 6.1.3

```
REM ------------------------------------------------------------------------------

2000 ' SUBROUTINE FOR CONFIGURATION FACTOR CALCULATION
   ' by GAUSS-QUADRATURE METHOD for strip dA1 to A2.
REM ------------------------------------------------------------------------------
DIM WFI(100), WFJ(100), SPI(100), SPJ(100)

READ P1, Q1, P3, Q3, W1, W3, HDIST, PI, STEPSIZE
DATA 0.12,1.4,0.0,1.46,0.1425,0.1325,0.12,3.141592,0.02
NPOINT = 1

PRINT "SEPARATION DISTANCE ="; HDIST; "[m]"
PRINT "LENGTH OF TOP TRAY ="; Q1 - P1; "[m]"
PRINT "WIDTH OF TOP TRAY ="; 2 * W1; "[m]"

2500 ON NPOINT GOSUB 5, 10, 20



3000   CFG1 = 0
     CFG3 = 0
     CFG2 = 0
     CFG4 = 0


     FOR I = 1 TO NITER

          FOR J = 1 TO NITER


      REM  PRINT "SPI("; I; ")="; SPI(I); "SPJ("; J; ")="; SPJ(J)


          X1X3 = ((Q1 + P1) + (Q1 - P1) * SPI(I)) / 2 - X3
          Y1Y3 = W1 * (1 + SPI(I)) / 2 - W3 * SPJ(J)
          Y3 = W3 * SPJ(J)
          W1Y3 = W1 - W3 * SPJ(J)


          UA1 = -W1 * (P1 - X3) / (4 * PI)
          UA2 = (P1 - X3) ^ 2
          UA3 = Y1Y3 ^ 2
          UA4 = HDIST ^ 2
          S1 = UA1 / (UA2 + UA3 + UA4)


          UB1 = (Q1 - P1) * Y3 / (4 * PI)
          UB2 = X1X3 ^ 2
          UB3 = Y3 ^ 2
          UB4 = HDIST ^ 2
          S2 = UB1 / (UB2 + UB3 + UB4)


          UC1 = W1 * (Q1 - X3) / (4 * PI)
          UC2 = (Q1 - X3) ^ 2
```

```
            UC3 = Y1Y3 ^ 2
            UC4 = HDIST ^ 2
            S3 = UC1 / (UC2 + UC3 + UC4)

            UD1 = (Q1 - P1) * W1Y3 / (4 * PI)
            UD2 = X1X3 ^ 2
            UD3 = W1Y3 ^ 2
            UD4 = HDIST ^ 2
            S4 = UD1 / (UD2 + UD3 + UD4)


      REM  PRINT "SPI("; I; ")="; SPI(I); "SPJ("; J; ")="; SPJ(J)
      REM  PRINT "S1="; S1; "S2="; S2; "S3="; S3
      REM  END

            CFG1 = CFG1 + WFI(I) * WFJ(J) * S1
            CFG2 = CFG2 + WFI(I) * WFJ(J) * S2
            CFG3 = CFG3 + WFI(I) * WFJ(J) * S3
            CFG4 = CFG4 + WFI(I) * WFJ(J) * S4
     REM   PRINT "CFG1="; CFG1; "CFG2="; CFG2; "CFG3="; CFG3; "CFG4="; CFG4

          NEXT J

        NEXT I


       REM  END


 REM  'CONFIGURTION FACTOR '


      VFACTOR = CFG1 + CFG2 + CFG3 + CFG4


 PRINT "X3="; X3; "VFACTOR="; VFACTOR

 IF NDATA > 75 THEN GOTO 5000

    X3 = X3 + STEPSIZE
    NDATA = NDATA + 1
    GOTO 3000

 5000 IF NPOINT > 3 THEN GOTO 6000
       NPOINT = NPOINT + 1
       GOTO 2500

 6000 END


 5 REM SAMPLING POINT = 5
  NITER = 5

 PRINT "SAMPLING POINTS ="; NITER

      X3 = 0
```

```
      NDATA = 1


      FOR I = 1 TO NITER
      READ SPI(I)
      READ WFI(I)
      NEXT I

      FOR J = 1 TO NITER
      READ SPJ(J)
      READ WFJ(J)
      NEXT J


REM DATA INPUT,   SPI(I), WFI(I)
DATA -.90618,.23693,-.53847,.47863,0.0,.56889,.53847,.47863,.90618,.23693


REM DATA INPUT  SPJ(J), WFJ(J),
DATA -.90618,.23693,-.53847,.47863,0.0,.56889,.53847,.47863,.90618,.23693

RETURN

10 REM SAMPLING POINT = 10
 NITER = 10
 PRINT
 PRINT "SAMPLING POINTS ="; NITER

      X3 = 0
      NDATA = 1


      FOR I = 1 TO NITER
      READ SPI(I)
      READ WFI(I)
      NEXT I

      FOR J = 1 TO NITER
      READ SPJ(J)
      READ WFJ(J)
      NEXT J


REM DATA INPUT,   SPI(I), WFI(I)
DATA -.97391,.06667,-.86506,.14945,-.67941,.21909,-.43339,.26927,-.14887,.29552
DATA .14887,.29552,.43339,.26927,.67941,.21909,.86506,.14945,.97391,.06667


REM DATA INPUT  SPJ(J), WFJ(J),
DATA -.97391,.06667,-.86506,.14945,-.67941,.21909,-.43339,.26927,-.14887,.29552
DATA .14887,.29552,.43339,.26927,.67941,.21909,.86506,.14945,.97391,.06667

RETURN


20 REM SAMPLING POINT = 20
 NITER = 20
 PRINT
```

```
PRINT "SAMPLING POINTS ="; NITER

    X3 = 0
    NDATA = 1


    FOR I = 1 TO NITER
    READ SPI(I)
    READ WFI(I)
    NEXT I

    FOR J = 1 TO NITER
    READ SPJ(J)
    READ WFJ(J)
    NEXT J


REM DATA INPUT,   SPI(I), WFI(I)
DATA -.99313,.01761,-.96397,.0406,-.91223,.06267,-.83912,.08328,-.74633,.10193
DATA -.63605,.11819,-.51087,.13169,-.37371,.14210,-.22778,.14917,-.07653,.15275
DATA .07653,.15275,.22778,.14917,.37371,.14210,.51087,.13169,.63605,.11819
DATA .74633,.10193,.83912,.08328,.91223,.06267,.96397,.0406,.99313,.01761


REM DATA INPUT  SPJ(J), WFJ(J),
DATA -.99313,.01761,-.96397,.0406,-.91223,.06267,-.83912,.08328,-.74633,.10193
DATA -.63605,.11819,-.51087,.13169,-.37371,.14210,-.22778,.14917,-.07653,.15275
DATA .07653,.15275,.22778,.14917,.37371,.14210,.51087,.13169,.63605,.11819
DATA .74633,.10193,.83912,.08328,.91223,.06267,.96397,.0406,.99313,.01761

RETURN
```

APPENDIX IV. Coefficients of the Regression Polynomials

Table 4A-1. Coefficients of the polynomial regression curves for moisture determination [Eq.(6-3)] for peas tempered to different moisture contents and micronized in the fixed-element configuration system.

coefficient	Fixed-element configuration system		
	19.1% initial MC, (wet basis)	25.2% initial MC, (wet basis)	29.8% initial MC, (wet basis)
M_0	19.07	24.98	30.22
a_1	-2.216×10^{-2}	-2.135×10^{-2}	-6.643×10^{-2}
a_2	1.185×10^{-4}	5.979×10^{-5}	5.499×10^{-4}
a_3	-1.399×10^{-6}	-1.317×10^{-6}	-2.953×10^{-6}

Table 4A-2. Coefficients of the polynomial regression curves for moisture determination [Eq.(6-4)] for peas tempered to different initial moisture contents and micronized in the moving-element configuration system.

coefficient	Moving-element configuration system		
	19.6 % initial MC, (wet basis)	24.1% initial MC, (wet basis)	28.8% initial MC, (wet basis)
M_0	19.41	23.81	28.98
a_1'	-1.675×10^{-3}	-1.893×10^{-2}	-1.677×10^{-2}
a_2'	-8.437×10^{-5}	-2.757×10^{-5}	-9.905×10^{-6}
a_3'	0.0	-1.961×10^{-7}	-3.779×10^{-8}

Table 4A-3. Coefficients of the polynomial regression curves [Eq.(6-5)] of the temperature for peas tempered to three different moisture contents and micronized in the fixed-element configuration system.

coefficient	Fixed-element configuration system		
	19.1% initial MC, (wet basis)	25.2% initial MC, (wet basis)	29.8% initial MC, (wet basis)
T_0	25.87	24.64	26.26
b_1	1.511	1.229	0.9706
b_2	-7.054×10^{-3}	-5.571×10^{-3}	-3.213×10^{-3}
b_3	1.147×10^{-5}	1.058×10^{-5}	2.825×10^{-6}

Table 4A-4. Coefficients of the polynomial regression curves [Eq.(6-6)] for the peas tempered to three different initial moisture contents and micronized in the moving-element configuration system.

coefficient	Moving-element configuration system		
	19.6% initial MC, (wet basis)	24.1% initial MC, (wet basis)	28.8% initial MC, (wet basis)
T_0	28.00	36.01	23.94
b_1'	0.2282	3.346×10^{-2}	0.4873
b_2'	7.624×10^{-4}	2.613×10^{-3}	5.244×10^{-3}
b_3'	-2.381×10^{-6}	-9.356×10^{-6}	-3.068×10^{-5}

Table 4A-5. Power indices in Eq.(6-7) and (6-8) of the moisture-temperature gradient for peas micronized in the fixed-element and the moving-element configuration system.

power index	Fixed-element configuration system		
	19.1% initial MC, (wet basis)	25.2% initial MC, wb	29.8% initial MC, wb
n	3.55	3.45	3.60
power index	Moving-element configuration system		
	19.6% initial MC, (wet basis)	24.1% initial MC, (wet basis)	28.8% initial MC, (wet basis)
n'	3.20	3.50	3.50

Appendix V. Table of Configuration Factor

Table 5A-1. Configuration factor for a different number of approximation in the Gauss-Quadrature numerical integration.

Trough distance, (cm)	Configuration factor, (N^* = 5, H = 12 cm), (-)	Configuration factor, (N = 10, H = 12 cm), (-)	Configuration factor, (N = 20, H = 12 cm), (-)
0	0.0779	0.0777	0.0777
10	0.2776	0.2760	0.2760
20	0.5415	0.5466	0.5466
30	0.6321	0.6402	0.6395
40	0.6969	0.6616	0.6632
50	0.6566	0.6726	0.6707
60	0.6307	0.6718	0.6736
70	0.7019	0.6761	0.6746
80	0.7179	0.6733	0.6747
90	0.6385	0.6747	0.6739
100	0.6442	0.6714	0.6716
110	0.6984	0.6648	0.6654
120	0.6471	0.6474	0.6469
130	0.5678	0.5766	0.5768
140	0.3406	0.3387	0.3387
146	0.1707	0.1699	0.1699

*N = number of approximation in the Gauss-Quadrature numerical integration.
H = separation distance between the emitter and the bottom tough of the micronizer.

Table 5A-2. Configuration factor with various separation distance of the micronizer.

Trough distance, (cm)	Configuration factor, (H^* = 8cm, N = 20), (-)	Configuration factor, (H = 12cm, N = 20), (-)	Configuration factor, (H = 20cm, N = 20), (-)
0	0.0482	0.0777	0.1075
10	0.2856	0.2760	0.2323
20	0.6811	0.5466	0.3770
30	0.7557	0.6402	0.4613
40	0.7693	0.6616	0.4964
50	0.7732	0.6726	0.5107
60	0.7749	0.6718	0.5168
70	0.7756	0.6761	0.5192
80	0.7756	0.6733	0.5193
90	0.7752	0.6747	0.5174
100	0.7740	0.6714	0.5124
110	0.7707	0.6648	0.5004
120	0.7602	0.6474	0.4711
130	0.7093	0.5766	0.3994
140	0.3882	0.3387	0.2632
146	0.1376	0.1699	0.1746

*H = separation distance between the emitter and the bottom trough of the micronizer.
*N = number of approximation in the Gauss-Quadrature numerical integration.

APPENDIX VI. Programs of Runge-Kutta 4th Order Method and Euler Method

'Simulation for a fixed element configuration _Euler method'

```
'Initial conditions
t=0
put t into cell(26,1)
T0=cell(25,11)
put T0 into cell(27,1)

B=cell(25,11)-273
put B into cell(28,1)
u=cell(25,16)
put u into cell(31,1)

for i=1 to 200 do

'simulation time calculation
t1=cell(26,i)+cell(25,1)
put t1 into cell(26,i+1)

'calculation of k=dM/dT
k=-1*(10^(-8)*cell(26,i)^3.65)
put k into cell(30,i)

'calculation of A=alfa
A=(1-cell(25,3))*(cell(25,6)*cell(25,7)*cell(25,8)^4*cell(25,5)+cell(25,9)
*cell(25,7)*cell(25,10)^4*(1-cell(25,5)))

'calculation of M=qf/(epss*dt)
M=(cell(25,18)*((-1)*cell(25,7)*cell(25,19)^4 *(cell(25,3)*(1-cell(25,4))-1)
  -cell(25,3)*cell(25,4)*cell(25,7)*cell(27,i)^4+A))/((1-cell(25,3)
  *(1-cell(25,18))*(1-cell(25,4)))*cell(25,4)*cell(25,1))
put M into cell(29,i)

'calculation of temperature
f1=(cell(25,1)*cell(25,2)*cell(25,17)*cell(25,3)*cell(25,4)*(cell(25,5)*cell(25,6)
   *cell(25,7)*cell(25,8)^4 + (1-cell(25,5))*cell(25,9)
```

```
    *cell(25,7)*cell(25,10)^4 - cell(25,7)*cell(27,i)^4+M))


 f4=100*cell(25,12)/(100-cell(31,i))
 put f4 into cell(37,i)
 f5=cell(25,13)/(100-cell(31,i))*cell(30,i)*cell(27,i)
 put f5 into cell(38,i)
 f6=cell(25,13)-(cell(25,14)/(100-cell(31,i))*cell(30,i))
 put f6 into cell(39,i)
 f2=f4*(f5+f6)
 put f2 into cell(36,i)

 f3=f1/f2


 f(t)=f3+cell(27,i)

 y=f(t)
 put y into cell (27,i+1)
 z=f(t)-273
 put z into cell(28,i+1)

 'calculation of moisture change
 L=(k*(cell(27,i+1)-cell(27,i)))+cell(31,i)
 put L into cell(31,i+1)
 end for
```

```
'Simulation for a fixed element configuration_R-K4

'Initial conditions
t=0
put t into cell(26,1)
ta=0
put ta into cell(40,1)
T0=cell(25,11)
put T0 into cell(27,1)

B=cell(25,11)-273
put B into cell(28,1)
u=cell(25,16)
put u into cell(31,1)


for i=1 to 200 do

'simulation time calculation
t1=cell(26,i)+cell(25,1)
put t1 into cell(26,i+1)

'calculation of k=dM/dT
k=-1*(10^(-8)*cell(26,i)^3.65)
put k into cell(30,i)

'calculation of A=alfa
A=(1-cell(25,3))*(cell(25,6)*cell(25,7)*cell(25,8)^4*cell(25,5)+cell(25,9)
*cell(25,7)*cell(25,10)^4*(1-cell(25,5)))

'calculation of M=qf/(epss*dt)
M=(cell(25,18)*((-1)*cell(25,7)*cell(25,19)^4 *(cell(25,3)*(1-cell(25,4))-1)
  -cell(25,3)*cell(25,4)*cell(25,7)*cell(27,i)^4+A))/((1-cell(25,3)
  *(1-cell(25,18))*(1-cell(25,4)))*cell(25,4)*cell(25,1))
put M into cell(29,i)

'calculation of temperature
f1=(cell(25,1)*cell(25,2)*cell(25,17)*cell(25,3)*cell(25,4)*(cell(25,5)*cell(25,6)
   *cell(25,7)*cell(25,8)^4 + (1-cell(25,5))*cell(25,9)
   *cell(25,7)*cell(25,10)^4 - cell(25,7)*cell(27,i)^4+M))


f4=100*cell(25,12)/(100-cell(31,i))
```

```
f5=cell(25,13)/(100-cell(31,i))*cell(30,i)*cell(27,i)

f6=cell(25,13)-(cell(25,14)/(100-cell(31,i))*cell(30,i))
put f6 into cell(39,i)
f2=f4*(f5+f6)


f3=f1/f2
put f3 into cell(36,i)

N=200
h=200/N

k1=h*f3
k2=h*(cell(36,i)+k1/2)
k3=h*(cell(36,i)+k2/2)
k4=h*(cell(36,i)+k3)
put k1 into cell(42,i+1)
put k2 into cell(43,i+1)
put k3 into cell(44,i+1)
put k4 into cell(45,i+1)

k5=(k1+2*k2+2*k3+k4)/6
put k5 into cell(41,i+1)

y=cell(27,i)+(k1+2*k2+2*k3+k4)/6
put y into cell (27,i+1)

z=y-273
put z into cell(28,i+1)

'calculation of moisture change
L=(k*(cell(27,i+1)-cell(27,i)))+cell(31,i)
put L into cell(31,i+1)

t2=i*h+ta
put t2 into cell(40,i+1)


end for
```

'Simulation for a moving element configuration_R-K4

```
'Initial conditions
t=0
put t into cell(26,1)
L1=0
put L1 into cell(40,1)
T0=cell(25,11)
put T0 into cell(27,1)

'Temp in deg. C
B=cell(25,11)-273
put B into cell(28,1)

'Moisture
M0=cell(25,16)
put M0 into cell(31,1)


for i=1 to 73 do

'calculation of k=dM/dT
k=-1*(10^(-8)*(cell(40,i)^cell(25,20)))
put k into cell(30,i)

'calculation of qb
z2=cell(25,18)*cell(25,7)*cell(25,19)^4
B1=(1-cell(25,3))*(cell(35,i)*cell(25,6)*cell(25,7)*cell(25,8)^4+
    (1-cell(35,i))*cell(25,9)*cell(25,7)*cell(25,10))
z1=cell(25,3)*cell(25,4)*cell(25,7)*cell(27,i)^4+B1
qb=(z2*(1-(1-cell(25,4))*cell(25,3))+cell(25,18)*z1)/(1-cell(25,3)+
    (1-cell(25,4))*(1-cell(25,18)))

put qb into cell(29,i)

'calculation of temperature
f1=cell(25,3)*cell(25,17)*cell(25,4)*(cell(35,i)*cell(25,6)
   *cell(25,7)*cell(25,8)^4 + (1-cell(35,i))*cell(25,9)
   *cell(25,7)*cell(25,10)^4 - cell(25,7)*cell(27,i)^4+qb/cell(25,4))


f4=100*cell(25,12)/(100-cell(31,i))
```

```
f5=cell(25,13)/(100-cell(31,i))*cell(30,i)*cell(27,i)

f6=cell(25,13)-(cell(25,14)/(100-cell(31,i))*cell(30,i))
put f6 into cell(39,i)
f2=f4*(f5+f6)


f3=f1/f2
put f3 into cell(36,i)

h=cell(25,2)

k1=h*f3
k2=h*(cell(36,i)+k1/2)
k3=h*(cell(36,i)+k2/2)
k4=h*(cell(36,i)+k3)
put k1 into cell(42,i+1)
put k2 into cell(43,i+1)
put k3 into cell(44,i+1)
put k4 into cell(45,i+1)

k5=(k1+2*k2+2*k3+k4)/6
put k5 into cell(41,i+1)

y=cell(27,i)+(k1+2*k2+2*k3+k4)/6
put y into cell (27,i+1)

z=y-273
put z into cell(28,i+1)

'calculation of moisture change
M=(k*(cell(27,i+1)-cell(27,i)))+cell(31,i)
put M into cell(31,i+1)

'Distance calculations
L2=100*i*h+L1
put L2 into cell(40,i+1)


end for
```